# PERFORMANCE OF CDMA SYSTEMS USING DIGITAL BEAMFORMING WITH MUTUAL COUPLING AND SCATTERING EFFECTS

by

Alexander M. Wyglinski

A thesis submitted to the
Department of Electrical and Computer Engineering
in conformity with the requirements
for the degree of Master of Science (Engineering)

Queen's University
Kingston, Ontario, Canada
September, 2000

# Abstract

The mobile communications market has seen an explosion of growth over the past several years. Moreover, trends indicate that this growth will continue uninterrupted into the next decade. To meet this increasing demand, the use of base station antenna arrays implementing digital beamforming is being proposed as a method to enhance both the performance and capacity of cellular systems. In this work, we will examine the effects of mutual coupling occurring within the base station antenna arrays of code division multiple access (CDMA) cellular systems.

First, we examine three different methods of incorporating mutual coupling effects within the base station antenna array. These methods are then applied to several antenna array models for comparison with the ideal case and with each other. Following this, we then improve a method for determining CDMA system uplink capacity, given by Earnshaw, by including the effects of mutual coupling.

Next, we derive a generalized model for the cross-correlation statistics between elements of an antenna array in a scattering environment to include mutual coupling effects and arbitrary distributions of angle-of-arrival (AOA) statistics. Using this model, we further improve the above method for determining CDMA system uplink capacity by including the effects of both scattering and mutual coupling.

Finally, we investigate an improved system capacity prediction where imperfect power control is assumed. In this derivation, the signal-to-noise ratio is a random

variable with a log-normal distribution, rather than a fixed value, as in the case of perfect power control. Furthermore, the outage probability associated with the imperfect power control case is derived.

# Acknowledgements

I would like to express my deepest gratitude to my supervisor, Dr. Steven D. Blostein, for his continuous support and guidance throughout my graduate studies at Queen's University. His knowledge, patience, and valuable advice over these past two years did much to achieve success in this work and are greatly appreciated.

I would also like to thanks the members of my defence committee, namely, Dr. L. K. Daneshmend, Dr. A. P. Freundorfer, Dr. T. Linder, and Dr. P. J. McLane, for their comments and suggestions with respect to my thesis.

The financial support provided by Dr. Blostein from the Canadian Institute for Telecommunications Research and the School of Graduate Studies and Research of Queen's University, as well as the financial support of Le Fonds pour la Formation de Chercheurs et l'Aide à la Recherche du Ministère de la Recherche, de la Science et de la Technologie du Québec, is gratefully acknowledged.

To all my friends that I have had the most fortunate pleasure of meeting during my stay at Queen's, thank you for all the good times and support. I would like to especially thank my labmates at the IPCL: Joseph, Noel, Yi, Lin, Qianfu, Wei, Neng, Li, Costi, Eric, Bin, and Ruifeng. Moreover, I would like to thank Zhihua, Jagdev, Kareem, Bohdan, Hany, Mohsen, Julian, Sebastien, Tony, Tom, Mark, Mike, Sr. Barbara, Mariola, Betty, Thomas, Cindy, Sally, and Rosa for their friendship.

I would like to thank my parents and my sisters, Joanne and Laura, as well as my other family members, for their continuous love, support, and encouragement ever since day one.

I would like to thank my best friend Linda for her love, support, and unwavering belief in me.

# Contents

# List of Tables

# List of Figures

# Symbols and Abbreviations

| | |
|---|---|
| AOA | angle-of-arrival |
| DOA | direction-of-arrival |
| $2\Delta$ | angle spread of the arriving signal |
| $\theta_d$ | mean AOA for the desired mobile |
| $\theta_k$ | mean AOA for the mobile $k$ |
| $P(\theta)$ | spatial distribution of the incoming signal |
| $\sigma_\Delta^2$ | variance of the spatial AOA distribution $P(\theta)$ |
| CDMA | code division multiple access |
| $\overrightarrow{I}$ | vector of currents distributed over the antenna array |
| $\overrightarrow{V}$ | vector of voltages distributed over the antenna array |
| $[Y]$ | antenna array mutual admittance matrix |
| $[Z]$ | antenna array mutual impedance matrix |
| $\rho_{RiRk}$ | correlation coefficient between the real component of the Rayleigh fading at antenna $i$ and the real component of the Rayleigh fading at antenna $k$ |
| $\rho_{RiIk}$ | correlation coefficient between the real component of the Rayleigh fading at antenna $i$ and the imaginary component of the Rayleigh fading at antenna $k$ |
| $N_A$ | number of antenna array elements |

| | |
|---|---|
| $B$ | bandwidth of the spreaded signal |
| $E_b/N_o$ | bit energy-to-noise ratio |
| $N_I$ | number of interfering mobiles |
| $N_M$ | total number of mobiles |
| $R_B$ | data bit rate |
| $\bar{a}$ | array response vector |
| $\bar{a}_\beta$ | array response vector which includes received signal strength information |
| $\bar{\omega}(\theta_d)$ | maximum SNR beamforming weights for the desired user as a function of the angle-of-arrival $\theta_d$ |
| $\bar{\omega}_{MC}(\theta_d)$ | maximum SNR beamforming weights for the desired user as a function of the angle-of-arrival $\theta_d$ which includes the effects of mutual coupling |
| $\alpha_{ki}$ | relative phase of the $i$th entry of mobile $k$ś array response vector |
| EM | electromagnetic |
| MoM | Method of Moments |
| MCE | Mutual Coupling Effects |
| $P_R$ | received signal power due to the desired user |
| $P_{I_k}$ | received interference power from $k$th mobile |
| $P_I$ | total received interference power |
| $\alpha$ | voice activity factor |
| $\eta$ | background noise power due to spurious interference and thermal noise contained in the total spreaded bandwidth |
| $\sigma_n^2$ | variance of the background noise |
| $\phi_k$ | fraction of interferer $k$'s signal power passed by the beamforming weights |
| N | total number of increments in antenna array |
| $\beta$ | wavenumber (equal to $2\pi/\lambda$) |

| | |
|---|---|
| $\sigma$ | surface charge density on a conducting surface $S$ |
| $\overrightarrow{J}$ | current vector on a conducting surface $S$ |
| $\mu$ | permeability of the dielectric |
| $\epsilon$ | permittivity of the dielectric |
| $\overrightarrow{A}$ | magnetic vector potential |
| $\Phi$ | magnetic scalar potential |
| $\overrightarrow{n}$ | outward direction normal to the conducting surface $S$ |
| $\overrightarrow{\nabla}$ | gradient operator |
| $\omega$ | angular frequency |
| $R$ | distance from a source point to a field point |
| $\lambda$ | wavelength of signal |
| $\phi_k$ | fraction of interferer $k$'s signal power passed by the beamforming weights of the array |
| $\phi_d$ | fraction of desired mobile $d$'s signal power passed by the beamforming weights of the array |
| $\beta_{ki}$ | received signal strength due to mobile $k$ at element $i$ |
| $\eta_k$ | path loss and shadowing effects factor at mobile $k$ |
| $R_{ki}$ | Rayleigh fading random variables for mobile $k$ at array element $i$ |
| $\mathcal{R}$ | cross-correlation matrix between antenna elements $i$ and $j$ |
| $b_o$ | the mean squared of the real or imaginary component of the Rayleigh fading at antenna $i$ or antenna $j$ |
| $k_u$ | number of users within a single cell |
| $K_o$ | maximum number of users that can be served simultaneously |
| LCH | lost call held |
| $P_k$ | steady-state occupancy probability for the $k$th state |
| $P_B$ | blocking probability |
| $I_oB$ | average noise-plus-interference power |

| | |
|---|---|
| $I_o$ | noise-plus-interference power |
| $P_{out}$ | probability of outage |

# Chapter 1

# Introduction

## 1.1 Motivation

The increase in demand for frequency bandwidth has made it one of the world's most valuable and sought-after resources. As a result, new technologies are required to further expand and exploit this resource to meet modern society's needs. One such technology, which has been proposed for the next generation of digital cellular phones in North America, is *code division multiple access* (CDMA). Although CDMA is capable of greater cell capacity by increasing the number of users within a given bandwidth as compared with other multiple access techniques, it is possible to further increase the capacity through the use of digital beamforming and base station antenna arrays.

One method of studying the capacity of CDMA communication systems is by investigating the electromagnetic behaviour of antenna array structures, usually modeled by combining the beampatterns of the individual antenna elements through superposition. One electromagnetic phenomenon associated with the closely-spaced array elements is mutual coupling. By definition, when a pair of antennas are in

close proximity to each other, whether one or both antennas are transmitting and/or receiving, some of the energy that is primarily intended for one antenna ends up at the other. Thus, mutual coupling effects do have an effect on the beampatterns of the array. Unfortunately, most beampattern synthesis models do not account for the effects of mutual coupling thus potentially leading to less accurate system performance predictions. Furthermore, studies which do include mutual coupling effects do not incorporate the effects of scatter due to multipath. Moreover, these studies do not bother to re-evaluate the effects of power control on the system performance, which is required since the mutual coupling and scattering effects change the statistics of received power levels, such as the mean and variance, which in turn affects power controllability. As a result, the performance predictions of these studies are potentially less accurate in relation to methods which include all three effects. Also, in many studies, the assumption of perfect power control is made, thus yielding overly-optimistic performance predictions.

In this thesis, the development of an improved method, where the effects of mutual coupling, scatter, and power control are included in the system capacity predictions, is presented and applied to system performance prediction. Using this improved method, it can be shown that the inclusion of both mutual coupling and scattering effects degrades the performance of the system. For example, as the effect of scatter increases, the capacity of multi-antenna systems decreases and ultimately converges to the capacity of a system consisting of one antenna. Moreover, the difference in capacity between a 5-antenna system which does and does not include the effects of mutual coupling ranges between 6 and 11 percent. With respect to the effects of power control, the constraint of perfect power control will be dropped and replaced with an imperfect power control assumption. A comparison of performance predictions, where the system either assumes perfect or imperfect power control, will follow.

## 1.2 Previous Work

One of the major contributions of this thesis is to accurately predict the capacity of CDMA communication systems using digital beamforming, where the effects of mutual coupling, scatter, and power control are included. In this section, we discuss the work carried out by other researchers who have addressed issues pertaining to capacity prediction as well as the above mentioned effects. Some researchers have only dealt with system capacity predictions without including any of these effects, while others have accounted for some of these effects in their analysis. After an extensive open literature search, it can be stated confidently that an analysis of system capacity, where all these effects are included, has not been performed. Therefore, the work presented in this thesis is considered original.

### 1.2.1 Mutual Coupling Effects

The study of mutual coupling effects in antenna arrays has been conducted for nearly a century. Thus, the literature on this subject is extensive and in-depth. In this area there exists three categories which this research can be classified under.

The oldest of these categories deals with the modeling of mutual coupling effects in antenna arrays. Carter [10], King [37], and Malherbe [50] have adapted an approach of modeling the mutual coupling effects within a dipole antenna array using the Induced EMF Method. In their derivations, the array geometry and the number of array elements were not specified. The mutual coupling information was then included in several beampattern synthesis problems, resulting in more accurate beampatterns. Another approach of modeling the effects of mutual coupling has been carried out by Harrington [30], Strait and Adams [81], Adams and Strait [2], and Strait and Hirasawa

[80]. In their method, they have modeling the mutual coupling effects within an array of parallel wire antennas using the Method of Moments, instead of the Induced EMF Method, and then applied to several problems of beampattern synthesis.

Another, more recent, category of mutual coupling research deals with the compensation of these effects in applications involving antenna arrays. For instance, Pasala and Friel [62] have investigated a technique of mutual coupling compensation in the multiple signal classification (MUSIC) algorithm operating over a wideband of frequencies. Adve and Sarkar [3] used the Method of Moments to obtain a mutual admittance matrix, which was then used to eliminate the effects of mutual coupling in the direct data domain adaptive algorithm. Friedlander and Weiss [25] used an eigenstructure approach to obtain estimates of directions of arrivals as well as estimates of gain, phase and mutual coupling of the observing array. Moreover, it was shown that the estimation of sensor characteristics is essential in order to estimate the direction-of-arrivals accurately. Leou, Yeh, and Ucci [42] devised two methods of counteracting the phase distortion associated with the effects of mutual coupling such that angel-of-arrival estimation can be performed accurately.

Finally, the last category of mutual coupling research deals with the performance of systems which employ antenna arrays and include mutual coupling effects. Gupta and Ksienski [29] investigated the steady-state and transient performance of adaptive arrays where the effects of mutual coupling are included. They have derived an expression for the steady-state output signal-to-interference-plus-noise ratio, the eigenvalues associated with the signal covariance matrix, the steering vector required to maximize the output signal-to-interference-plus-noise ratio of Applebaum-type adaptive arrays, all in the presence of mutual coupling. Cheng [11] investigated optimization techniques for antenna arrays in the presence of mutual coupling. Specifically, he used the Method of Moments to generate the mutual coupling information, which

was then included in the maximization procedures for array directivity and signal-to-noise power ratio. Diouris, McLaughlin, and Zeidler [16] evaluated the performance of a compact space-time diversity receiver for mobile communications and derived several expressions for the bit error rate and outage probability as a function of the channel covariance matrix.

### 1.2.2 Scatter due to Multipath

Another physical effect associated with antenna arrays is scatter due to multipath propagation. In the past, much of the research involving antenna arrays assumed that the envelopes of the received signals were either uncorrelated, as in diversity research, or perfectly correlated, as in beamforming research. Unfortunately, with these assumptions, the resulting performance predictions of the system are inaccurate and optimistic. Thus, there exists several researchers who are currently examining the cross-correlation statistics between antennas within the antenna array to resolve this inaccuracy. Within this collection of researchers, there exist two groups with different research emphasis concerning the cross-correlation statistics.

The first group is concerned with understanding and adequately modeling the spatial characteristics of the channel. Ertel et al. [22] investigated several spatial models used to characterize the channel in different environments, such as the Gaussian Wide Sense Stationary Uncorrelated Scattering, Gaussian Angle-of-Arrival, Typical Urban, and Bad Urban models. Furthermore, Ertel and Reed [23] investigated the time and angle of arrival statistics for circular and elliptical scattering models, resulting in the derivation of the joint and marginal time-of-arrival and angle-of-arrival probability density functions.

The second group is interested in the effect of correlations among the fading

signals at the array elements. Salz and Winters [74] [75], Jakes [33], Colman [12], and Bramley [8] examined the cross-correlation statistics between the antennas in the antenna array. These researchers all approached the problem the same way by investigating the cross-correlation statistics received from the same source at a pair of antennas. Most of these researchers assumed a specific spatial distribution in their analysis. Only Colman in [12] derived an expression of the cross-correlation statistics which does not assume an specific spatial distribution.

### 1.2.3 Power Control

A critical component of CDMA systems is power control. Power control techniques are used to overcome the near-far effects by varying transmitted power levels to ensure that all the signals are received with equal power levels. As a result, many researchers, such as [9], [14], [19], [31], [44], [45], [51], [91], [92], [93], and [99], have conducted extensive investigations into these techniques and their impact on the system capacity. Cameron and Woerner [9] examined the performance of a CDMA system which assumes imperfect power control, multiple access interference, and a single cell. The results are then compared to the case where perfect power control is assumed. Comparing the results between the two cases, it was shown that a 10 to 30 percent loss in capacity from the perfect power control case occurs when imperfect power control is assumed. Corazza, De Maio, and Vatalaro [14] determined the outage probabilities as a function of interference from both inside and outside the reference cell, path loss, fading, shadowing, and power control. Earnshaw [19] investigated and compared both perfect and imperfect power control techniques and considered in the analysis the effect of mobile call initialization, including the initialization of its transmission power. Hsu and Lee [31] established a system model which included the effects of shadowing, multipath fading, antenna diversity, voice activity.

The performance of this system was then evaluated when perfect and imperfect power control was assumed. In both cases, the outage probability was determined. They determined that the system performance was sensitive to multipath fading, antenna diversity, and power control error. Lin, Huang, and Wu [44] implemented an uplink power control scheme for a CDMA system based on the IS-95 standard. The cases of perfect and imperfect power control were assumed. Linnartz [45] derived am exact mathematical expression for the outage probability where the effects of multiple interfering signals combined with log-normal and Rayleigh fading are present. Manji and Zhuang [51] examined the reverse link power control in an indoor environment characterized by a slowly Rayleigh fading channel. Furthermore, three algorithms were discussed and their performance compared. These algorithms are: open loop, channel estimation, and closed loop power control. Both perfect and imperfect power control schemes are investigated although the perfect power control is calculated while the imperfect power control is simulated. Viterbi [91], as well as Viterbi and Viterbi [92], presented an approach to the evaluation of the reverse link capacity of a CDMA cellular voice system which employs power control and a variable rate vocoder based on voice activity. In fact, the derivations in Chapter 5 for the outage probabilities, when either perfect or imperfect power control is assumed, follows an approach similar to the one presented in [91] [92] with the exception that in our work mutual coupling and scatter effects are accounted-for. Wu, Wu, and Zhou [93] investigated an optimum power control scheme for several centralized power control algorithms for CDMA systems. Finally, Zhou, Onozato, and Yamamoto [99] examined the performance of CDMA systems with hierarchical macrocell/microcell architectures where power control, both perfect and imperfect, are assumed.

### 1.2.4 System Capacity

One of the motivations for using CDMA is its ability to support multiple users simultaneously within the same frequency band via unique pseudo-noise sequence assignment for each user. Thus, the study of system cellular capacity has been a major objective of many researchers.

With respect to capacity determination, extensive research has been conducted with respect to CDMA systems employing omnidirectional antennas. Gilhousen et al. [27] presented one of the first and most cited papers on CDMA system capacity. In [27], the problem of calculating the capacity of a CDMA system employing omnidirectional antennas and cell sectorization was addressed. Moreover, effects such as path loss and shadowing as well as voice activity were included in the analysis. Although our analysis of system capacity throughout this thesis is based on the approach used in [27], we do not address voice activity, even though to include it would be a simple extension to our work. Cameron and Woerner [9] compared differences in system capacity when imperfect power control is used rather than a perfect power control assumption in a CDMA system where omnidirectional antennas are employed and the analysis performed for a single cell. Milstein, Rappaport, and Barghouti [53] studied the effects of the path loss exponent, total number of mobiles, and diversity on the bit-error probability for both the uplink and downlink. Stuber and Kchao [82] determined the bit-error rates as a function of path loss, fading, multiple access interference, and background noise assuming power control and compared it against the case when power control is not assumed.

Several researchers have adopted queuing theory viewpoint when investigating system capacity by examining the outage probability and Erlang capacity. As was mentioned before, Viterbi [91], as well as Viterbi and Viterbi [92], determined the

outage probability for a power controlled CDMA system from which the Erlang capacity was obtained. Baiocchi, Delli Priscoli, and Sestini [6] defined traffic control mechanisms to counteract the detrimental effects of large fluctuations of bursty user mobility on the Erlang capacity of the CDMA cellular network. The improvement in capacity was also determined and compared against the case where none of these control mechanisms were in place. Shen and Krzymien [77] investigated the effect of fading on the reverse link Erlang capacity of the IS-95 CDMA communication system. The fading channel multipath intensity profile was included in the Erlang capacity formula. Lee and Miller [40] calculated the CDMA blocking probability based on a new analysis of the total squared power of other-cell interference. From this analysis, the results obtained exhibit higher Erlang capacity relative to previous methods.

Although cellular CDMA systems are capable of handling multiple users simultaneously within the same frequency band, the increasing demand for mobile communications can potentially strain the capacity of the CDMA system and affect the quality of service for each user. Digital beamforming employing the use of base station antenna arrays is one proposed method of significantly increasing the cellular capacity of a CDMA system within a single cell. In this thesis, we determine the increase in capacity due to beamforming with antenna arrays where the effects of mutual coupling, scatter, and power control are included. This work is partially an extension of the work carried out by Colman in [12], who studied the performance of cellular CDMA communication systems using digital beamforming in environments with scatter. Furthermore, Earnshaw [19] [20] as well as Naguib and Paulraj [56] - [59] have presented work also closely related to our own. Finally, other works digital beamforming and antenna arrays are used to increase capacity of CDMA systems include [28], [43], [46], [86], and [89].

## 1.3 Summary of Contributions

The major contributions of this thesis are:

- A method of including the effects of mutual coupling, generated using either the Induced EMF Method [37], method of moments [30], or full-wave electromagnetic numerical computation [98], in our beampattern synthesis models of base station antenna arrays used in CDMA communication systems employing digital beamforming.
- The illustration of mutual coupling effects in antenna beamforming.
- Improved CDMA power and capacity predictions from Colman in [12] for both single and multiple element antenna array cases by including the effects of mutual coupling.
- A comparison of CDMA system capacity predictions between models which do and do not include the adverse effects of mutual coupling.
- A model for the cross-correlation statistics between two array elements, similar to the model developed by Salz and Winters in [75], assuming an unspecified angle-of-arrival probability distribution $P(\theta)$, as in [12], with the effects of mutual coupling included.
- The extension of the CDMA power and capacity predictions to the scattering environment case using the cross-correlation statistics at the antenna array where the effects of mutual coupling are included.
- The illustration of the effects of angle spread, angle-of-arrival spatial distributions, and number of array elements on CDMA system capacity predictions.

- Improved probability of outage expressions for CDMA systems assuming perfect or imperfect power control from Viterbi and Viterbi in [91] and [92] by including the effects of mutual coupling and scatter due to multipath.
- The illustration of the effects of mutual coupling, scatter due to multipath, and power control on the Erlang capacity of the CDMA communication system.

## 1.4 Thesis Outline

The following chapters examine the effects of mutual coupling, scatter due to multipath, and power control on CDMA cellular communication systems employing digital beamforming and base station antenna arrays. The goal of this study is to investigate the impact of these effects on the performance of CDMA systems using smart antennas via system capacity predictions.

Chapter 2 examines the power and uplink capacity prediction of CDMA systems which employ digital beamforming and antenna arrays in an ideal environment, i.e., no scattering due to multipath and no mutual coupling effects, presented in Colman [12] and Naguib [56]. Furthermore, we introduce background material in digital beamforming and define the array response vectors associated with antenna arrays.

Chapter 3 examines two analytical methods, the Induced EMF Method, from [37], and the Method of Moments, from [30], as well as a full-wave electromagnetic numerical computation, from [98], are used to include the effects of mutual coupling in the system models from Chapter 2. The implementation of these methods in our beampattern synthesis models and system capacity predictions is meticulously described in our analysis. A comparison of beampatterns and capacity predictions when mutual coupling is and is not included is performed.

Chapter 4 takes the system model we developed in Chapter 3 one step further by assuming the environment also includes the effects of scatter due to multipath. This is achieved by determining the cross-correlation statistics between antennas of the array, as was performed by Salz and Winters [75], but improving it by including the effects of mutual coupling and using an unspecified angle-of-arrival spatial distribution. Hence, we can further increase the accuracy of our system model by including both the effects of mutual coupling and scatter. An illustration of the effects of mutual coupling scatter on system capacity as a function of angle spread and number of array elements is performed.

Chapter 5 presents an approach to the evaluation of the reverse link capacity of a CDMA system using digital beamforming and employing a base station antenna array under imperfect power control where the effects of mutual coupling and scatter due to multipath are included. The derivation for the probability of outage for a system with perfect power control uses an approach based on [91] and [92]. The end result is two expressions for the outage probability, one is an upper bound and other is a Gaussian approximation. This derivation is then extended to the case of imperfect power control, also obtaining the upper-bound and Gaussian approximation of the outage probability. Finally, we present some comparisons which highlight the relative effects of digital beamforming with different numbers of antenna elements, mutual coupling, scatter due to multipath, and power control.

# Chapter 2

# Capacity Enhancement using Digital Beamforming and Antenna Arrays

## 2.1 Introduction

One of the primary restrictions for current code-division multiple access (CDMA) communication systems is their susceptibility to interference from other co-channel users. Although several remedies have been proposed, CDMA systems which employ digital beamforming and base station antenna arrays, also known as *smart antennas*, have been shown to be capable of achieving greater capacity relative to other multiple access techniques [57]. In this chapter, we examine the uplink power and capacity prediction of CDMA systems which employ digital beamforming and antenna arrays in an ideal environment, i.e., no scattering due to multipath and no mutual coupling effects. Furthermore, we shall introduce some background material on digital beamforming and define several array response vectors associated with antenna arrays.

### 2.1.1 Chapter Outline

The first half of this chapter deals with the concepts of digital beamforming. These concepts are then reinforced with an explanation of array response vectors and its dependency on the array geometry. In particular, the array response vectors for circular and uniform linear antenna arrays are derived in detail. Following this subsection, we will discuss beampattern synthesis. This is crucial to understanding how digital beamforming works since it provides insight into the electromagnetic behaviour of the antenna array, which can be used to study the performance of the system.

The second half of this chapter addresses system capacity predictions. Specifically, a derivation of the system capacity will be carried out and then applied to the case of a circular antenna array ranging from one to six array elements. Using this example, the benefits of using antenna arrays to increase system capacity will be exhibited.

## 2.2 Digital Beamforming

### 2.2.1 Introduction

Digital beamforming is used to maximize the ratio of the desired mobile's signal power to the noise and interference power by taking the weighted sum of the antenna outputs in the multi-element base station antenna array. This maximization is achieved by suppressing the noise and interference power using a suitable set of beamforming coefficients.

One critical required component for performing digital beamforming is the knowledge of the array response vector, that contains the relative phases of received signals

at each array element. The array response vector is used by a digital beamformer to isolate desired signals and suppress interfering signals.

Using the array response vector, the beampatterns generated for an array which is beamforming towards a particular direction can be found. This process is called *beampattern synthesis* and it is an important and useful tool in determining the performance of the system.

### 2.2.2 Array Response Vectors

The use of multi-element antenna arrays in the reception of signals requires the knowledge of the array response vector $\bar{a}$ for a signal arriving from direction $\theta_k$. The array response vector consists of the relative phases of the received signal at each of the antennas within the array. Using the array response vector, an amplification of the desired signals and the suppression of the undesirable signals occurs. This type of spatial filtering is called *beamforming*.

#### 2.2.2.1 Array Response Vector for a Uniform Linear Array

Suppose the distance between the desired mobile and the base station is large relative to the carrier wavelength, $\lambda$. Therefore, the incoming signals from that mobile can be treated as plane waves. When these signals from the $k$th mobile arrive at the base station antenna array, as in Figure 2.1 for example, and are incident upon it with angle $\theta_k$, each antenna receives the signal out-of-phase with respect to the other antennas. Thus, assuming the distance between adjacent antennas to be $\lambda/2$, the relative phase of a signal with angle-of-arrival $\theta_k$ being received by the $i$th element of

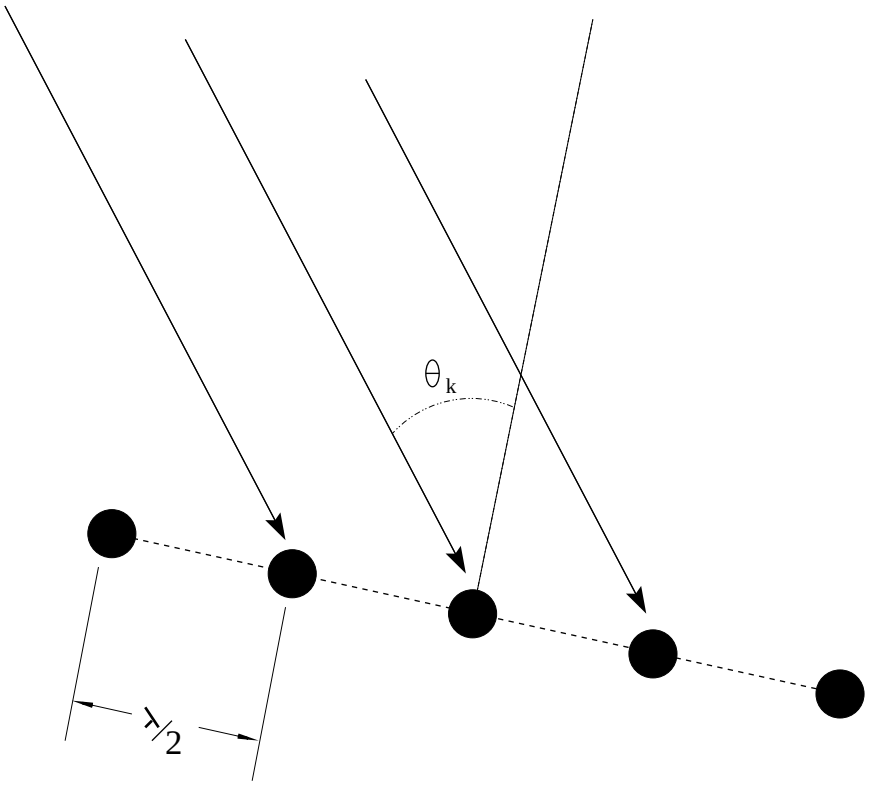


Figure 2.1: Linear array geometry

an $N_A$-element uniform linear array, where $1 \leq i \leq N_A$, is given as [90]

$$\bar{a}\left(\theta_k\right) = \begin{bmatrix} 1 \\ e^{j\pi\cos(\theta_k)} \\ e^{j2\pi\cos(\theta_k)} \\ \vdots \\ e^{j(N_A)\pi\cos(\theta_k)} \end{bmatrix} \tag{2.1}$$

where $\bar{a}$ is the array response vector. It should be noted that in this case, each element of $\bar{a}$ has unity magnitude for simplicity. As will be shown later, when the effects of mutual coupling and scatter are considered, no such simplification will be made.

#### 2.2.2.2 Array Response Vector for a Circular Array

Using the previously made assumptions concerning the distances between the antenna array and desired mobile as well as between the array elements, suppose the antennas are arranged in a circular geometry, as in Figure 2.2. Therefore, the relative phase of a signal with angle-of-arrival $\theta_k$ being received by the $i$th element of an $N_A$-element circular array, where $1 \leq i \leq N_A$, is given as [19]

$$\bar{a}\left(\theta_k\right) = \begin{bmatrix} 1 \\ e^{j\alpha_1(\theta_k)} \\ e^{j\alpha_2(\theta_k)} \\ \vdots \\ e^{j\alpha_{(N_A-1)}(\theta_k)} \end{bmatrix} \tag{2.2}$$

such that the phase delay for $i$th element of the array, $\alpha_i$, is

$$\alpha_i\left(\theta_k\right) = \frac{\pi \cos\left(\theta_k - i\frac{2\pi}{N_A}\right)}{2\sin\left(\frac{\pi}{N_A}\right)} \tag{2.3}$$

where $\bar{a}$ is the array response vector. Just as in the uniform linear array case, each element of $\bar{a}$ has unity magnitude for simplicity.

### 2.2.3 Beampattern Synthesis

Once the array response vector is obtained for a particular geometry, one is capable of creating the array beamforming pattern. This is accomplished by using

$$\phi_k\left(\theta_k, \theta_d\right) = \left|\bar{\omega}^{\mathbf{H}}\left(\theta_d\right)\bar{a}\left(\theta_k\right)\right|^2 \tag{2.4}$$

where $\bar{a}\left(\theta_k\right)$ is the array response vector for a mobile $k$ with direction of arrival $\theta_k$, $\bar{\omega}\left(\theta_d\right)$ is the beamforming weight vector for a desired mobile $d$ with direction of arrival

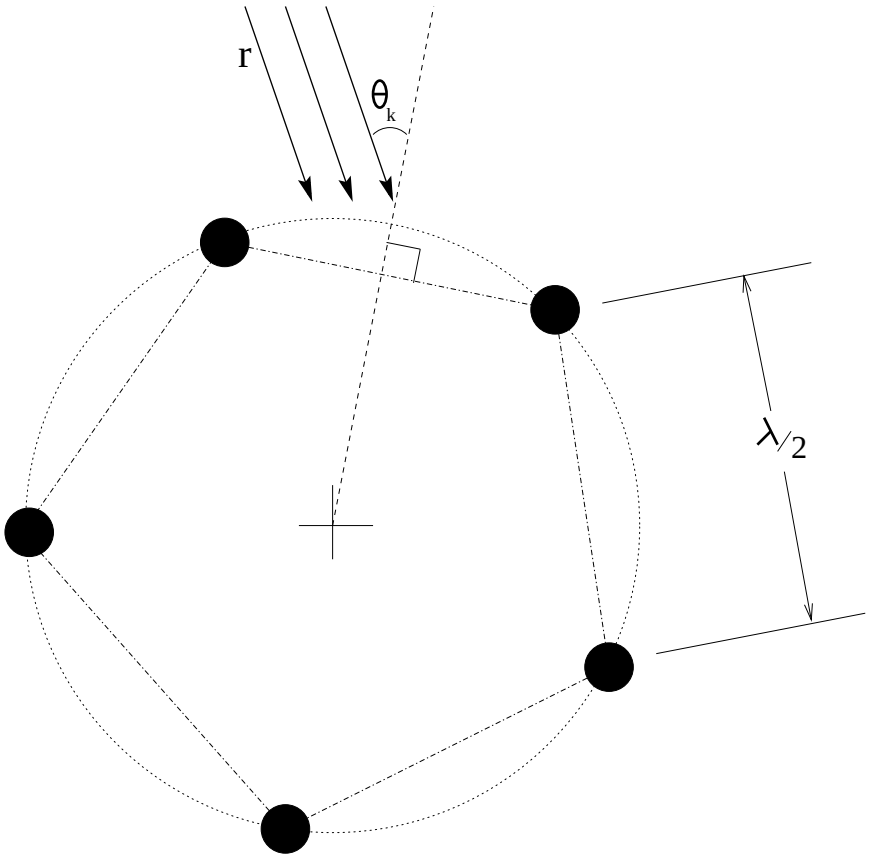


Figure 2.2: Circular array geometry

$\theta_d$, $\bar{\omega}^{\mathbf{H}}(\theta_d)$ is the conjugate transpose of $\bar{\omega}(\theta_d)$,and $\phi_k$ is the fraction of interferer $k$'s signal passed by the beamforming weights of the antenna array.

The result of Equation (2.4) is a beampattern which has a main lobe directed towards $\theta_d$. Thus, the signal of the desired mobile is easily passed through the beampattern while signals from the interfering mobiles located at other angles-of-arrival are suppressed.

As an example, suppose we are using maximum signal-to-noise ratio (SNR) beamforming weights. Therefore, the beamforming weight vector is identical to the array response vector. Using a 5-element circular array with adjacent array elements being

a half wavelength apart, $\bar{\omega}(\theta_d)$ is

$$\bar{\omega}(\theta_d) = \begin{bmatrix} 1 \\ e^{jw_1(\theta_d)} \\ e^{jw_2(\theta_d)} \\ \vdots \\ e^{jw_{(N_A-1)}(\theta_d)} \end{bmatrix} \tag{2.5}$$

where the phase delay for $i$th element of the array, $w_i(\theta_d)$, is

$$w_i(\theta_d) = \frac{\pi \cos\left(\theta_d - i\frac{2\pi}{N_A}\right)}{2\sin\left(\frac{\pi}{N_A}\right)} \tag{2.6}$$

and $N_A = 5$.

To create the beampattern, for each $\theta_k$ we vary $\theta_d$ from $-\pi$ to $\pi$ radians. Therefore, if the direction of arrival is $\pi/6$ radians for our circular array, Figure 2.3 results. Likewise, if the direction of arrival is 0 radians, Figure 2.4 results.

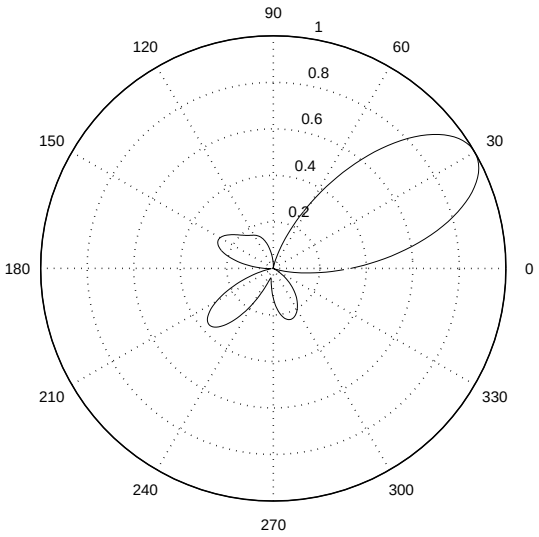


Figure 2.3: Beampattern of a 5-element circular array DOA of $30^o$

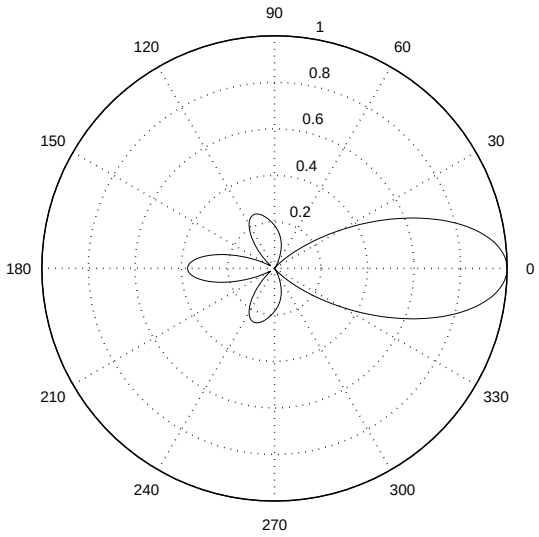


Figure 2.4: Beampattern of a 5-element circular array with DOA of $0^o$

## 2.3 System Capacity Predictions

In this section, the capacity of the CDMA system uplink is derived for both the single antenna element and multiple antenna element array cases. The approach used in these derivations are based upon the calculations found in [12] and [27].

### 2.3.1 Cellular CDMA Reverse Link

Although there exists several standards defining the complete implementation protocol of a CDMA communication system, such as [55], [87], and [70], we nevertheless investigate only the reverse link (mobile-to-base station) of such a communication system within the context of this thesis.

In our system setup, we assume that the base station employs a single $N_A$-element antenna array to receive and transmit signals from and to mobiles. Moreover, the mobiles in our system do not possess antenna arrays. To simplify the analysis within this thesis, a single cell system is considered and BPSK modulation is assumed.

Suppose we consider the signal component from a single mobile in a cell containing $N_M$ mobiles. We can express the digital baseband transmitted signal for the $i$th mobile, spread by pseudo-noise (PN) sequence $\tilde{c}_i(t)$, as

$$s_i(t) = WC(b_i(t))\,\tilde{c}_i(t) \quad , \quad i = 1, 2, 3..., N_M \tag{2.7}$$

where $WC(b_i(t))$ is the Walsh code corresponding to the data bit $b_i(t)$ for period $[t, t + T_b)$. The bit sequence transmitted by the mobile is defined as

$$b_i(t) = \sum_{k=-\infty}^{\infty} b_{i,k}\, p(t - kT_b) \tag{2.8}$$

where $b_{i,k}$ are assumed to be i.i.d. random variables, $T_b$ is the bit duration, and $p(t)$ is the pulse shape, which is constant over $T_b$ and assumed to be rectangular. Furthermore, we define the PN sequence for user $i$ as

$$\tilde{c}_i(t) \;=\; c_i^I(t) + jc_i^Q(t) \tag{2.9}$$

such that the in-phase (I) and quadrature (Q) components of $\tilde{c}_i(t)$ are

$$c_i^I(t) = \sum_{k=-\infty}^{\infty} c_{i,k}^I p(t - kT_c) \qquad\qquad c_i^Q(t) = \sum_{k=-\infty}^{\infty} c_{i,k}^Q p(t - kT_c)$$

where $c_{i,k}^I$ and $c_{i,k}^Q$ are assumed to be i.i.d. random variables taking values of $\pm 1$ with equal probability, $T_c$ is the bit duration, and $p(t)$ is the pulse shape, which is constant over $T_c$ and assumed to be rectangular.

Assuming that the channel parameters vary slowly relative to the bit duration $T_b$, such that they are constant over several bit durations, the complex baseband received signal vector from the $i$th user at the base station antenna array is

$$\mathbf{x}_i(t) \;=\; \sum_{l=1}^{L} s_i(t - \tau_{l,i})\, e^{j\phi_{l,i}} \mathbf{a}_{l,i} \tag{2.10}$$

where $\phi_{l,i} = \omega_c \tau_{l,i}$, $\omega_c$ is the carrier frequency in radians per second, $\tau_{l,i}$ is the integer chip time delay for multipath component $l$ of user $i$, $L$, is the number of multipath components, and $\mathbf{a}_{l,i}$ is the array response vector for the $i$th user and $l$th multipath component.

Thus, using Equation (2.10), the total received signal at the base station is the sum of all the users' signals plus noise is

$$\mathbf{x}(t) \;=\; \sum_{i=1}^{N_M} \sum_{l=1}^{L} \mathbf{x}_{l,i}(t) + \mathbf{n}(t) \tag{2.11}$$

where $N_M$ is the total number of mobiles within the cell, and $\mathbf{n}(t)$ represents additive white Gaussian noise.

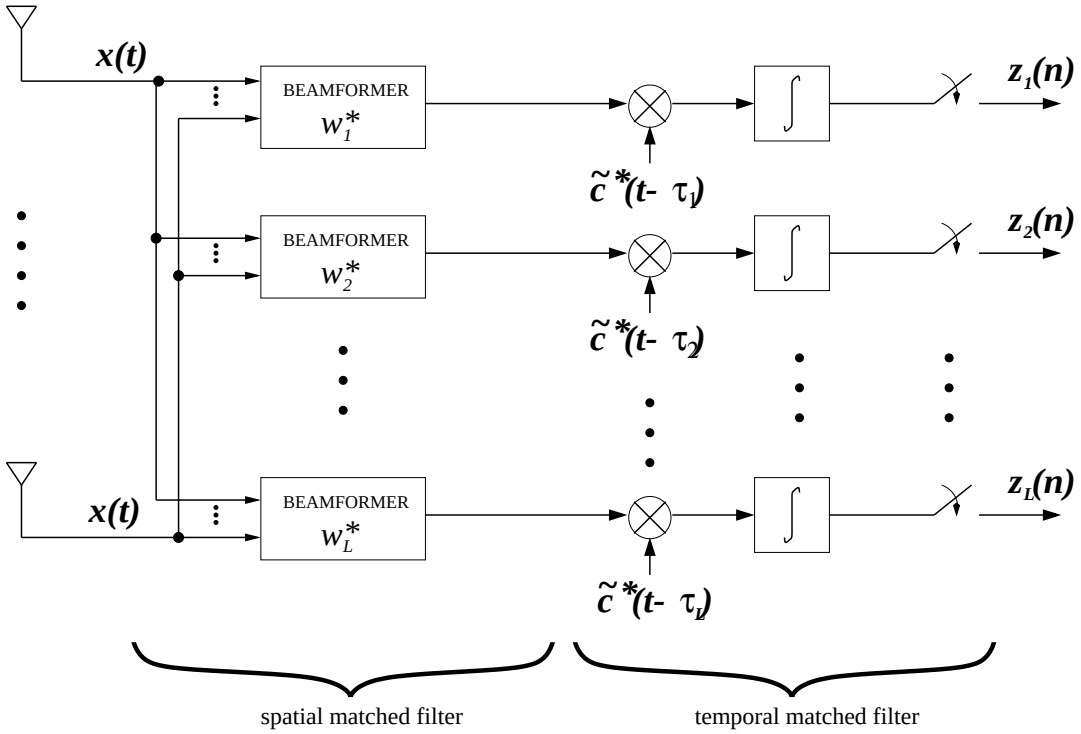


Figure 2.5: Space-time matched filter [56]

At the receiver end of the system, as shown in Figure 2.5, the first process that the received signal encounters is a parallel multi-beamformer, a form of spatial matched filtering used to reduce the interference from other mobiles by taking the weighted sum of the antenna array outputs, thus maximizing the ratio of the desired mobile's signal power to the noise and interference power.

The weighted sum is performed by using the elements of a complex baseband beamforming weight vector that is assigned to each mobile. Assuming there exists $L$ multipath components of mobile $i$'s signal, the receiver in Figure 2.5 possesses a bank of $L$ beamformers, each with beamforming weight vector $\mathbf{w}_l$, corresponding to the $l$th multipath component of the $i$th mobile's signal.

After beamforming has been performed, we enter the temporal matched filtering

process of the receiver, consisting of a bank of $L$ correlators. In this process, the $l$th matched filter is matched to the code waveform in the $l$th path by $\tilde{c}^*(t-\tau_l)$, such that we obtain the $l$th sufficient statistic

$$z_l(n) = \int_{(n-1)T_b+\tau_l}^{nT_b+\tau_l} \tilde{c}^*(t-\tau_l)\,\mathbf{w}_l^*\mathbf{x}(t)\,dt \quad , \quad l = 1,2,3,...,L \tag{2.12}$$

In the following section as well as the remainder of this thesis, the emphasis of the analysis will be focused on the use of digital beamforming for purpose of increasing the system cellular capacity.

### 2.3.2 Single Antenna Element Power and Capacity Calculations

The system in this derivation uses perfect power control in a single-cell environment where the base station antenna array consists of only one antenna. Power control is used to establish a state of equilibrium in CDMA systems with respect to transmission power levels of each mobile since these systems are strictly interference limited. This topic is further discussed in Chapter 5

Assuming there are $N_M$ mobiles in the CDMA uplink, where each mobile has received signal power $P_R$, the total received interference power, $P_I$, is

$$P_I = N_I P_R \tag{2.13}$$

where $N_I = N_M - 1$ is the number of interfering mobiles, and the voice activity factor $\alpha$ is assumed to be unity.

Therefore, the signal-to-noise ratio is given as

$$SNR = \frac{P_R}{P_I + \eta} \tag{2.14}$$

where $\eta$ is the background noise due to spurious interference and thermal noise within the bandwidth of the spread signal.

Using Equation (2.14), the bit energy-to-noise density ratio can be obtained by dividing the desired signal power by the data bit rate, $R_B$, and dividing the noise and interference power by the bandwidth of the spread signal, $B$. Therefore, the bit energy-to-noise density ratio is

$$\frac{E_b}{N_o} = \frac{P_R/R_B}{P_I/B + \sigma_n^2} \tag{2.15}$$

where $\sigma_n^2$ is the variance of the background noise. It should be noted that Equation (2.15) agrees with Equation (2) in [27] and Equation (4.4) in [12].

Therefore, using Equation (2.13), we solve for $P_R$ in Equation (2.15), yielding

$$P_R = \left(\frac{E_b}{N_o}\right)\sigma_n^2 \left\{\frac{1}{R_B} - \frac{N_I}{B}\left(\frac{E_b}{N_o}\right)\right\}^{-1} \tag{2.16}$$

which is used to predict the signal power and interference power for one array element given a target signal-to-noise ratio.

To calculate the maximum number of mobiles which the system can support, we start by isolating $N_I$ in Equation (2.16), yielding

$$\begin{aligned}
\frac{P_R}{\left(\frac{E_b}{N_o}\right)\sigma_n^2} &= \frac{1}{\frac{1}{R_B} - \frac{N_I}{B}\left(\frac{E_b}{N_o}\right)} \\
\frac{\left(\frac{E_b}{N_o}\right)\sigma_n^2}{P_R} &= \frac{1}{R_B} - \frac{N_I}{B}\left(\frac{E_b}{N_o}\right) \\
\frac{1}{R_B} - \frac{\left(\frac{E_b}{N_o}\right)\sigma_n^2}{P_R} &= \frac{N_I}{B}\left(\frac{E_b}{N_o}\right) \\
N_I &= \left\lfloor \frac{B}{R_B\left(\frac{E_b}{N_o}\right)} - \frac{B\sigma_n^2}{P_R} \right\rfloor
\end{aligned} \tag{2.17}$$

where $\lfloor . \rfloor$ is the floor function.

Since the total number of mobiles is equal to the number of interfering mobiles plus the desired mobile, using Equation (2.17), the system cell capacity is

$$N_M = N_I + 1 = \left\lfloor \frac{B}{R_B\left(\frac{E_b}{N_o}\right)} - \frac{B\sigma_n^2}{P_R} \right\rfloor + 1 \tag{2.18}$$

where $N_M$ is the total number of mobiles within the cell.

Assuming that $E_b/N_o = 7$dB, $R_B = 9600$bits/second, and $B = 1.2288$MHz, as well as $\sigma_n^2 = (4.5 \times 10^{-11})^2$ [69], Equation (2.18) can be approximated by

$$N_M \approx \left\lfloor \frac{B}{R_B\left(E_b/N_o\right)} \right\rfloor + 1 \tag{2.19}$$

since the minimum signal level is constrained by the receiver sensitivity. According to [88], the receiver sensitivity was measured to be $-92$dBm. Therefore, letting $P_R = -92$dBm, we see that

$$\frac{B}{R_B\left(\frac{E_b}{N_o}\right)} = 25.5393 \quad \gg \quad \frac{B\sigma_n^2}{P_R} = 3.9437 \times 10^{-3}$$

thus justifying the approximation of Equation (2.18).

### 2.3.3 Multiple Antenna Element Array Power Calculations

Following a methodology similar to the one used to determine the predicted power values for the single antenna element case, an expression for $P_R$, and ultimately $N_M$, is determined for the multiple antenna element array case. In this case, the suppression of signals arriving from certain directions due to beamforming, as well as the effects of mutual coupling, are considered in the following derivations.

In the multiple antenna element case, the expression for the bit energy-to-noise density ratio from Equation (2.15) becomes

$$\frac{E_b}{N_o} = \frac{P_R/R_B}{P_I/B + N_A\sigma_n^2} \tag{2.20}$$

where $N_A$ is the number of array elements and $P_R$ is the total received signal power at the array due to the desired mobile. The factor $N_A$ in Equation (2.20) is due to the fact that the additive noise is assumed to be statistically independent at each array element.

Therefore, the interference contribution by mobile $k$ is given by

$$P_{I_k} = \phi_k P_R \tag{2.21}$$

where

$$\sum_{k=1}^{N_I} P_{I_k} = P_I \tag{2.22}$$

and $\phi_k$ is the fraction of interferer $k$'s signal power passed by the beamforming weights.

Thus, the expected value of the total interference power is given as

$$\begin{aligned} E\{P_I\} &= E\left\{\sum_{k=1}^{N_I} P_{I_k}\right\} \\ &= E\left\{\sum_{k=1}^{N_I} \phi_k P_R\right\} \\ &= E\left\{P_R \sum_{k=1}^{N_I} \phi_k\right\} \\ &= P_R \sum_{k=1}^{N_I} E\{\phi_k\} \\ &= P_R N_I E\{\phi_k\} \end{aligned} \tag{2.23}$$

which is then substituted into Equation (2.20) to solve for the received predicted power level $E\{P_R\}$, namely

$$E\{P_R\} = \left(\frac{E_b}{N_o}\right) N_A \sigma_n^2 \left\{\frac{1}{R_B} - \frac{E\{\phi_k\} N_I}{B}\left(\frac{E_b}{N_o}\right)\right\}^{-1} \tag{2.24}$$

where $E\{\phi_k\}$ is the expected fraction of interferer $k$'s signal power, which we shall determine in the next subsection.

### 2.3.4 Derivation of $E\{\phi_k\}$

In this derivation, we will consider a circular array without loss of generality. The maximum SNR beamforming weights for a desired user $d$ at an angle $\theta_d$ relative to the circular antenna array is given as

$$\bar{\omega}(\theta_d) = \begin{bmatrix} e^{jw_0(\theta_d)} \\ e^{jw_1(\theta_d)} \\ e^{jw_2(\theta_d)} \\ \vdots \\ e^{jw_{(N_A-1)}(\theta_d)} \end{bmatrix} \tag{2.25}$$

where the phase delay for $i$th element of the array, $w_i(\theta_d)$, is

$$w_i(\theta_d) = \frac{\pi \cos\left(\theta_d - i\frac{2\pi}{N_A}\right)}{2\sin\left(\frac{\pi}{N_A}\right)} \tag{2.26}$$

It should be noted that these beamforming weights can be reconfigured to other array geometries as well.

Therefore, the amount of interference power seen from an interferer $k$ at an angle-of-arrival $\theta_k$ is

$$\phi_k(\theta_d, \theta_k) = \left|\bar{\omega}^{\mathbf{H}}(\theta_d)\bar{a}(\theta_k)\right|^2 \tag{2.27}$$

where $\bar{\omega}^{\mathbf{H}}(\theta_d)$ denotes the complex conjugate transpose of $\bar{\omega}(\theta_d)$ and $\bar{a}(\theta_k)$ is an array response vector for an $N_A$-element array, as described in Section 2.2.2.

Assuming both $\theta_k$ and $\theta_d$ are random variables uniformly distributed over $[0, 2\pi)$, the expected value of $\phi_k$ can be determined by substituting Equation (2.2) and Equation (2.25) into Equation (2.27), for the case of a circular array, and average over $\theta_k$ and $\theta_d$, yielding [12]

$$E\{\phi_k(\theta_d, \theta_k)\} = \frac{1}{4\pi^2 N_A}\int_0^{2\pi}\int_0^{2\pi}\left|e^{j\left(\frac{\pi\cos(\theta_d - q2\pi/N_A)}{2\sin(\pi/N_A)} - \frac{\pi\cos(\theta_k - q2\pi/N_A)}{2\sin(\pi/N_A)}\right)}\right|^2 d\theta_d d\theta_k \tag{2.28}$$

The results of Equation (2.28) for a circular array, where the number of array elements ranges from $N_A = 1$ to 6 antennas, are shown in Table 2.1. Note that the effects of mutual coupling are not included in Equation (2.28) and will be discussed later in Chapter 3.

#### 2.3.4.1 Results

From Table 2.1, we observe that as the number of antennas increases, the expected values of $\phi_k$, $E\{\phi_k\}$, decrease. Thus, there is an inverse relationship between the number of antennas and $E\{\phi_k\}$. These results, which were determined numerically using Matlab, are the same as the results found in [12].

| $N_A$ | 1 | 2 | 3 | 4 | 5 | 6 |
|---|---|---|---|---|---|---|
| $E\{\phi_k\}$ | 1.0000 | 0.5463 | 0.3950 | 0.3241 | 0.2460 | 0.2058 |

Table 2.1: Expected values of $\phi_k$

Using the derived expressions for $E\{\phi_k\}$ as well as the tabulated values in Table 2.1, one is now capable of predicting the capacity of a CDMA system using base station antenna arrays, as we will see in the next section.

### 2.3.5 Multiple Antenna Element Array Capacity Calculations

Using the same technique as in the single antenna element case, the system capacity can be determined by isolating the total number of mobiles within the cell,

$N_M$, in Equation (2.24), thus yielding

$$\begin{aligned}
\frac{E\{P_R\}}{\left(\frac{E_b}{N_o}\right) N_A \sigma_n^2} &= \frac{1}{\frac{1}{R_B} - \frac{E\{\phi_k\} N_I}{B}\left(\frac{E_b}{N_o}\right)} \\
\frac{\left(\frac{E_b}{N_o}\right) N_A \sigma_n^2}{E\{P_R\}} &= \frac{1}{R_B} - \frac{E\{\phi_k\} N_I}{B}\left(\frac{E_b}{N_o}\right) \\
\frac{1}{R_B} - \frac{\left(\frac{E_b}{N_o}\right) N_A \sigma_n^2}{E\{P_R\}} &= \frac{E\{\phi_k\} N_I}{B}\left(\frac{E_b}{N_o}\right) \\
N_I &= \left\lfloor \frac{B}{E\{\phi_k\}} \left( \frac{1}{\left(\frac{E_b}{N_o}\right) R_B} - \frac{N_A \sigma_n^2}{E\{P_R\}} \right) \right\rfloor
\end{aligned} \tag{2.29}$$

where $\lfloor . \rfloor$ is the floor function.

Since the total number of mobiles is equal to the number of interfering mobiles plus the desired mobile, using Equation (2.29), the system cell capacity is

$$N_M = N_I + 1 = \left\lfloor \frac{B}{E\{\phi_k\}} \left( \frac{1}{\left(\frac{E_b}{N_o}\right) R_B} - \frac{N_A \sigma_n^2}{E\{P_R\}} \right) \right\rfloor + 1 \tag{2.30}$$

Letting $E_b/N_o = 7$dB, $R_B = 9600$bits/second, $B = 1.2288$MHz, $\sigma_n^2 = (4.5 \times 10^{-11})^2$ [69], and $P_R = -92$dBm [88], Equation (2.30) can be approximated by

$$N_M \approx \left\lfloor \frac{B}{E\{\phi_k\}} \left( \frac{1}{\left(\frac{E_b}{N_o}\right) R_B} \right) \right\rfloor + 1 \tag{2.31}$$

since

$$\frac{B}{R_B \left(\frac{E_b}{N_o}\right)} = 25.5393 \gg N_A \frac{B \sigma_n^2}{P_R} = N_A \left(3.9437 \times 10^{-3}\right)$$

where in this study $1 \leq N_A \leq 6$.

Using Equation (2.31), the predicted capacity for CDMA systems employing base station antenna arrays with circular geometries, where adjacent array elements are a half-wavelength apart and the number of array elements range from one to six, are given in Table 2.2. Note that the effects of mutual coupling are not included in Equation (2.31) and will be discussed later in Chapter 3.

Inspecting these values, it can be seen that as the number of antennas increases, the number of mobiles which the system can support also increases for all three cases. Furthermore, when compared against the results in [12], they match.

| $N_A$ | 1 | 2 | 3 | 4 | 5 | 6 |
|---|---|---|---|---|---|---|
| Capacity | 26 | 47 | 65 | 79 | 104 | 125 |

Table 2.2: Predicted capacity values using perfect power control and correlation of 1.0 between array elements

## 2.4 Chapter Summary

In this chapter, the rationale and concepts of digital beamforming were presented. In particular, we focused on the array response vectors and their significance in beamforming. Furthermore, we looked at two types of array response vectors associated with different array geometries: the circular array, and the uniform linear array. We also looked at beampattern synthesis, using an example of maximum SNR beamforming weights, and plotted the beampatterns for two different direction of arrivals.

In the second half of the chapter, we examined a simple derivation of system capacity. Furthermore, the resulting analysis was applied to a system where the array possessed a circular geometry and consisted of $N_A$ array elements, where $1 \leq N_A \leq 6$. The results show that an increase in the number of array elements will cause an increase in the number of mobiles that can be supported by the system.

# Chapter 3

# Effects of Mutual Coupling on System Performance

## 3.1 Introduction

Extensive research has been carried out worldwide to investigate the performance of CDMA systems which employ digital beamforming and base station antenna arrays by using a variety of models. Unfortunately, many of these models neglect the effects of mutual coupling, an electromagnetic phenomenon which affects closely-spaced antenna arrays. This potentially leads to less accurate system performance predictions. In this chapter, two analytical methods, the Induced EMF Method [7] [10] [37] [38] [50] and the Method of Moments [2] [30] [81], as well as a full-wave electromagnetic numerical computation, are used to include the effects of mutual coupling in our system models. The implementation of these methods in our beampattern synthesis models and system capacity predictions is described in detail.

### 3.1.1 Chapter Outline

The first section of this chapter deals with the effects of mutual coupling in antenna arrays. We commence with a brief qualitative explanation of mutual coupling effects and how these effects behave within the confines of a closely-spaced antenna array. Two examples of mutual coupling, namely transmission-mode and reception-mode coupling, are presented.

The next section deals with the methods used to include the effects of mutual coupling in our beampattern synthesis models and system capacity predictions. The Induced EMF Method is the first method examined, followed by the Method of Moments, and finally the full-wave electromagnetic numerical computation. In all three cases, the basic formulation of the method is described which is then followed by its application to our system models. The impact of our improved beampattern synthesis models on system performance is presented.

Finally, system capacity prediction is the last topic in this chapter. The analysis commences with the case of a single antenna element in a CDMA system. This is then followed by and extended to the more complicated case of a multiple antenna element array by utilizing the beampattern models developed in the second section of this chapter. In particular, the beampatterns are used to determine the power levels that are influenced by interfering mobiles. The results of our system capacity predictions where mutual coupling effects are considered is presented.

## 3.2 Mutual Coupling Effects

### 3.2.1 Introduction

When two antennas are in close proximity, whether one and/or both are transmitting or receiving, some of the energy that is primarily intended for one ends up at the other. According to [7], the amount of energy transferred between antennas mainly depends on:

- radiation characteristics of each antenna
- relative separation between the pair of antennas
- relative orientation of each antenna

This energy transfer is known as *mutual coupling*. Various phenomena exist which may cause this transfer of energy, such as when both antennas are transmitting or when they are both receiving.

In order to understand transmission mode coupling, let us refer to Figure 3.1. As our system is transmitting, (a) energy is travelling through antenna $n$, where (b) it is radiated into space, and (c) towards antenna $m$. Upon being received by antenna $m$, the energy is rescattered either (d) into space, or (f) back to antenna $n$, while the remaining energy (e) travels to the generator of antenna $m$. It should be noted that when both antennas are excited simultaneously, vector addition is required to perform the analysis.

Similarly, following Figure 3.2 closely, we see that (a) a phase wave front is incident upon the array which excites antenna $n$ first. At antenna $n$, (c) some of the energy will be rescattered into space, (d) some of the energy will be reflected to antenna $m$

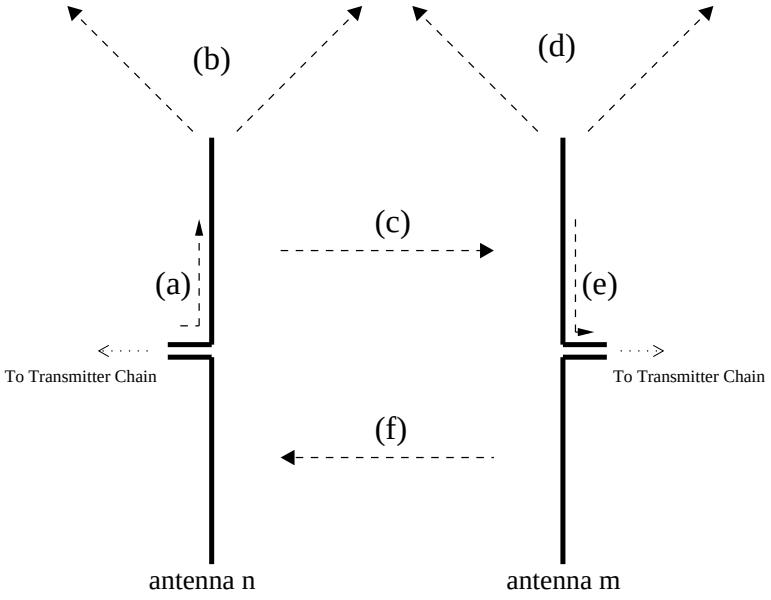


Figure 3.1: Transmission mode coupling

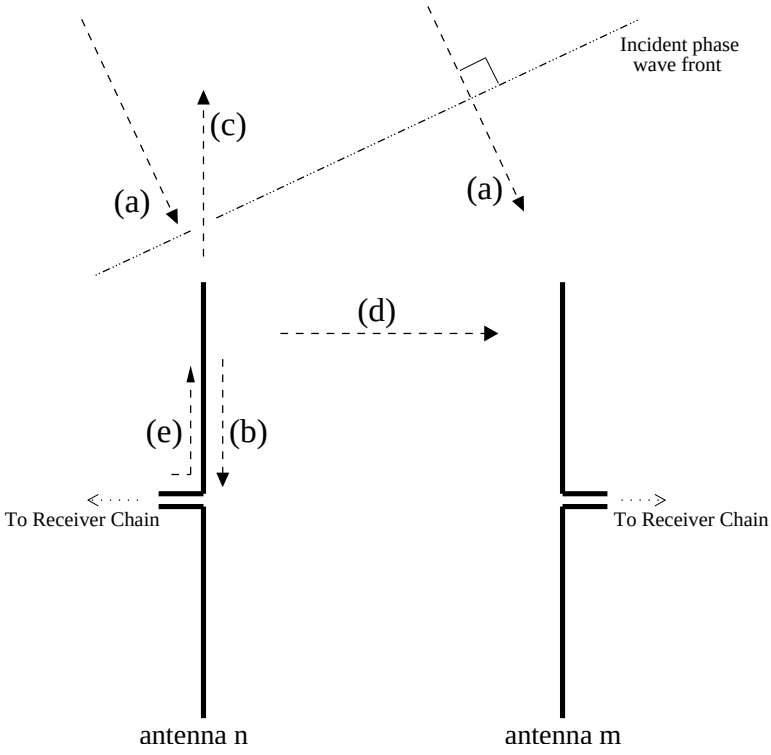


Figure 3.2: Reception mode coupling

where it will be added vectorially with (a) to obtain the net received energy, and (b) the rest will travel towards the receiver chain. Some of this energy in (b) will be (e) reflected back due to impedance mismatch.

Although the inclusion of mutual coupling effects will complicate our analysis of CDMA systems using antenna arrays, it is necessary to include them due to the significant potential impact on the performance of the systems being studied.

## 3.3 Beampattern Synthesis Models

### 3.3.1 Mutual Impedance Data Generation Methods

The methods used in this chapter to include mutual coupling effects in our beampattern synthesis models of CDMA systems utilizing base station antenna arrays all follow a similar formulation. The methods covered, namely, the *induced EMF method*, the *Method of Moments*, and a *finite-element numerical computation method*, are all based upon representing an $N_A$ element array as a $N$ port network, as shown in Figure 3.3. In this figure and in our study, all the array elements are of equal length and the increments are equally distributed over all of them, although these methods are applicable to non-uniform length array elements as well. Furthermore, the IE3D software package used in the finite-element numerical computation method subdivides the array into a mesh of two-dimensional increments rather than a collection of one-dimensional increments, as in the Induced EMF Method and Method of Moments, but the use of a mesh does not change the network representation of the array.

The goal of representing the array as a network of $N$-ports is to exploit the circuit parameters associated with such a representation, namely, the driving-point impedances looking into each port. These impedances can be organized into a mutual

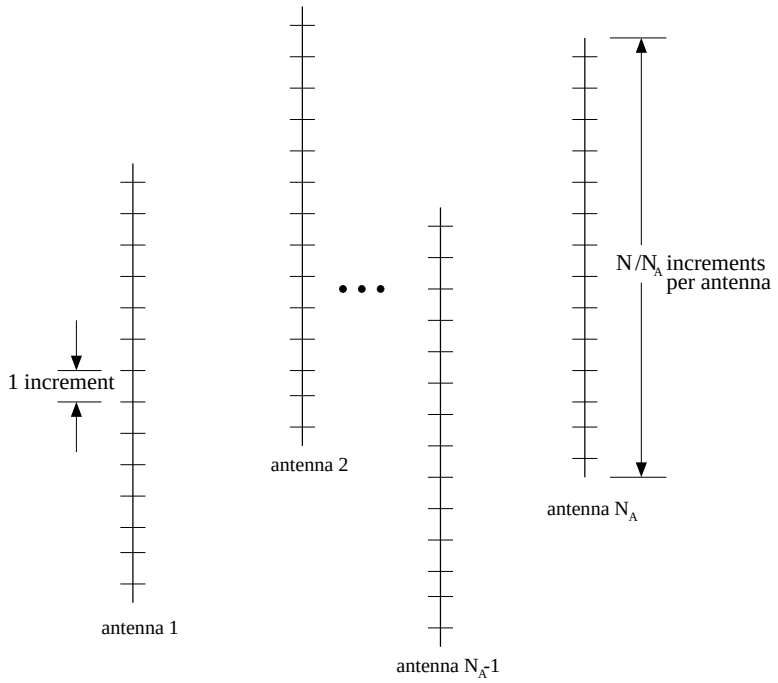


Figure 3.3: Equivalent representation of an $N_A$ element array as a $N$-port network

impedance matrix, $[Z]$, which contains information of the mutual coupling effects in the array. The matrix $[Z]$ can be applied to a beampattern synthesis formulation or a capacity prediction using the matrix equation

$$[Z]\overrightarrow{I} = \overrightarrow{V} \tag{3.1}$$

where $\overrightarrow{V}$ and $\overrightarrow{I}$ are vectors of the voltage and current distributions, respectively, over the array elements of length $N$.

Therefore, the main difference between the methods of the following three subsections is the way they obtain the mutual impedance matrix $[Z]$. Each of the techniques used to obtain these matrices will be described in detail as well as their implementation in a beampattern synthesis model.

#### 3.3.1.1 Induced EMF Method

The induced EMF (electromagnetic fields) method, described in [7] [10] [37] [38] [50], is a classical method to compute the self and mutual impedances of a collection of two-port networks, such as antenna arrays. Thus, we are able to obtain an $N_A \times N_A$ mutual impedance matrix $[Z]$ and employ it to perform beampattern synthesis. Although the method is restricted to straight and parallel elements in formation as well as possessing difficulties in accurately accounting for wire radii and feed gaps, its advantage is that it can lead to closed-form solutions. Although [7] [10] [37] [38] [50] all approach the induced EMF method in a similar fashion, King's approach [37] was adopted to our analysis.

Referring to Figure 3.4, we have two center-fed dipole antennas, antenna 1 and antenna 2, both with half-lengths $l_1$ and $l_2$ separated by a distance $d$ and staggered in elevation by $h$. The mutual impedance between the two antennas is given by

$$Z_{21} = -\frac{V_{21}}{I_{1b}} \tag{3.2}$$

where $V_{21}$ is the open-circuit voltage at the terminals of antenna 2, due to a base current $I_{1b}$ in antenna 1. We can determine $V_{21}$ by applying the reciprocity theorem [36] to obtain

$$V_{21} = \frac{1}{I_{2b}} \left( \int_{h}^{l_2+h} E_{z1} I_2(z) dz + \int_{l_2+h}^{2l_2+h} E_{z1} I_2(z) dz \right) \tag{3.3}$$

where $I_{2b}$ is the base current of antenna 2 and $E_{z1}$ is the component of electric intensity parallel to the axis of the antenna at a point $z$ along antenna 2 due to the current in antenna 1. Assuming the current distribution of antenna 2, namely $I_2$, is sinusoidal, we get

$$I_2(z) \;=\; \begin{cases} I_{2m} \sin \beta(z-h) & , \quad h < z < l_2 + h \\ I_2(z) = I_{2m} \sin \beta(2l_2 + h - z) & , \quad h + l_2 < z < 2l_2 + h \end{cases} \tag{3.4}$$

where $I_{2m}$ is the value of the current at the current loop or current maximum and $\beta = 2\pi/\lambda$ is the wave number. Furthermore, the expression for the parallel component of the electric field is given as [37]

$$E_{z1} = 30I_{1m}\left[\frac{-j\exp^{-j\beta r_1}}{r_1} + \frac{-j\exp^{-j\beta r_2}}{r_2} + \frac{2j\cos\beta l_1\exp^{-j\beta r_0}}{r_0}\right] \tag{3.5}$$

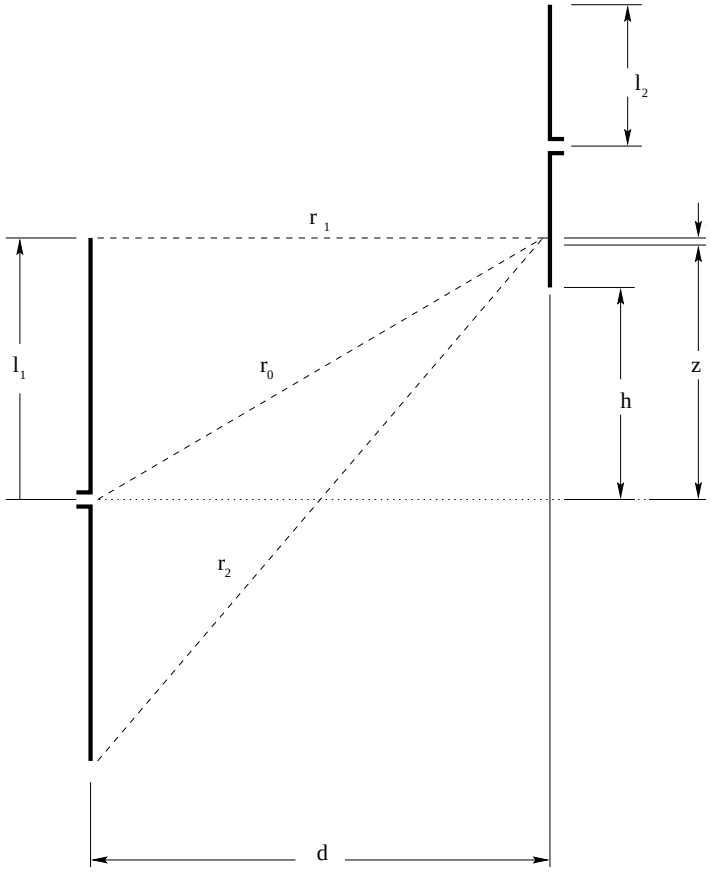


Figure 3.4: Two parallel antennas of arbitrary length in-echelon [37]

Thus, the mutual impedance related to the loop currents is given by

$$Z_{12loop} = \frac{I_{1b}I_{2b}}{I_{1m}I_{2m}}Z_{12base} \tag{3.6}$$

Using these equations, we obtain

$$Z_{12} = -30\int_{h}^{l_2+h}\sin\beta(z-h)$$

$$\cdot\left(\frac{-j\exp^{-j\beta r_1}}{r_1}+\frac{-j\exp^{-j\beta r_2}}{r_2}+\frac{2j\cos\beta l_1\exp^{-j\beta r_0}}{r_0}\right)dz$$
$$-30\int_{l_2+h}^{2l_2+h}\sin\beta(2l_2+h-z)$$
$$\cdot\left(\frac{-j\exp^{-j\beta r_1}}{r_1}+\frac{-j\exp^{-j\beta r_2}}{r_2}+\frac{2j\cos\beta l_1\exp^{-j\beta r_0}}{r_0}\right)dz \tag{3.7}$$

Observing the geometry in Figure 3.4, we see that

$$r_0=\sqrt{d^2+z^2} \tag{3.8}$$
$$r_1=\sqrt{d^2+(l_1-z)^2} \tag{3.9}$$
$$r_2=\sqrt{d^2+(l_1+z)^2} \tag{3.10}$$

Thus, using Equations (3.7), (3.8), (3.9), and (3.10), as well as using dipole array elements of equal length in a non-staggered arrangement, we obtain the following expressions for components $Z_{mn}$ of the $N_A\times N_A$ mutual impedance matrix $[Z]$

$$Z_{mn}=\begin{cases}30\left(0.5772+\ln(2\beta l)-Ci(2\beta l)\right) & \\ \qquad +j30\left(Si(2\beta l)\right) & ,m=n\\ \\ R_{mn}+jX_{mn} & ,m\neq n\end{cases} \tag{3.11}$$

where

$$R_{mn}=30\cos(2\beta l)(Ci(u_0)+Ci(v_0)-2Ci(u_1)-2Ci(v_1)$$
$$+2Ci(\beta d))+30\sin(2\beta l)(-Si(u_0)+Si(v_0)+2Si(u_1)$$
$$-2Si(v_1))+30(-2Ci(u_1)-2Ci(v_1)+4Ci(\beta d))$$

$$X_{mn}=30\cos(2\beta l)(-Si(u_0)-Si(v_0)+2Si(u_1)+2Si(v_1)$$
$$-2Si(\beta d))+30\sin(2\beta l)(-Ci(u_0)+Ci(v_0)+2Ci(u_1)$$
$$-2Ci(v_1))+30(2Si(u_1)+2Si(v_1)-4Si(\beta d))$$

$$u_0 = \beta(\sqrt{d^2 + 4l^2} - 2l) \qquad v_0 = \beta(\sqrt{d^2 + 4l^2} + 2l)$$
$$u_1 = \beta(\sqrt{d^2 + l^2} - l) \qquad v_1 = \beta(\sqrt{d^2 + l^2} + l)$$
$$Ci(u) = \int_{\infty}^{u} \frac{\cos(x)}{x} dx \qquad Si(u) = \int_{0}^{u} \frac{\sin(x)}{x} dx$$

and $d$ is the horizontal distance between two dipole antennas, $l = l_1 = l_2$ is the half-length of the dipole antennas, $Ci(.)$ and $Si(.)$ are the cosine and sine integral equations, respectively, and $1 \leq m, n \leq N_A$.

After creating the mutual impedance matrix $[Z]$, we must augment Equation (3.1) and solve the matrix equation

$$[Z]^{-1}\overrightarrow{V} = \overrightarrow{I} \tag{3.12}$$

where $[Z]^{-1}$ is the inverse matrix of $[Z]$. Using the maximum SNR beamforming weight vector described in Subsection 2.2.3, we can define the elements of the voltage distribution vector, $\overrightarrow{V}$. Therefore, we can determine the current for each antenna using Equation (3.12) and perform beampattern synthesis for a circular array using [50]

$$A(\theta) = \left| \sum_{m=1}^{N_A} I_m e^{j\left(\frac{\pi \cos(\theta - m(2\pi/N_A))}{2\sin(\pi/N_A)}\right)} \right|^2 \tag{3.13}$$

where $I_m$ is an element of $\overrightarrow{I}$, $\theta$ is the angle-of-arrival, and $1 \leq m \leq N_A$.

#### 3.3.1.2 Method of Moments

The Method of Moments is another technique for obtaining the mutual impedance matrix $[Z]$. For this method, we referred to [2] [30] [81] for a detailed overview and analysis. In particular, we used [30] as the basis for the following work concerning the method of moments.

From basic electromagnetics, we have the following equations [34] [72] [71]

$$\overrightarrow{E} = j\omega\overrightarrow{A} + \overrightarrow{\nabla}\Phi \tag{3.14}$$

$$\overrightarrow{A} = \mu \int \int_S \overrightarrow{J} \frac{\exp^{-j\beta R}}{4\pi R} ds \tag{3.15}$$

$$\Phi = \frac{1}{\varepsilon} \int \int_S \sigma \frac{\exp^{-j\beta R}}{4\pi R} ds \tag{3.16}$$

$$\sigma = \frac{-1}{j\omega} \overrightarrow{\nabla} \cdot \overrightarrow{J} \tag{3.17}$$

$$\overrightarrow{n} \times \overrightarrow{E}_{scatter} = -\overrightarrow{n} \times \overrightarrow{E} \tag{3.18}$$

where $\beta = 2\pi/\lambda$ is the wavenumber, $\sigma$ is the surface charge density on a conducting surface $S$, $\overrightarrow{J}$ is the current vector on a conducting surface $S$, $\mu$ is the permeability of the dielectric, $\epsilon$ is the permittivity of the dielectric, $\overrightarrow{A}$ is the magnetic vector potential, $\Phi$ is the magnetic scalar potential, $\overrightarrow{n}$ is the outward direction normal to the conducting surface $S$, $\overrightarrow{\nabla}$ is the gradient operator, $\omega$ is the angular frequency of operation, $R$ is the distance from a source point to a field point, and $\overrightarrow{E}$ is the impressed field vector. Applying these equations to a thin wire structure, where the current flows in one direction and the current and charge densities are approximated by filaments of current and charge on the wire axis, we obtain

$$E_l = j\omega A_l + \frac{\partial \Phi}{\partial l} \tag{3.19}$$

$$\overrightarrow{A} = \mu \int_{axis} \overrightarrow{I}_{filament}(l) \frac{\exp^{-j\beta R}}{4\pi R} dl \tag{3.20}$$

$$\Phi = \frac{1}{\varepsilon} \int_{axis} \sigma_{filament}(l) \frac{\exp^{-j\beta R}}{4\pi R} dl \tag{3.21}$$

$$\sigma_{filament} = \frac{-1}{j\omega} \frac{dI_{filament}}{dl} \tag{3.22}$$

where $l$ is the length variable along the wire axis, $\overrightarrow{I}_{filament}$ is the current vector of the filament, and $\sigma_{filament}$ is the charge of the filament.

A convenient way to obtain a simple solution to Equations (3.19), (3.20), (3.21), and (3.22) is by using matrices. For instance, we can approximate the above integrals by the sum of integrals over $N$ small increments by treating $I_{filament}$ and $q_{filament}$ as

constants over each increment. Moreover, derivatives can be approximated by finite differences over the same increments.

Therefore, referring to Figure 3.5, we see that the $n$th segment is identified by its starting position, $n^-$, its midpoint, $n$, and finally its endpoint, $n^+$. Furthermore, we define the increment $\Delta l_n$ as the distance between $n^-$ and $n^+$ while $\Delta l_n^-$ and $\Delta l_n^+$ are increments shifted one-half increments minus or plus along $l$.

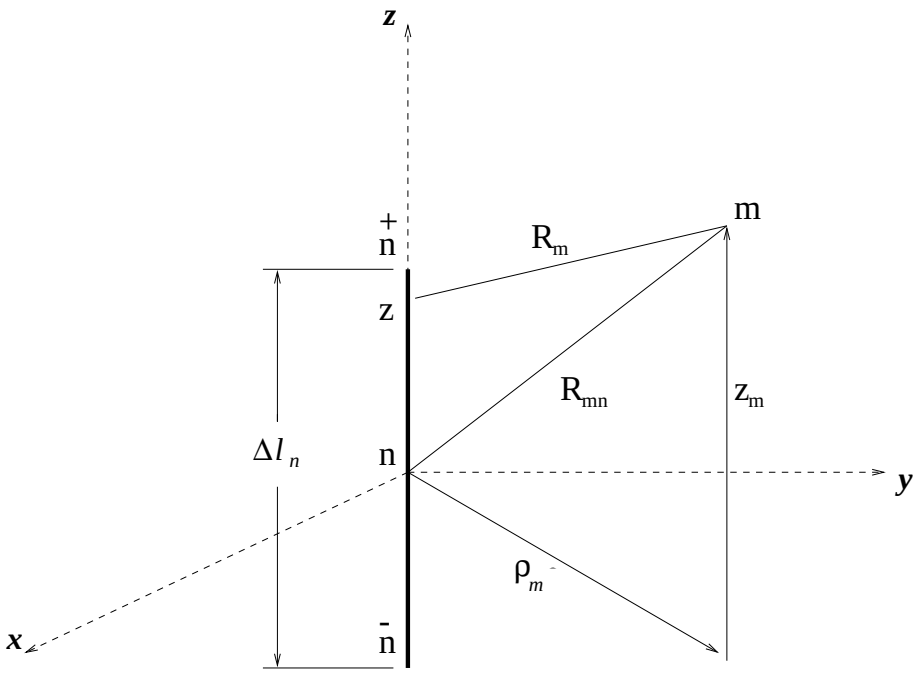


Figure 3.5: Geometry of a dipole antenna increment [30]

Using these approximations, we obtain the following

$$E_l(m) \approx j\omega A_l(m) + \frac{\Phi(m^-) - \Phi(m^+)}{\Delta l_m} \tag{3.23}$$

$$\overrightarrow{A}(m) \approx \mu \sum_n \overrightarrow{I}_{filament}(n) \int_{\Delta l_n} \frac{\exp^{-j\beta R}}{4\pi R} dl \tag{3.24}$$

$$\Phi(m^+) \approx \frac{1}{\varepsilon}\sum_n \sigma_{filament}(n^+) \int\limits_{\Delta l_n} \frac{\exp^{-j\beta R}}{4\pi R} dl \tag{3.25}$$

$$\sigma(n^+)_{filament} \approx \frac{-1}{j\omega}\frac{I_{filament}(n+1) - I_{filament}(n)}{\Delta l_n^+} \tag{3.26}$$

Note that the cases where we have $\Phi(m^-)$ and $\sigma(n^-)$ are treated similarly.

We can view the $N$ equations above as the equations for an $N$-port network, with terminal pairs $n^+$ and $n^-$, and an applied voltage $\overrightarrow{E} \cdot \mathbf{\Delta}\overrightarrow{l}_n$. Applying Equations (3.24) and (3.25) to two representative elements, $n$ and $m$, as shown in Figure 3.5, and noticing that they possess the same integral form, we obtain

$$\psi(n,m) = \frac{1}{\Delta l_n}\int\limits_{\Delta l_n} \frac{\exp^{-j\beta R_m}}{4\pi R_m} dl \tag{3.27}$$

and

$$R_m = \begin{cases} \sqrt{\rho^2 + (z - z_m)^2} & : \quad m \neq n \\ \sqrt{a^2 + z^2} & : \quad m = n \end{cases} \tag{3.28}$$

where $\rho$ is the horizontal distance between antennas containing points $n$ and $m$, $a$ is the dipole antenna radius, $k$ is the wave number, $z_m$ is the vertical distance between points $n$ and $m$, $\Delta l_n$ is the length of the $n^{th}$ increment, $\omega$ is the frequency of operation (in radians per second), and $R_m$ is the distance from a point on $\Delta l_n$ to the point $m$.

Let the increment $n$ of Figure 3.5 consist of a current filament $I_{filament}(n)$ and two charge filaments of net charge

$$q(n^+) = \frac{1}{j\omega} I_{filament}(n) \qquad q(n^-) = \frac{-1}{j\omega} I_{filament}(n) \tag{3.29}$$

Therefore, using Equation (3.24) we obtain

$$\overrightarrow{A} = \mu \overrightarrow{I}_{filament}(n)\Delta l_n \psi(n,m) \tag{3.30}$$

Using Equations (3.27) and (3.29), knowing that $q = \sigma_{filament}\Delta l$, Equation (3.25) can be rewritten such that the scalar potentials at $m^+$ and $m^-$ are

$$\Phi(m^+) = \frac{1}{j\omega\varepsilon}\left[I_{filament}(n)\psi(n^+, m^+) - I_{filament}(n)\psi(n^-, m^+)\right] \tag{3.31}$$

$$\Phi(m^-) = \frac{1}{j\omega\varepsilon}\left[I_{filament}(n)\psi(n^+, m^-) - I_{filament}(n)\psi(n^-, m^-)\right] \tag{3.32}$$

Substituting equations (3.31), (3.32), and (3.30) into equation (3.23) yields the impedance equation

$$\begin{aligned} Z_{mn} &= j\omega\mu\Delta\overrightarrow{l}_{\mathbf{n}} \cdot \Delta\overrightarrow{l}_{\mathbf{m}}\psi(n,m) \\ &+ \frac{1}{j\omega\varepsilon}\left[\psi(n^+, m^+) - \psi(n^-, m^+) - \psi(n^+, m^-) + \psi(n^-, m^-)\right] \end{aligned} \tag{3.33}$$

where $1 \leq m, n \leq N$, $\psi(n,m)$ is given in Equation (3.27), and $Z_{mn}$ is an element of the mutual impedance matrix $[Z]$.

Numerically integrating $\psi(n,m)$, we obtain the mutual impedance matrix $[Z]$. Specifying a vector of voltage distribution over all the filaments, $\overrightarrow{V}$, where a filament may also be referred to as an increment, one can solve the matrix equation

$$[Z_{mn}]^{-1}[V_n] = [I_m] \tag{3.34}$$

where $\overrightarrow{I}$ specifies a vector of the increment currents over the entire array.

In this thesis, we have assumed that the antennas in the array are center-fed such that only the increments corresponding to the centers of the antennas possess non-zero voltages while the remaining entries are zero.

Upon obtaining $\overrightarrow{I}$, we perform beampattern synthesis by determining the far-zone field at a point $i$ using [2]

$$A_i = \frac{\mu e^{-j\beta r_i}}{4\pi r_i}\sum_{j=1}^{n} I_j e^{j\beta r_j \cos\xi_{ij}}\Delta l_j \tag{3.35}$$

where $r_i$ and $r_j$ are the radius vectors to the distant field and source points, respectively, $\xi_{ij}$ is the angle between them, and $I_j$ is an element from the current vector $\overrightarrow{I}$.

#### 3.3.1.3 Full-Wave Electromagnetic Numerical Computation using IE3D

One commercially-available full-wave electromagnetic numerical computation software package is known as IE3D [98]. It is capable of modeling both the electric current on a metallic structure as well as a magnetic current representing the field distribution on a metallic aperture. The computation process of IE3D is based upon solving an integral equation derived using Green's Functions and the Method of Moments [98]. The $N \times N$ matrix equation is given as

$$[Z]\overrightarrow{I} = \overrightarrow{V} \tag{3.36}$$

such that

$$Z_{mn} = \int_S \{Z_s \vec{B_m} \cdot \vec{B_n}\} ds + \int_S ds \int_S \{\vec{B_m} \cdot \vec{G}(\vec{r}|\vec{r}') \cdot \vec{B_n}\} ds' \tag{3.37}$$

and

$$V_n = \int_S \{\vec{E_i}(\vec{r}) \cdot \vec{B_n}\} ds \tag{3.38}$$

where we compute the voltage vector $\overrightarrow{V}$ and mutual impedance matrix $[Z]$ and use (3.36) to solve for the current vector $\overrightarrow{I}$.

The differences among full-wave electromagnetic formulations are based on the choice of basis functions $\vec{B_n}(\vec{r})$ for the current distribution representation and the Green's function $\vec{G}(\vec{r}|\vec{r}')$.

The rationale for a full-wave electromagnetic numerical computation approach is that it is capable of predicting the patterns of larger classes of antenna arrays which cannot be analytically studied, such as those that have directional radiation which could be employed in fixed wireless applications.

### 3.3.2 Results

Using the Induced EMF Method and the Method of Moments beampattern synthesis models, as well as full-wave electromagnetic numerical computation to include the effects of mutual coupling, beampattern synthesis can be performed for a number of desired angle-of-arrivals based on array geometries consisting of equal-length dipoles positioned in a side-by-side configuration. Figures 3.6 to 3.24 are the normalized beampatterns of $N_A$ half wavelength dipole antennas arranged in a circular array, where $N_A$ ranges from 2 to 6. Figures 3.6, 3.10, 3.14, 3.18, and 3.22 do not consider the effects of mutual coupling while the other figures do include these effects.

It is observed that figures which include the effects of mutual coupling compare relatively close to one another in terms of there sidelobe levels, null depth, and beamwidth. When compared to the figures where no mutual coupling is considered, we see that the figures which do include the effects of mutual coupling all exhibit higher sidelobe levels, shallower nulls, and wider beamwidths relative to the figures which do not consider these effects.

Thus, the effects of mutual coupling degrade the beamforming patterns which ultimately result in a decrease in performance for the CDMA system using these base station antenna arrays.

It should be noted that in several instances, there exist a difference in the sidelobe levels between the beampatterns generated using IE3D and the Method of Moments. For example, Figure 3.12 exhibits smaller sidelobes relative to Figure 3.13 even though they both include the effects of mutual coupling. The reason why a difference exists is due to the physical setup of each method. The Method of Moments uses cylindrical increments with a specified finite radius while the model used in IE3D uses an hexagonal polyhedron, where each face is considered an increment. As a result, the IE3D

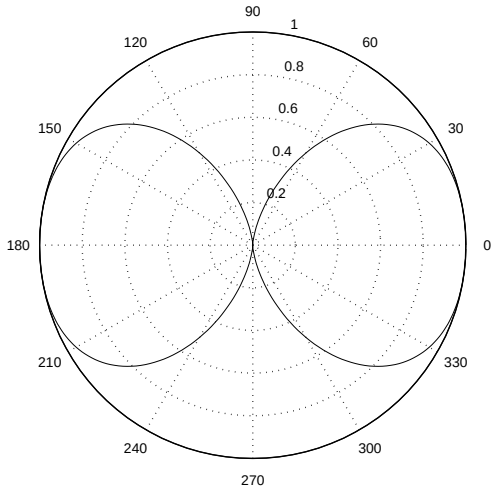


Figure 3.6: Beampattern of a 2 element circular array with AOA=$0^o$ and no MCE

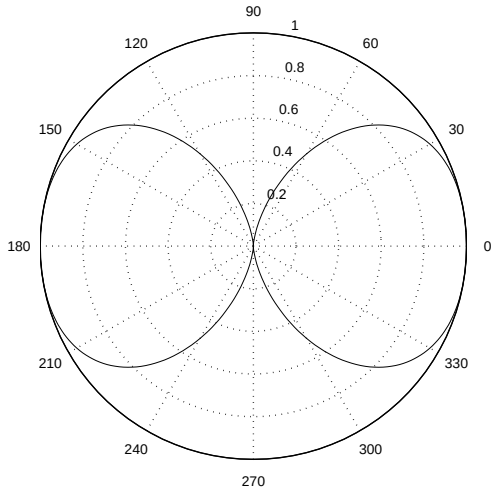


Figure 3.7: Beampattern of a 2 element circular array with AOA=$0^o$ and Induced EMF Method-generated MCE

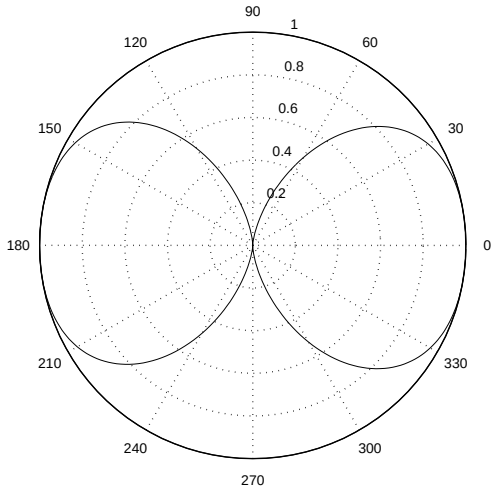


Figure 3.8: Beampattern of a 2 element circular array with AOA=$0^o$ and MoM-generated MCE

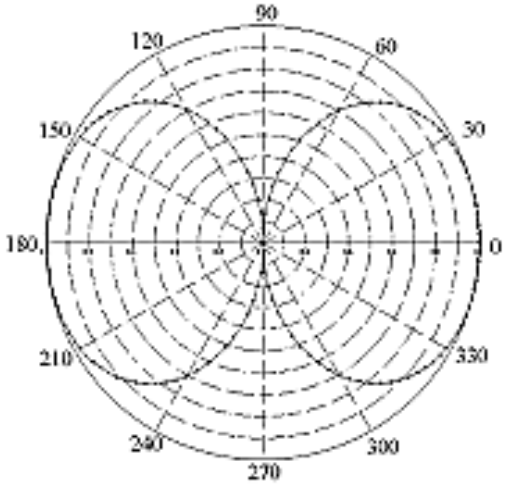


Figure 3.9: Beampattern of a 2 element circular array with AOA=$0^o$ and IE3D-generated MCE

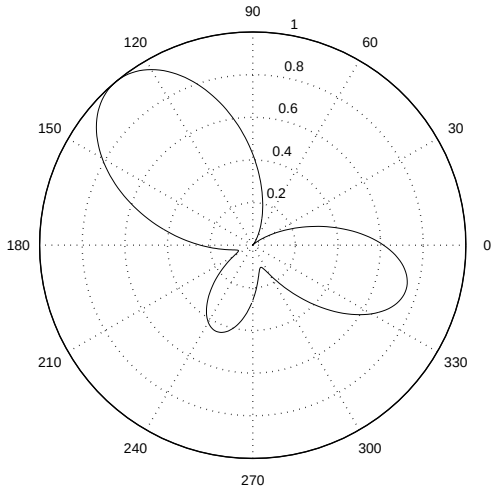


Figure 3.10: Beampattern of a 3 element circular array with AOA=135$^o$ and no MCE

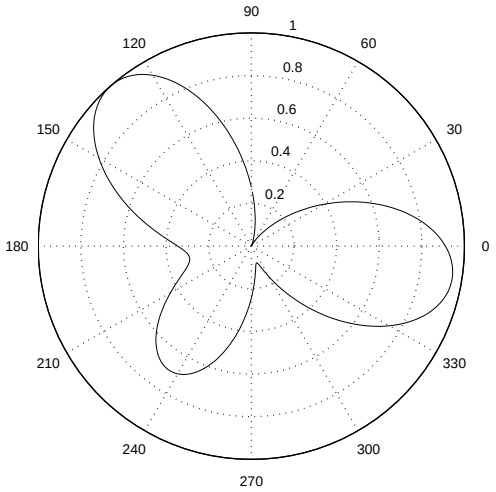


Figure 3.11: Beampattern of a 3 element circular array with AOA=135$^o$ and Induced EMF-generated MCE

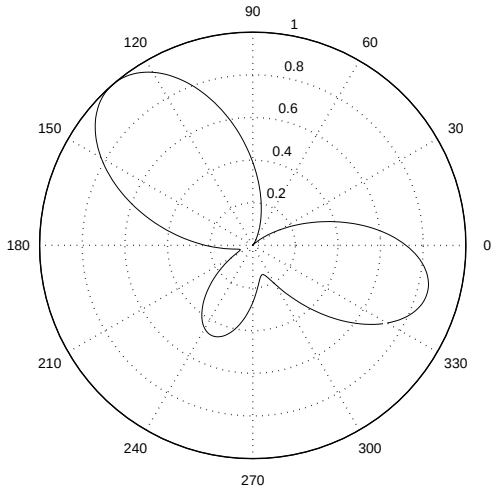


Figure 3.12: Beampattern of a 3 element circular array with AOA=135$^o$ and MoM-generated MCE

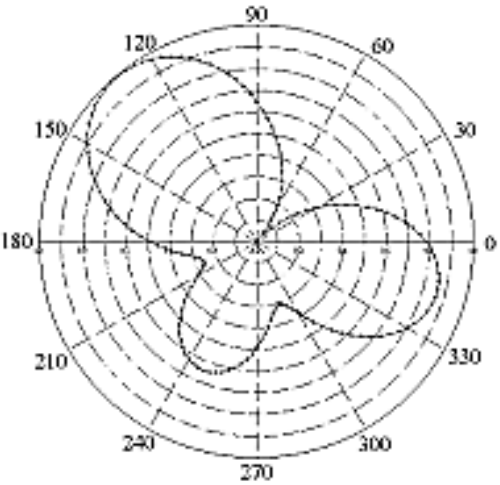


Figure 3.13: Beampattern of a 3 element circular array with AOA=135$^o$ and IE3D-generated MCE

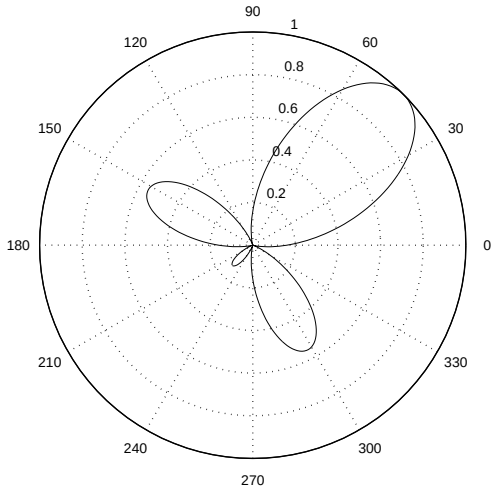


Figure 3.14: Beampattern of a 4 element circular array with AOA=$45^o$ and no MCE

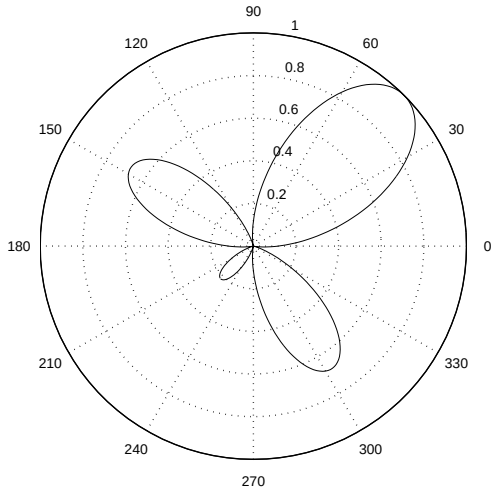


Figure 3.15: Beampattern of a 4 element circular array with AOA=$45^o$ and Induced EMF Method-generated MCE

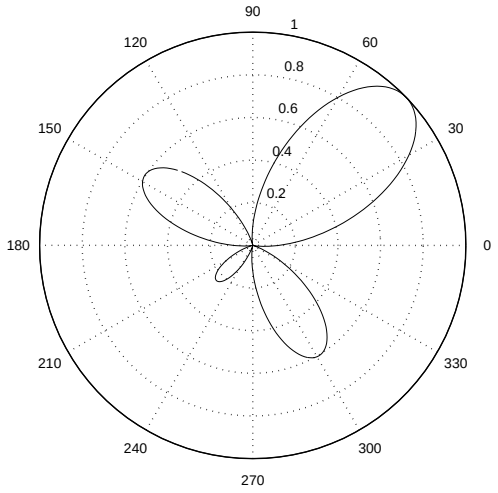


Figure 3.16: Beampattern of a 4 element circular array with AOA=$45^o$ and MoM-generated MCE

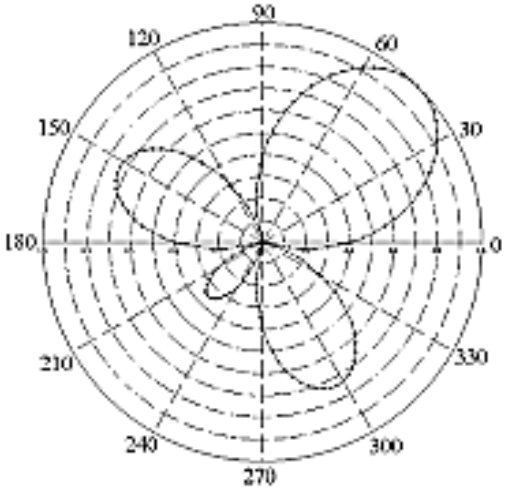


Figure 3.17: Beampattern of a 4 element circular array with AOA=$45^o$ and IE3D-generated MCE

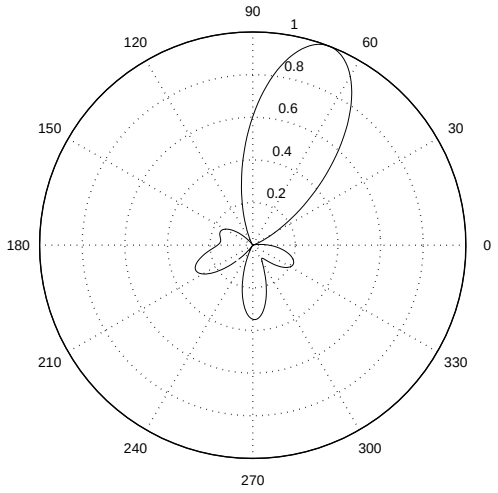


Figure 3.18: Beampattern of a 5 element circular array with AOA=$80^o$ and no MCE

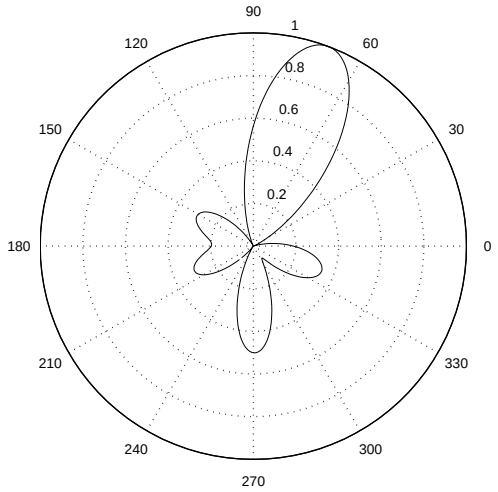


Figure 3.19: Beampattern of a 5 element circular array with AOA=$80^o$ and Induced EMF Method-generated MCE

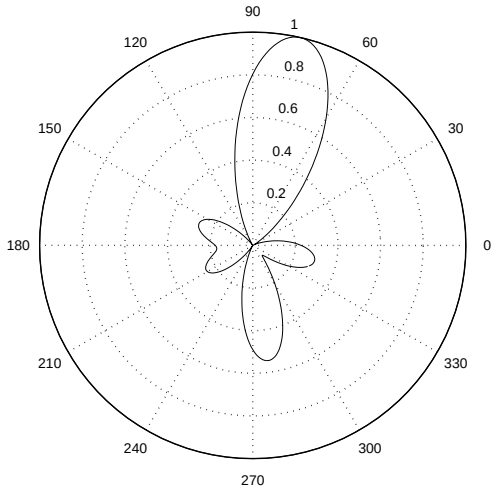


Figure 3.20: Beampattern of a 5 element circular array with AOA=$80^o$ and MoM-generated MCE

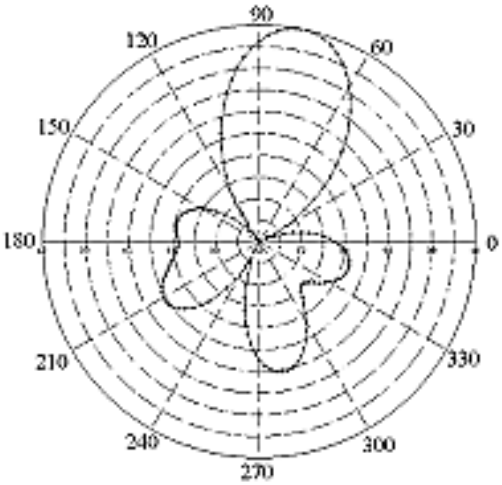


Figure 3.21: Beampattern of a 5 element circular array with AOA=$80^o$ and IE3D-generated MCE

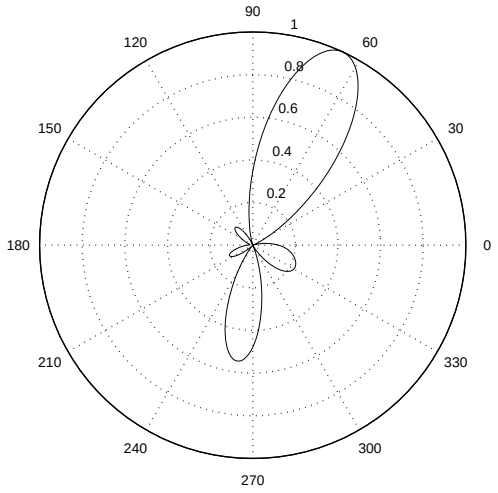


Figure 3.22: Beampattern of a 6 element circular array with AOA=$80^o$ and no MCE

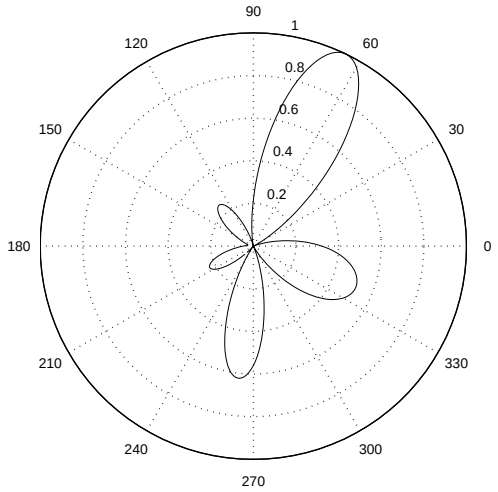


Figure 3.23: Beampattern of a 6 element circular array with AOA=$80^o$ and Induced EMF Method-generated MCE

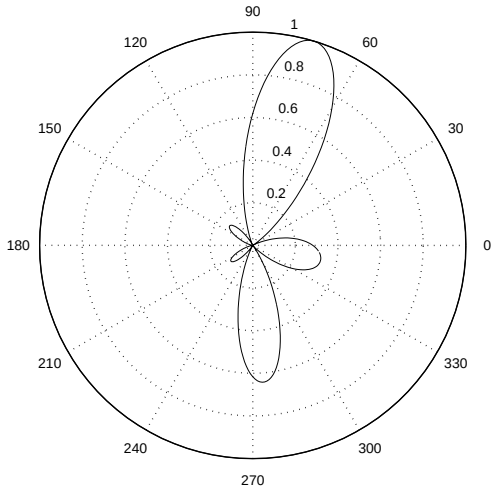


Figure 3.24: Beampattern of a 6 element circular array with AOA=$80^o$ and MoM-generated MCE

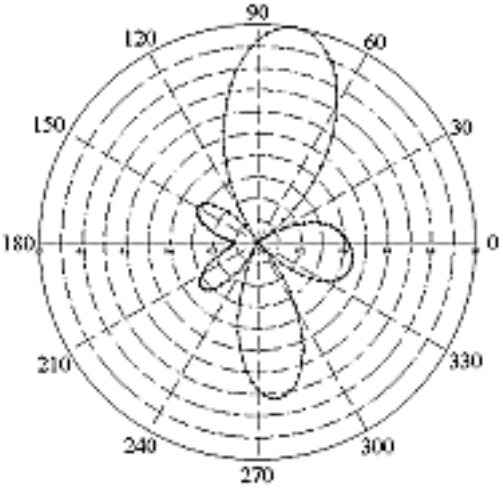


Figure 3.25: Beampattern of a 6 element circular array with AOA=$80^o$ and IE3D-generated MCE

model experiences volume effects which leads to the difference in sidelobe levels. For more information about the setup of the IE3D antenna array model, please refer to Appendix B.

## 3.4 System Capacity Predictions

The derivation of the system uplink capacity for both the single and multiple antenna element array cases, where the effects of mutual coupling are accounted-for, is identical to the work performed in Section 2.3, with one exception which shall be discussed in the next paragraph. As a result, the received predicted power level, $E\{P_R\}$, is given by Equation (2.24) as

$$E\{P_R\} = \left(\frac{E_b}{N_o}\right)\sigma_n^2\left\{\frac{1}{R_B} - \frac{E\{\phi_k\}N_I}{B}\left(\frac{E_b}{N_o}\right)\right\}^{-1} \tag{3.39}$$

The only difference between this section and Section 2.3 is the resulting expression for the expected fraction of interferer $k$'s signal power passed by the beamforming weights, $E\{\phi_k\}$, since we have included the mutual coupling information in this term. Therefore, the derivation of $E\{\phi_k\}$, which accounts for the effects of mutual coupling, is performed in the following subsection.

### 3.4.1 Derivation of $E\{\phi_k\}$

In our derivation, $E\{\phi_k\}$ is a critical factor since it accounts for both the effects of the beamforming weights on the received signal power and the effects of mutual coupling associated with closely-spaced array elements.

In this derivation, the maximum SNR beamforming weights for a desired user $d$ at an angle $\theta_d$ relative to the circular antenna array is given as

$$\bar{\omega}\left(\theta_d\right) = \begin{bmatrix} e^{jw_0(\theta_d)} \\ e^{jw_1(\theta_d)} \\ e^{jw_2(\theta_d)} \\ \vdots \\ e^{jw_{(N_A-1)}(\theta_d)} \end{bmatrix} \tag{3.40}$$

where the phase delay for $i$th element of the array, $w_i\left(\theta_d\right)$, is

$$w_i\left(\theta_d\right) = \frac{\pi \cos\left(\theta_d - i\frac{2\pi}{N_A}\right)}{2\sin\left(\frac{\pi}{N_A}\right)} \tag{3.41}$$

It should be noted that these beamforming weights can be reconfigured to other array geometries as well.

According to [32], to account for the effects of mutual coupling, the beamforming weight vector must also contain the mutual impedance information of the antenna array. This can be approached in two different fashions: (a) using the mutual impedance information generated with the Induced EMF Method, or (b) using the mutual impedance information generated with the Method of Moments. The following two subsections illustrates these two techniques.

#### 3.4.1.1 Including Mutual Coupling Effects in $E\{\phi_k\}$ with Induced EMF Method-Generated Data

Using the $N_A \times N_A$ mutual impedance matrix $[Z]$ derived earlier in this chapter in the Induced EMF Method section, we must first perform a matrix inversion such that

$$[Y] = [Z]^{-1} \tag{3.42}$$

where $[Y]$ is also a $N_A \times N_A$ matrix.

Using Equation (3.40) and (3.42), we perform matrix multiplication such that we obtain the modified beamforming weight vector [32]

$$\bar{\omega}_{MC}(\theta_d) = [Y]\bar{\omega}(\theta_d) \tag{3.43}$$

where $\bar{\omega}(\theta_d)$ is a maximum SNR beamforming weight vector with unity magnitude, $\bar{\omega}_{MC}(\theta_d)$ is the combination of the beamforming weight vector and the mutual coupling effects, and $\bar{\omega}_{MC}(\theta_d)$, $[Y]$, and $\bar{\omega}(\theta_d)$ have units of amperes, siemens, and volts, respectively.

Therefore, the normalized amount of interference power seen from an interferer $k$ at an angle-of-arrival $\theta_k$ is

$$\phi_k(\theta_d, \theta_k) = \left| \frac{\bar{\omega}_{MC}^{\mathbf{H}}(\theta_d)}{\|\bar{\omega}_{MC}^{\mathbf{H}}(\theta_d)\|} \frac{\bar{a}(\theta_k)}{\|\bar{a}(\theta_k)\|} \right|^2 \tag{3.44}$$

where $\bar{\omega}_{MC}^{\mathbf{H}}(\theta_d)$ denotes the complex conjugate transpose of $\bar{\omega}_{MC}(\theta_d)$, $\bar{a}(\theta_k)$ is an array response vector for an $N_A$-element array, $\theta_d$ is the mean AOA for the desired mobile, and $\|.\|$ is the Euclidean norm over the complex domain.

Assuming that both $\theta_k$ and $\theta_d$ are random variables uniformly distributed over $[0^o, 360^o)$, the expected value of $\phi_k$ can be determined by substituting Equation (2.2) and Equation (3.43) into Equation (3.44), for the case of a circular array, and computing the expected value. Thus, we obtain

$$E\{\phi_k\} = \frac{1}{N_\theta^2} \sum_{\theta_d \in \Theta_d} \sum_{\theta_k \in \Theta_k} \left| \frac{\bar{\omega}_{MC}^{\mathbf{H}}(\theta_d)}{\|\bar{\omega}_{MC}^{\mathbf{H}}(\theta_d)\|} \frac{\bar{a}(\theta_k)}{\|\bar{a}(\theta_k)\|} \right|^2 \tag{3.45}$$

where $\Theta_k$ and $\Theta_d$ are sets of $N_\theta$ angles-of-arrival that range uniformly over $[0^o, 360^o)$.

The results of Equation (3.45) for a circular array with array elements ranging from one to six where the effects of mutual coupling, generated using the Induced EMF Method, where $N_\theta$ consists of $1^o$ increments uniformly distributed over $[0^o, 360^o)$, are shown in the second column of Table 3.1.

| $N_A$ | With MCE (MoM) | With MCE (Induced EMF) | Without MCE (from [12]) |
|---|---|---|---|
| 1 | 1.0000 | 1.0000 | 1.0000 |
| 2 | 0.5603 | 0.5970 | 0.5463 |
| 3 | 0.4178 | 0.4314 | 0.3950 |
| 4 | 0.3286 | 0.3283 | 0.3241 |
| 5 | 0.2751 | 0.2642 | 0.2460 |
| 6 | 0.2293 | 0.2307 | 0.2058 |

Table 3.1: Expected values of $\phi_k$. Mutual coupling effects, generated using the Method of Moments (MoM) and the Induced EMF Method, are included in the first two columns of results, respectively.

#### 3.4.1.2 Including Mutual Coupling Effects in $E\{\phi_k\}$ with Method of Moments-Generated Data

The technique by which the effects of mutual coupling, generated using the Method of Moments, are included in $E\{\phi_k\}$ follows closely to the technique described previously, where the mutual impedance information was generated using the Induced EMF Method, but with several exceptions.

Using the $N \times N$ mutual impedance matrix $[Z]$ derived earlier in this chapter in the Method of Moments section, we must perform matrix inversion, yielding

$$[Y] = [Z]^{-1} \tag{3.46}$$

where the dimensions of admittance matrix $[Y]$ is also $N \times N$.

The next step is to change the dimension of our beamforming weight vector to

be $N\times1$ instead of $N_A\times1$, in order to perform matrix multiplication with Equation (3.46). According to [30], if all our antennas are of the same length and center-fed, the non-zero entries of the new beamforming weight vector must coincide with the position of the increments corresponding to the feed points of the antenna array. As for the other entries, they are all zero. Therefore, using Equation (3.40), our new beamforming weight vector is

$$\bar{\omega}\left(\theta_d\right) = \begin{bmatrix} \bar{\omega}_0\left(\theta_d\right) \\ \bar{\omega}_1\left(\theta_d\right) \\ \vdots \\ \bar{\omega}_{N_A-1}\left(\theta_d\right) \end{bmatrix} \tag{3.47}$$

where the vector $\bar{\omega}_i\left(\theta_d\right)$ is defined as

$$\bar{\omega}_i\left(\theta_d\right) = \left.\begin{bmatrix} 0 \\ \vdots \\ 0 \\ e^{jw_i(\theta_d)} \\ 0 \\ \vdots \\ 0 \end{bmatrix}\right\} N/N_A \quad elements \tag{3.48}$$

and the phase delay for $i$th element of the array, $w_i\left(\theta_d\right)$, is

$$w_i\left(\theta_d\right) = \frac{\pi\cos\left(\theta_d - i\frac{2\pi}{N_A}\right)}{2\sin\left(\frac{\pi}{N_A}\right)} \tag{3.49}$$

Note that the middle element of Equation (3.48) is the only non-zero element of this vector. Thus, the number of increments per antenna, $N_A/N$, must be an odd number for the increment corresponding to the midpoint of the antenna to exist. Furthermore, since the number of increments can never be less than the number of array elements, we require that $N_A\leq N$.

Once the new beamforming weight vector is obtained, we use Equation (3.47) and Equation (3.46) to perform matrix multiplication, thus yielding the modified beamforming weight vector

$$\bar{\omega}_{MC}(\theta_d) = [Y]\bar{\omega}(\theta_d) \tag{3.50}$$

which is identical to Equation (3.43).

Therefore, the normalized amount of interference power seen from an interferer $k$ at an angle-of-arrival $\theta_k$ is

$$\phi_k(\theta_d, \theta_k) = \left| \frac{\bar{\omega}_{MC}^{\mathbf{H}}(\theta_d)}{\|\bar{\omega}_{MC}^{\mathbf{H}}(\theta_d)\|} \frac{\bar{a}(\theta_k)}{\|\bar{a}(\theta_k)\|} \right|^2 \tag{3.51}$$

where $\bar{a}(\theta_k)$ is an array response vector for an $N_A$-element array specified in Equation (2.2). Note that this expression is identical to Equation (3.44).

Assuming that both $\theta_k$ and $\theta_d$ are random variables uniformly distributed over $[0^o, 360^o)$, the expected value of $\phi_k$ can be determined by substituting Equation (2.2) and Equation (3.50) into Equation (3.51) and computing the expected value. Therefore

$$E\{\phi_k\} = \frac{1}{N_\theta^2} \sum_{\theta_d \in \Theta_d} \sum_{\theta_k \in \Theta_k} \left| \frac{\bar{\omega}_{MC}^{\mathbf{H}}(\theta_d)}{\|\bar{\omega}_{MC}^{\mathbf{H}}(\theta_d)\|} \frac{\bar{a}(\theta_k)}{\|\bar{a}(\theta_k)\|} \right|^2 \tag{3.52}$$

where $\Theta_k$ and $\Theta_d$ are sets of $N_\theta$ angles-of-arrival that range uniformly over $[0^o, 360^o)$. Note that this expression is identical to Equation (3.45).

The results of Equation (3.52) for a circular array with array elements ranging from one to six where the effects of mutual coupling, generated using the Method of Moments, are shown in the third column of Table 3.1.

#### 3.4.1.3 Results

From Table 3.1, we see that as the number of antennas increases, the expected values of $\phi_k$ decrease. Thus there is an inverse relationship between the number

of antennas and $E\{\phi_k\}$. Furthermore, the effects of mutual coupling increases the value of $E\{\phi_k\}$, for both the Induced EMF Method and the Method of Moments derived mutual impedance, relative to the case where the mutual coupling effects are unaccounted for, such as in [12].

Using the derived expressions for $E\{\phi_k\}$ as well as the tabulated values in Table 3.1, one is now capable of predicting the capacity of a CDMA system using base station antenna arrays, as will be discussed in the next section.

### 3.4.2 Multiple Antenna Element Array Capacity Calculations

Using the same technique as in the single antenna element case, the system capacity can be determined by isolating $N_I$ in Equation (3.39), resulting with the number of interfering mobiles within the cell

$$N_I = \left\lfloor \frac{B}{E\{\phi_k\}} \left( \frac{1}{\left(\frac{E_b}{N_o}\right) R_B} - \frac{N_A \sigma_n^2}{E\{P_R\}} \right) \right\rfloor \tag{3.53}$$

Therefore, the total number of mobiles within a cell is

$$N_M = \left\lfloor \frac{B}{E\{\phi_k\}} \left( \frac{1}{\left(\frac{E_b}{N_o}\right) R_B} - \frac{N_A \sigma_n^2}{E\{P_R\}} \right) \right\rfloor + 1 \tag{3.54}$$

which can then be approximated, as was done with Equation (2.30), to yield

$$N_M \approx \left\lfloor \frac{1}{E\{\phi_k\}} \frac{B}{R_B \left(E_b/N_o\right)} \right\rfloor + 1 \tag{3.55}$$

where $\lfloor . \rfloor$ is the floor function. It should be pointed out that the effects of mutual coupling are included in $E\{\phi_k\}$.

The predicted capacity for CDMA systems which use circular arrays, such that the adjacent array elements are a half-wavelength apart and the number of array elements range from one to six, are given in Table 3.2.

Inspecting these values, it can be seen that as the number of antennas increases, the number of mobiles which the system can support also increases for all three cases. Furthermore, the predicted capacity values which correspond to models where the effects of mutual coupling are included are noticeably lower relative to the capacity values of models which do not consider them. For instance, the case of five antennas exhibits a difference of six to eleven percent between the models which do include MCE and those which do not. Moreover, the two sets of capacity values which do include MCE compare very closely.

| $N_A$ | With MCE (MoM) | With MCE (Induced EMF) | Without MCE (from [12]) |
|---|---|---|---|
| 1 | 26 | 26 | 26 |
| 2 | 46 | 43 | 47 |
| 3 | 62 | 60 | 65 |
| 4 | 78 | 78 | 79 |
| 5 | 93 | 97 | 104 |
| 6 | 112 | 111 | 125 |

Table 3.2: Predicted capacity values versus number of antennas assuming perfect power control and correlation of unity between array elements. Mutual coupling effects are included in the first two columns.

## 3.5 Chapter Summary

The impact of mutual coupling effects on the performance of CDMA systems using base station antenna arrays has been analyzed in this chapter.

Firstly, the phenomenon of mutual coupling was explained in detail and several examples were provided to illustrate the mechanisms involved. In particular, the transmission mode coupling and reception mode coupling cases were examined.

Then the techniques used to incorporate MCE into our beampattern synthesis models as well as our capacity predictions were outlined, namely, the Induced EMF Method, the Method of Moments, and a full-wave electromagnetic numerical computation. The mutual impedance information derived from these methods were then used in several comparisons between beampatterns which accounted for MCE against those which do not. These comparisons show that when MCE is included in the beampattern synthesis process, the beampatterns have higher sidelobe levels, shallower nulls, and wider beamwidths relative to beampatterns which do not include MCE. Moreover, the beampatterns which do account for MCE generated using the three methods all compare very closely with one another.

Finally, this chapter ends with a detailed analysis of the effects of mutual coupling upon our capacity predictions. In particular, our analysis focused on computing the power and predicted capacity of the single antenna element and multiple antenna element array cases. Furthermore, with respect to the multiple antenna element array case, a technique of including the MCE within the expected value of $\phi_k$ was derived and presented. Note that the MCE information was generated using both the Induced EMF Method and the Method of Moments. The predicted capacity results for the cases where MCE are included show a noticeable decrease relative to the case where the MCE is unaccounted for. For example, we observe a difference in system capacity of six to eleven percent when the effects of mutual coupling are and are not considered in the $N_A = 5$ antennas case.

# Chapter 4

# System Performance in Scattering Environments

## 4.1 Introduction

In our investigation of CDMA systems which use digital beamforming in Chapter 3 , we have examined the performance and behaviour of antenna arrays that include the effects of mutual coupling with the underlying assumption that the operating environment for the array consists of noise and interference due to other mobiles. In this chapter, we take our model one step further by assuming the environment also includes the effects of scatter due to multipath. This is achieved by determining the cross-correlation statistics between antennas of the array. Hence, we can further increase the accuracy of our system model during analysis.

### 4.1.1 Chapter Outline

We begin this chapter with a brief introduction to the phenomenon of scattering due to multipath propagation, as well as a quick overview of various spatial channel

models. Following this section, the remainder of our chapter is subdivided into two major parts.

The first part deals with a model for the cross-correlation statistics between signals received from the same source point by a pair of antennas. Although the basic derivations may be found in [8], [12], [56], [74], and [75], the overall model was re-derived such that the mutual coupling effects occuring within the antenna array were included. Furthermore, as in [12], the resulting model is generalized for an arbitrary angle-of-arrival distribution.

The second part deals with the capacity of the CDMA system uplink in a scattering environment. This analysis makes use of the derived power value expressions, found in [12], [19], and the previous chapter, in order to determine the threshold for the number of mobiles the system can support before power control begins to fail. Furthermore, the scattering effects are included in this analysis by converting the effects of increasing scatter into decreased amplitude cross-correlation statistics and through a scatter-induced phase distortion calculation from the beampattern. We will then assess the impact of scattering relative to the results found in [12] and [19].

## 4.2 Scatter

Scatter is a phenomenon associated with multipath propagation. It occurs when signals from a single source arrive at a base station from several directions within an angular region after being reflected by objects in the surrounding environment. A graphical representation of this definition is shown in Figure 4.1. This angular region, known as the *angle spread*, varies according to the operating environment. Table 4.1, from [56], gives us several typical angle spreads for different environments.

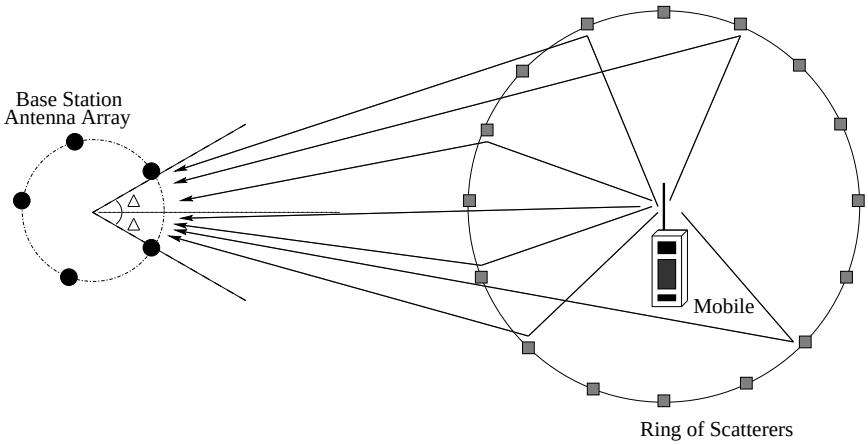


Figure 4.1: Graphical representation of scatter

| Environment | Angle Spread ($2\Delta$) |
|---|---|
| Flat Rural (Macro) | $1^o$ |
| Urban (Macro) | $20^o$ |
| Hilly (Macro) | $30^o$ |
| Microcell (Mall) | $120^o$ |
| Picocell (Indoors) | $360^o$ |

Table 4.1: Several typical angle spreads ($2\Delta$) [56]

Throughout this chapter, most of the work carried out requires the use of cross-correlation statistics, either directly or indirectly. Thus, the choice of the probability distribution of the arriving signal power, $P(\theta)$, will have a large impact on our analysis. Several spatial channel models which can be chosen are found in [22]. In this thesis, we develop a cross-correlation statistics model, based on a simpler method found in [12] and [75], using a generalized $P(\theta)$ which can be used for an arbitrary angle-of-arrival (AOA) distribution. We then apply the calculation to the the cases

of a Gaussian distributed AOA modelwhich we refer to later as GAA, and a Uniformly distributed AOA model, which we refer to later as UAA, although the same methodology can be applied to distributions corresponding to other environments as well.

## 4.3 Cross-Correlation Model

In this section we derive the cross-correlation statistics of the multipath fading channel where the mutual coupling effects within the antenna array are included. Although it is based on the derivations given in [8], [12], [56], [74], and [75], this derivation takes the model one step further by also including the antenna array mutual coupling effects. Furthermore, in the spirit of the derivation found in [12], we shall assume that there is no specific AOA distribution used. Thus we can apply this result later on to cases where an arbitrary distribution is specified.

Assume that we have two identical antennas, $i$ and $k$, that are spaced a distance $d$ apart receiving signals from the same source, as shown in Figure 4.2. Let the direction of the $r^{th}$ wave make an angle $\theta_{k_r}$ with a line passing through antennas $i$ and $k$. Suppose the $r^{th}$ wave produces the voltages

$$v_{ir} = a_r \cos\left(\omega t + \psi_r + \frac{\pi d}{\lambda}\cos\left(\theta_{k_r}\right)\right) \tag{4.1}$$

and

$$v_{kr} = a_r \cos\left(\omega t + \psi_r - \frac{\pi d}{\lambda}\cos\left(\theta_{k_r}\right)\right) \tag{4.2}$$

on antennas $i$ and $k$ for a coplanar wave of frequency $f = \omega/2\pi$ and wavelength $\lambda$. The phase delay of the ray $r$ is represented by the value $\phi_r$ while the amplitude of the ray $r$ is defined as $a_r$.

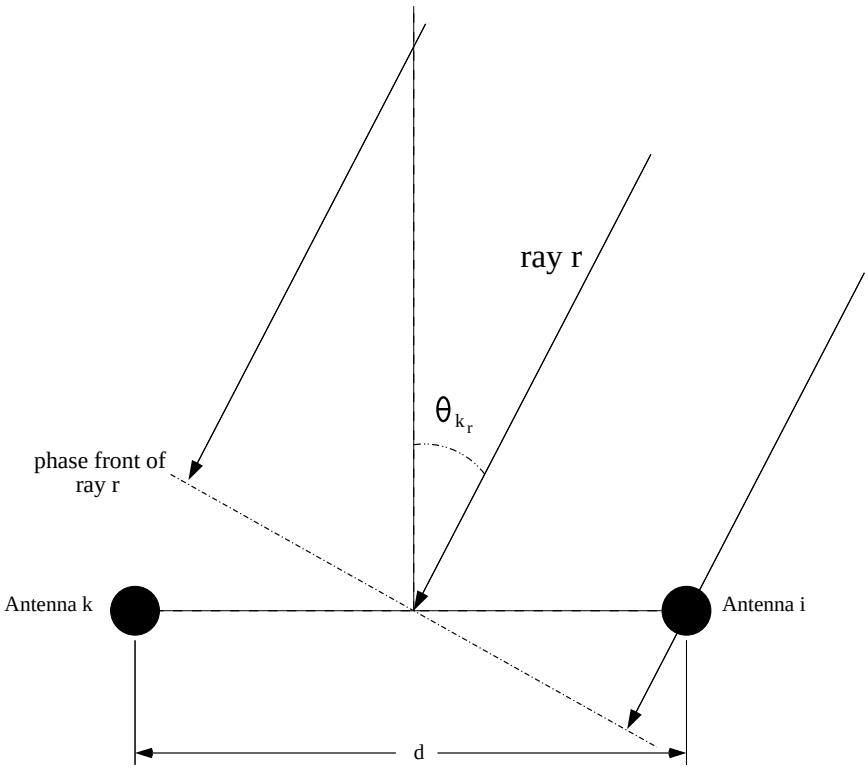


Figure 4.2: Model used in our cross-correlation derivation

Therefore, by the principle of superposition, the total voltages produced by all the waves at antennas $i$ and $k$ are given by

$$v_i = \sum_{r=1}^{n} a_r \cos\left(\omega t + \psi_r + \frac{\pi d}{\lambda}\cos\left(\theta_{k_r}\right)\right) \tag{4.3}$$

and

$$v_k = \sum_{r=1}^{n} a_r \cos\left(\omega t + \psi_r - \frac{\pi d}{\lambda}\cos\left(\theta_{k_r}\right)\right) \tag{4.4}$$

which can respectively be rewritten as

$$v_i = A_1 \cos\left(\omega t + \Psi_1\right) \tag{4.5}$$

and

$$v_k = A_2 \cos\left(\omega t + \Psi_2\right) \tag{4.6}$$

such that the amplitudes and phases are generally different at the two antennas.

Using Equations (4.5) and (4.6), it can be easily shown that the mean signal voltage at antennas $i$ and $k$ is

$$v_i = v_k = 0 \tag{4.7}$$

while their mean-squared signal voltage is

$$\overline{v_i^2} = \overline{v_k^2} = \frac{1}{2}\sum_{r=1}^{n} a_r^2 \tag{4.8}$$

Furthermore, the mean-squared signal amplitude at antennas $i$ and $k$ is

$$\overline{A_1^2} = \overline{A_2^2} = \sum_{r=1}^{n} a_r^2 \tag{4.9}$$

Suppose now that instead of receiving a collection of individual rays at the antenna elements, we are dealing with a whole distribution of waves. As a result, the summations of Equations (4.8) and (4.9) become integrals over the entire distribution of the received waves. Therefore, given a distribution of the arriving signal power, $P(\theta)$, the total power received from the whole distribution of waves is given as

$$P_o = \int_0^{2\pi} P(\theta)d\theta \tag{4.10}$$

such that Equations (4.8) and (4.9) now become

$$\overline{v_i^2} = \overline{v_k^2} = P_o = \int_0^{2\pi} P(\theta)d\theta \tag{4.11}$$

$$\overline{A_1^2} = \overline{A_2^2} = 2P_o = 2\int_0^{2\pi} P(\theta)d\theta \tag{4.12}$$

Therefore, using Equations (4.11) and (4.12), we obtain

$$\frac{1}{2}\sum_{r=1}^{m} a_r^2 = \int_0^{2\pi} P(\theta)d\theta \tag{4.13}$$

which will be used later in our derivation.

To include the effects of mutual coupling, we must pass these voltages through a mutual admittance matrix $[Y]$, which is the inverse of the mutual impedance matrix $[Z]$ derived in the previous chapter using the Induced EMF Method. Thus the total voltages which include mutual coupling effects, $v_{i,mc}$ and $v_{k,mc}$, are, respectively,

$$\begin{bmatrix} v_{i,mc} \\ v_{k,mc} \end{bmatrix} = \begin{bmatrix} |Y_{ii}|\, e^{j\angle Y_{ii}} & |Y_{ik}|\, e^{j\angle Y_{ik}} \\ |Y_{ki}|\, e^{j\angle Y_{ki}} & |Y_{kk}|\, e^{j\angle Y_{kk}} \end{bmatrix} \begin{bmatrix} v_i \\ v_k \end{bmatrix} \tag{4.14}$$

where, for example, $|Y_{ik}|$ and $\angle Y_{ik}$ represent the magnitude and phase of the mutual admittance between antenna elements $i$ and $k$, respectively. We can rewrite the above matrix equation as

$$v_{i,mc} = |Y_{ii}|\, A_1 \cos(\omega t + \Psi_1)\, e^{j\angle Y_{ii}} + |Y_{ik}|\, A_2 \cos(\omega t + \Psi_2)\, e^{j\angle Y_{ik}} \tag{4.15}$$

and

$$v_{k,mc} = |Y_{ki}|\, A_1 \cos(\omega t + \Psi_1)\, e^{j\angle Y_{ki}} + |Y_{kk}|\, A_2 \cos(\omega t + \Psi_2)\, e^{j\angle Y_{kk}} \tag{4.16}$$

Using the trignometric identity

$$\cos(A + B) = \cos(A)\cos(B) - \sin(A)\sin(B) \tag{4.17}$$

we obtain

$$\begin{aligned} v_{i,mc} &= |Y_{ii}|A_1\Big(\cos(\omega t)\cos(\Psi_1)e^{j\angle Y_{ii}} - \sin(\omega t)\sin(\Psi_1)e^{j\angle Y_{ii}}\Big) \\ &+ |Y_{ik}|A_2\Big(\cos(\omega t)\cos(\Psi_2)e^{j\angle Y_{ik}} - \sin(\omega t)\sin(\Psi_2)e^{j\angle Y_{ik}}\Big) \end{aligned} \tag{4.18}$$

and

$$\begin{aligned} v_{k,mc} &= |Y_{ki}|A_1\Big(\cos(\omega t)\cos(\Psi_1)e^{j\angle Y_{ki}} - \sin(\omega t)\sin(\Psi_1)e^{j\angle Y_{ki}}\Big) \\ &+ |Y_{kk}|A_2\Big(\cos(\omega t)\cos(\Psi_2)e^{j\angle Y_{kk}} - \sin(\omega t)\sin(\Psi_2)e^{j\angle Y_{kk}}\Big) \end{aligned} \tag{4.19}$$

Equations (4.18) and (4.19) can respectively be rewritten as

$$\begin{aligned} v_{i,mc} &= \left(|Y_{ii}|A_1\cos(\Psi_1)e^{j\angle Y_{ii}} + |Y_{ik}|A_2\cos(\Psi_2)e^{j\angle Y_{ik}}\right)\cos(\omega t) \\ &- \left(|Y_{ii}|A_1\sin(\Psi_1)e^{j\angle Y_{ii}} + |Y_{ik}|A_2\sin(\Psi_2)e^{j\angle Y_{ik}}\right)\sin(\omega t) \end{aligned} \tag{4.20}$$

and

$$\begin{aligned} v_{k,mc} &= (|Y_{ki}|A_1\cos(\Psi_1)e^{j\angle Y_{ki}} + |Y_{kk}|A_2\cos(\Psi_2)e^{j\angle Y_{kk}})\cos(\omega t) \\ &- (|Y_{ki}|A_1\sin(\Psi_1)e^{j\angle Y_{ki}} + |Y_{kk}|A_2\sin(\Psi_2)e^{j\angle Y_{kk}})\sin(\omega t) \end{aligned} \tag{4.21}$$

In practice, since we usually observe the signal amplitude, we thus need to calculate the correlation coefficient between the total received voltage amplitudes at antennas $i$ and $k$. Therefore, let us respectively rewrite Equations (4.20) and (4.21) as

$$v_{i,mc} = B_{1c}\cos(\omega t) + B_{1s}\sin(\omega t) \tag{4.22}$$

and

$$v_{k,mc} = B_{2c}\cos(\omega t) + B_{2s}\sin(\omega t) \tag{4.23}$$

where

$$\begin{aligned} B_{1c} &= |Y_{ii}|A_1\cos(\Psi_1)e^{j\angle Y_{ii}} + |Y_{ik}|A_2\cos(\Psi_2)e^{j\angle Y_{ik}} \\ &= |Y_{ii}|\sum_{r=1}^{m} a_r\cos(\psi_r + \chi_r)e^{j\angle Y_{ii}} + |Y_{ik}|\sum_{r=1}^{m} a_r\cos(\psi_r - \chi_r)e^{j\angle Y_{ik}} \end{aligned} \tag{4.24}$$

$$\begin{aligned} B_{1s} &= |Y_{ii}|A_1\sin(\Psi_1)e^{j\angle Y_{ii}} + |Y_{ik}|A_2\sin(\Psi_2)e^{j\angle Y_{ik}} \\ &= |Y_{ii}|\sum_{r=1}^{m} a_r\sin(\psi_r + \chi_r)e^{j\angle Y_{ii}} + |Y_{ik}|\sum_{r=1}^{m} a_r\sin(\psi_r - \chi_r)e^{j\angle Y_{ik}} \end{aligned} \tag{4.25}$$

$$\begin{aligned} B_{2c} &= |Y_{ki}|A_1\cos(\Psi_1)e^{j\angle Y_{ki}} + |Y_{kk}|A_2\cos(\Psi_2)e^{j\angle Y_{kk}} \\ &= |Y_{ki}|\sum_{r=1}^{m} a_r\cos(\psi_r + \chi_r)e^{j\angle Y_{ki}} + |Y_{kk}|\sum_{r=1}^{m} a_r\cos(\psi_r - \chi_r)e^{j\angle Y_{kk}} \end{aligned} \tag{4.26}$$

$$\begin{aligned} B_{2s} &= |Y_{ki}|A_1\sin(\Psi_1)e^{j\angle Y_{ki}} + |Y_{kk}|A_2\sin(\Psi_2)e^{j\angle Y_{kk}} \\ &= |Y_{ki}|\sum_{r=1}^{m} a_r\sin(\psi_r + \chi_r)e^{j\angle Y_{ki}} + |Y_{kk}|\sum_{r=1}^{m} a_r\sin(\psi_r - \chi_r)e^{j\angle Y_{kk}} \end{aligned} \tag{4.27}$$

and

$$\chi_r = \frac{\pi d}{\lambda}\cos(\theta_{k_r}) \tag{4.28}$$

Since the phase angles $\psi_r$ are assumed to be random and $m$ is assumed to be large, we can then say that $B_{1c}$, $B_{1s}$, $B_{2c}$, and $B_{2s}$ are each distributed normally with zero mean.

To determine the joint probability distribution of the total received voltage amplitudes at antennas $i$ and $k$, we must derive their second moments, namely, $\overline{B_{1c}B_{1c}^*}$, $\overline{B_{1s}B_{1s}^*}$, $\overline{B_{2c}B_{2c}^*}$, $\overline{B_{2s}B_{2s}^*}$, $\overline{B_{1c}B_{2c}^*}$, $\overline{B_{1s}B_{2s}^*}$, $\overline{B_{1c}B_{1s}^*}$, $\overline{B_{2c}B_{2s}^*}$, $\overline{B_{1c}B_{2s}^*}$, and $\overline{B_{2c}B_{1s}^*}$, where $\overline{(\cdot)}$ is the expectation of $(\cdot)$. After some extensive derivation (see Appendix A), we obtain

$$\begin{aligned}\overline{B_{1c}B_{1c}^*} = \overline{B_{1s}B_{1s}^*} &= \left(|Y_{ii}|^2 + |Y_{ik}|^2\right)\frac{1}{2}\sum_{r=1}^{m} {a_r}^2 \\ &+ |Y_{ii}||Y_{ik}|\sum_{r=1}^{m} {a_r}^2 \cos\left(\frac{2\pi d}{\lambda}\cos\left(\theta_{k_r}\right)\right)\cos\left(\angle Y_{ii} - \angle Y_{ik}\right) \quad (4.29)\end{aligned}$$

$$\begin{aligned}\overline{B_{2c}B_{2c}^*} = \overline{B_{2s}B_{2s}^*} &= \left(|Y_{ki}|^2 + |Y_{kk}|^2\right)\frac{1}{2}\sum_{r=1}^{m} {a_r}^2 \\ &+ |Y_{ki}||Y_{kk}|\sum_{r=1}^{m} {a_r}^2 \cos\left(\frac{2\pi d}{\lambda}\cos\left(\theta_{k_r}\right)\right)\cos\left(\angle Y_{ki} - \angle Y_{kk}\right) \quad (4.30)\end{aligned}$$

$$\overline{B_{1c}B_{1s}^*} = j\,|Y_{ii}|\,|Y_{ik}|\sin\left(\angle Y_{ik} - \angle Y_{ii}\right)\sum_{r=1}^{m} a_r^2 \sin\left(\frac{2\pi d}{\lambda}\cos\left(\theta_{k_r}\right)\right) \quad (4.31)$$

$$\overline{B_{2c}B_{2s}^*} = -j\,|Y_{kk}|\,|Y_{ki}|\sin\left(\angle Y_{ki} - \angle Y_{kk}\right)\sum_{r=1}^{m} a_r^2 \sin\left(\frac{2\pi d}{\lambda}\cos\left(\theta_{k_r}\right)\right) \quad (4.32)$$

$$\begin{aligned}\overline{B_{1c}B_{2c}^*} = \overline{B_{1s}B_{2s}^*} &= |Y_{ii}||Y_{ki}|\frac{1}{2}\sum_{r=1}^{m} a_r^2 e^{j\left(\angle Y_{ii} - \angle Y_{ki}\right)} \\ &+ |Y_{ik}||Y_{kk}|\frac{1}{2}\sum_{r=1}^{m} a_r^2 e^{j\left(\angle Y_{ik} - \angle Y_{kk}\right)} \\ &+ |Y_{ii}||Y_{kk}|\frac{1}{2}\sum_{r=1}^{m} a_r^2 \cos\left(\frac{2\pi d}{\lambda}\cos\left(\theta_{k_r}\right)\right) e^{j\left(\angle Y_{ii} - \angle Y_{kk}\right)} \\ &+ |Y_{ik}||Y_{ki}|\frac{1}{2}\sum_{r=1}^{m} a_r^2 \cos\left(\frac{2\pi d}{\lambda}\cos\left(\theta_{k_r}\right)\right) e^{j\left(\angle Y_{ik} - \angle Y_{ki}\right)} \quad (4.33)\end{aligned}$$

$$\begin{aligned}\overline{B_{1c}B_{2s}^*} = -\overline{B_{2c}B_{1s}^*} &= -|Y_{ii}||Y_{kk}|\frac{1}{2}\sum_{r=1}^{m}a_r^2\sin\left(\frac{2\pi d}{\lambda}\cos\left(\theta_{k_r}\right)\right)e^{j\left(\angle Y_{ii}-\angle Y_{kk}\right)} \\ &+ |Y_{ik}||Y_{ki}|\frac{1}{2}\sum_{r=1}^{m}a_r^2\sin\left(\frac{2\pi d}{\lambda}\cos\left(\theta_{k_r}\right)\right)e^{j\left(\angle Y_{ki}-\angle Y_{ik}\right)} \quad (4.34)\end{aligned}$$

Equations (4.29), (4.30), (4.33), and (4.34) can be further simplified using the fact that the mutual admittance matrix is symmetric, namely, $\angle Y_{ii} = \angle Y_{kk}$, $\angle Y_{ik} = \angle Y_{ki}$, $|Y_{ii}| = |Y_{kk}|$, and $|Y_{ik}| = |Y_{ki}|$. Thus we obtain

$$\begin{aligned}\overline{B_{1c}B_{2c}^*} = \overline{B_{1s}B_{2s}^*} &= |Y_{ii}||Y_{ki}|\sum_{r=1}^{m}a_r^2\cos\left(\angle Y_{ii}-\angle Y_{ki}\right) \\ &+ \left(|Y_{ii}|^2+|Y_{ik}|^2\right)\frac{1}{2}\sum_{r=1}^{m}a_r^2\cos\left(\frac{2\pi d}{\lambda}\cos\left(\theta_{k_r}\right)\right) \\ &= \rho_{R_iR_k} \quad (4.35)\end{aligned}$$

and

$$\begin{aligned}\overline{B_{1c}B_{2s}^*} = -\overline{B_{2c}B_{1s}^*} &= -\left(|Y_{ii}|^2-|Y_{ik}|^2\right)\frac{1}{2}\sum_{r=1}^{m}a_r^2\sin\left(\frac{2\pi d}{\lambda}\cos\left(\theta_{k_r}\right)\right) \\ &= \rho_{R_iI_k} \quad (4.36)\end{aligned}$$

$$\begin{aligned}\overline{B_{1c}B_{1c}^*} = \overline{B_{1s}B_{1s}^*} &= \overline{B_{2c}B_{2c}^*} = \overline{B_{2s}B_{2s}^*} \\ &= \left(|Y_{ii}|^2+|Y_{ik}|^2\right)\frac{1}{2}\sum_{r=1}^{m}{a_r}^2 \\ &+ |Y_{ii}||Y_{ik}|\sum_{r=1}^{m}{a_r}^2\cos\left(\frac{2\pi d}{\lambda}\cos\left(\theta_{k_r}\right)\right)\cos\left(\angle Y_{ii}-\angle Y_{ik}\right) \\ &= b_o \quad (4.37)\end{aligned}$$

where $\rho_{R_iR_k}$ is the cross-correlation factor of the real component of the Rayleigh fading value at antenna element $i$ with the real component of the Rayleigh fading value at antenna element $k$, $\rho_{R_iI_k}$ is the cross-correlation factor of the real component of the Rayleigh fading value at antenna $i$ with the imaginary component of the Rayleigh fading value at element $j$, and $b_o$ is the mean-squared value of $B_{1c}$, $B_{1s}$, $B_{2c}$, and $B_{2s}$.

Substituting Equation (4.13) into Equations (4.35) and (4.36), we obtain

$$\begin{aligned}\rho_{R_iR_k} &= 2|Y_{ii}||Y_{ki}|\int_0^{2\pi} P(\theta)\cos\left(\angle Y_{ii} - \angle Y_{ki}\right)d\theta \\ &+ \left(|Y_{ii}|^2 + |Y_{ik}|^2\right)\int_0^{2\pi} P(\theta)\cos\left(\frac{2\pi d}{\lambda}\cos\left(\theta\right)\right)d\theta \end{aligned} \tag{4.38}$$

$$\rho_{R_iI_k} = -\left(|Y_{ii}|^2 - |Y_{ik}|^2\right)\int_0^{2\pi} P(\theta)\sin\left(\frac{2\pi d}{\lambda}\cos\left(\theta\right)\right)d\theta \tag{4.39}$$

Our derivation of a cross-correlation model assuming a generalized spatial distribution $P(\theta)$ is now complete, resulting with Equations (4.38) and (4.39). In the subsequent subsections, the cases of uniform and Gaussian AOA distributions will be examined.

### 4.3.1 Use of a Gaussian Distribution for $P(\theta)$

If a Gaussian distribution is used for $P(\theta)$ with mean AOA $\theta_k$ and variance $\sigma_\Delta^2$, namely

$$P(\theta) = \frac{1}{\sqrt{2\pi\sigma_\Delta^2}} e^{\frac{-(\theta-\theta_k)^2}{2\sigma_\Delta^2}} \tag{4.40}$$

then Equations (4.38) and (4.39) become

$$\begin{aligned}\rho_{R_iR_k} &= 2|Y_{ii}||Y_{ki}|\cos\left(\angle Y_{ii} - \angle Y_{ki}\right)\left(erf\left(\frac{2\pi-\theta_k}{\sigma_\Delta}\right) + erf\left(\frac{\theta_k}{\sigma_\Delta}\right)\right) \\ &+ \left(|Y_{ii}|^2 + |Y_{ik}|^2\right)\left(J_o\left(\frac{2\pi d}{\lambda}\right) + 2\sum_{m=1}^{\infty} J_{2m}\left(\frac{2\pi d}{\lambda}\right)\cos\left(2m\theta_k\right)e^{-2m^2\sigma_\Delta^2}\right)\end{aligned} \tag{4.41}$$

$$\rho_{R_iI_k} = -\left(|Y_{ii}|^2 - |Y_{ik}|^2\right)\left(2\sum_{m=1}^{\infty} J_{2m+1}\left(\frac{2\pi d}{\lambda}\right)\sin\left(\left(2m+1\right)\theta_k\right)e^{\frac{-(2m+1)^2\sigma_\Delta^2}{2}}\right) \tag{4.42}$$

where $erf(.)$ is the error function, defined as

$$erf\left(x\right) = \frac{2}{\sqrt{\pi}}\int_0^x e^{-t^2}dt$$

In determining Equations (4.41) and (4.42), the integration is performed over $[0, 2\pi)$. Furthermore, it should be noted that for these integrals, the Gaussian AOA distribution is being truncated. Thus, as $\sigma_\Delta^2$ increases, Equations (4.41) and (4.42) become less close to a true Gaussian AOA distribution.

Figures 4.3, 4.4, 4.5, and 4.6 exhibit the relationship of the cross-correlation between antennas and their spacing. In these figures, mean arrival angles of $0^o$ and $90^o$, as well as angle spreads of $3^o$, $5^o$, $10^o$, $20^o$, $40^o$, $90^o$, and $180^o$, were used. In particular, the graphs show the relationship for the cross-correlation coefficients between the real components of the Rayleigh fading between two antennas as a function of antenna spacing. Figures 4.3 and 4.5 assume a (truncated) Gaussian AOA distribution where the arrival angles are $0^o$ and $90^o$, respectively, and where the effects of mutual coupling in the antenna array are not considered. We can compare these figures to Figures 3.4 and 3.5 in [12], where the same assumptions were also made. From this comparison, we see that they compare closely. Figures 4.4 and 4.6 also assume a Gaussian AOA distribution where the mean arrival angles are $0^o$ and $90^o$, respectively, but also contain the effects of mutual coupling in the antenna array. Figures 4.3 to 4.6 were generated using Equation (4.41). Similar plots may also be obtained for the correlation coefficient between the real component of the Rayleigh fading value at one antenna and the imaginary component of the Rayleigh fading value at another using Equation (4.42).

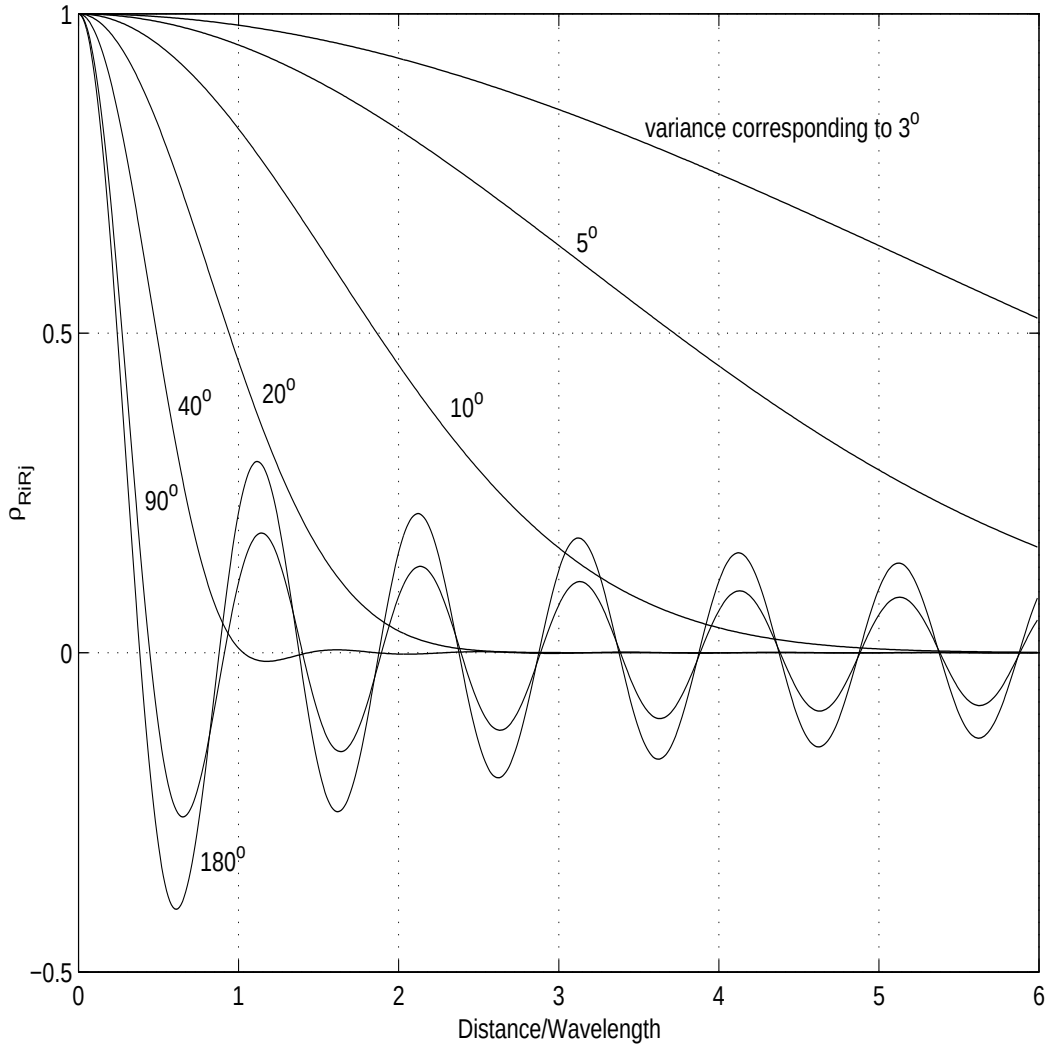


Figure 4.3: Correlation of the real portion of the fading versus antenna spacing for $\theta = 0^o$ and Gaussian angle-of-arrival distribution (mutual coupling effects ignored)

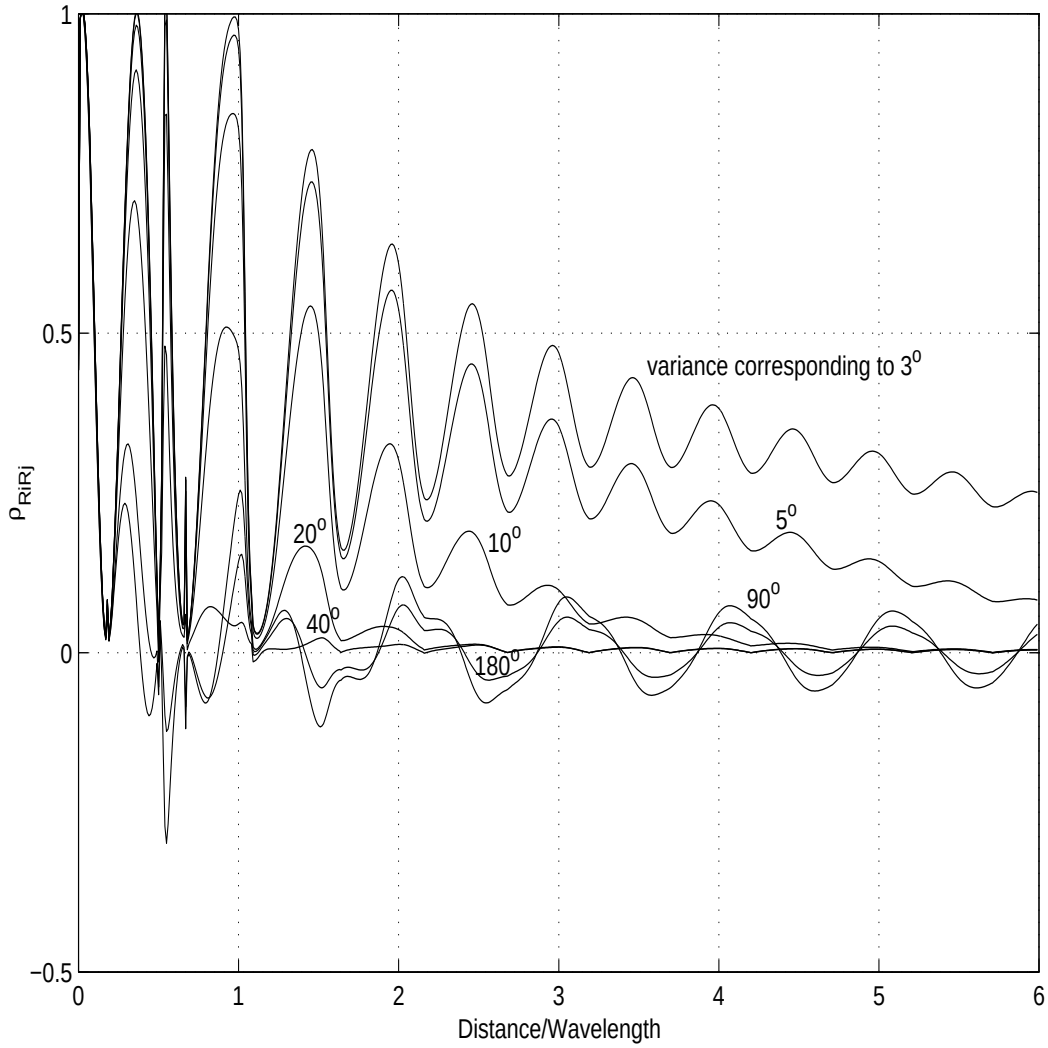


Figure 4.4: Correlation of the real portion of the fading versus antenna spacing for $\theta = 0^o$ and Gaussian angle-of-arrival distribution (mutual coupling effects included)

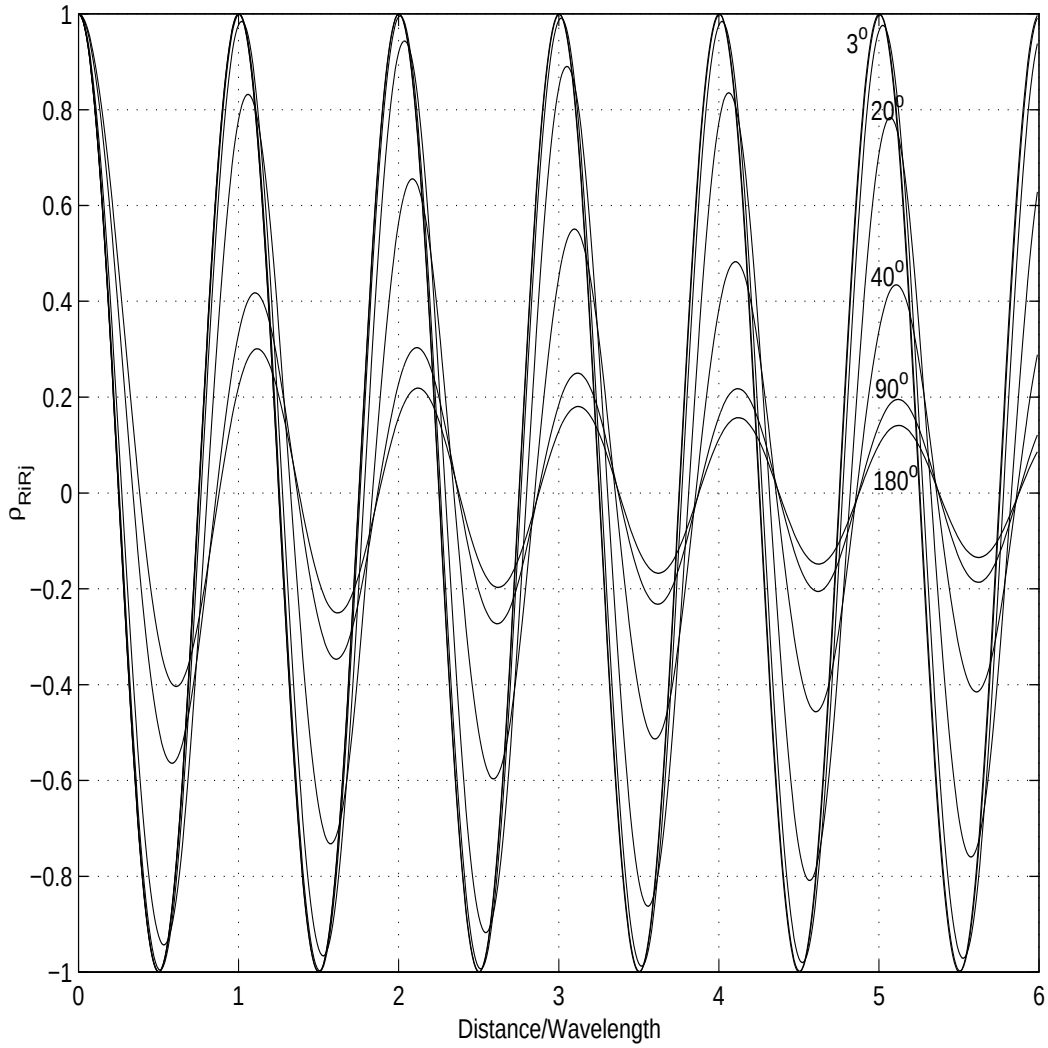


Figure 4.5: Correlation of the real portion of the fading versus antenna spacing for $\theta = 90^o$ and Gaussian angle-of-arrival distribution (mutual coupling effects ignored)

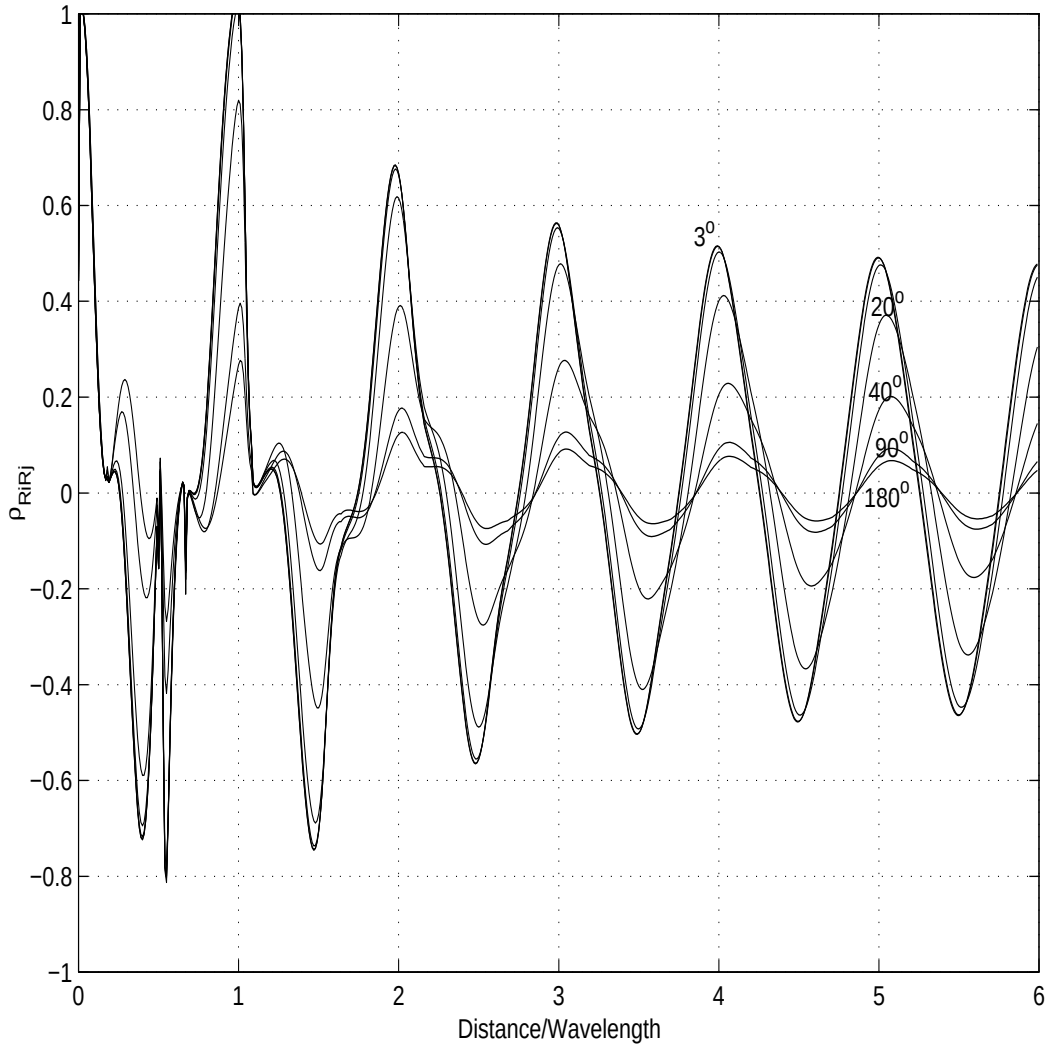


Figure 4.6: Correlation of the real portion of the fading versus antenna spacing for $\theta = 90^o$ and Gaussian angle-of-arrival distribution (mutual coupling effects included)

### 4.3.2 Use of a Uniform Distribution for $P(\theta)$

If an uniform distribution is used for $P(\theta)$ with beamwidth $[\theta_k - \Delta, \theta_k + \Delta]$, namely

$$P(\theta) = \begin{cases} \frac{1}{2\Delta}, & \theta_k - \Delta \leq \theta \leq \theta_k + \Delta \\ 0, & otherwise \end{cases} \tag{4.43}$$

then Equations (4.38) and (4.39) become

$$\begin{aligned} \rho_{R_i R_k} &= 2|Y_{ii}||Y_{ki}|\cos\left(\angle Y_{ii} - \angle Y_{ki}\right) \\ &+ \left(|Y_{ii}|^2 + |Y_{ik}|^2\right)\left(J_o\left(\frac{2\pi d}{\lambda}\right) + 2\sum_{m=1}^{\infty} J_{2m}\left(\frac{2\pi d}{\lambda}\right)\cos\left(2m\theta_k\right)\frac{\sin(2m\Delta)}{2m\Delta}\right) \end{aligned} \tag{4.44}$$

$$\rho_{R_i I_k} = -\left(|Y_{ii}|^2 - |Y_{ik}|^2\right)\left(2\sum_{m=1}^{\infty} J_{2m+1}\left(\frac{2\pi d}{\lambda}\right)\sin\left((2m+1)\,\theta_k\right)\frac{\sin((2m+1)\Delta)}{(2m+1)\Delta}\right) \tag{4.45}$$

Figures 4.7, 4.8, 4.9, and 4.10 are coefficients generated using Equation (4.44) and exhibit the cross-correlation coefficients between the real components of the Rayleigh fading between two antennas as a function of antenna spacing for both mean arrival angles of $0^o$ and $90^o$ as well as angle spreads of $3^o$, $5^o$, $10^o$, $20^o$, $40^o$, and $90^o$. Figures 4.7 and 4.9 assume a Uniform AOA distribution where the effects of mutual coupling in the antenna array are not considered. They compare closely to Figures 3.2 and 3.3 in [12], where the same assumptions were made. Figures 4.8 and 4.10 also assume a Uniform AOA distribution but the effects of mutual coupling in the antenna array are also considered. Similar plots can be obtained for $\rho_{R_i I_k}$ using Equation (4.45).

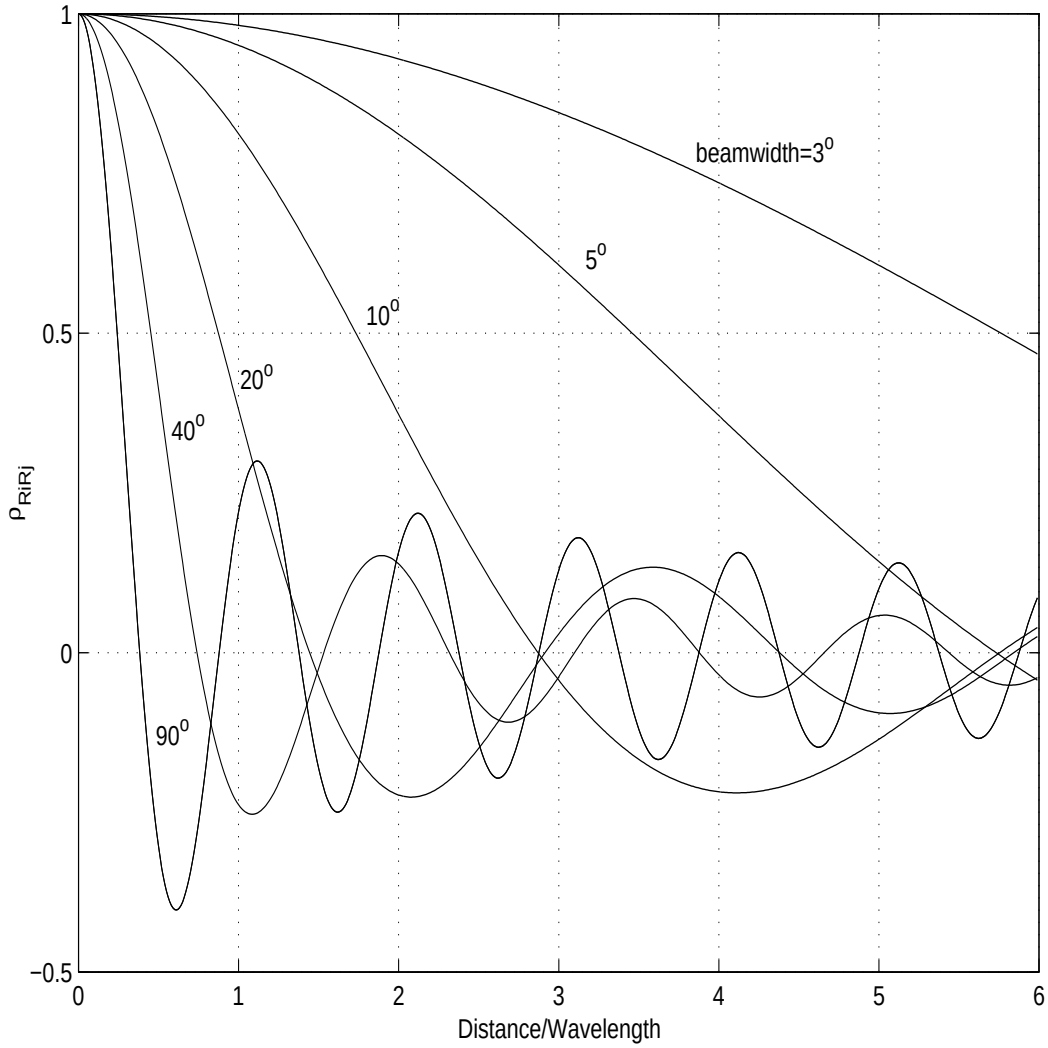


Figure 4.7: Correlation of the real portion of the fading versus antenna spacing for $\theta = 0^o$ and Uniform angle-of-arrival distribution (mutual coupling effects ignored)

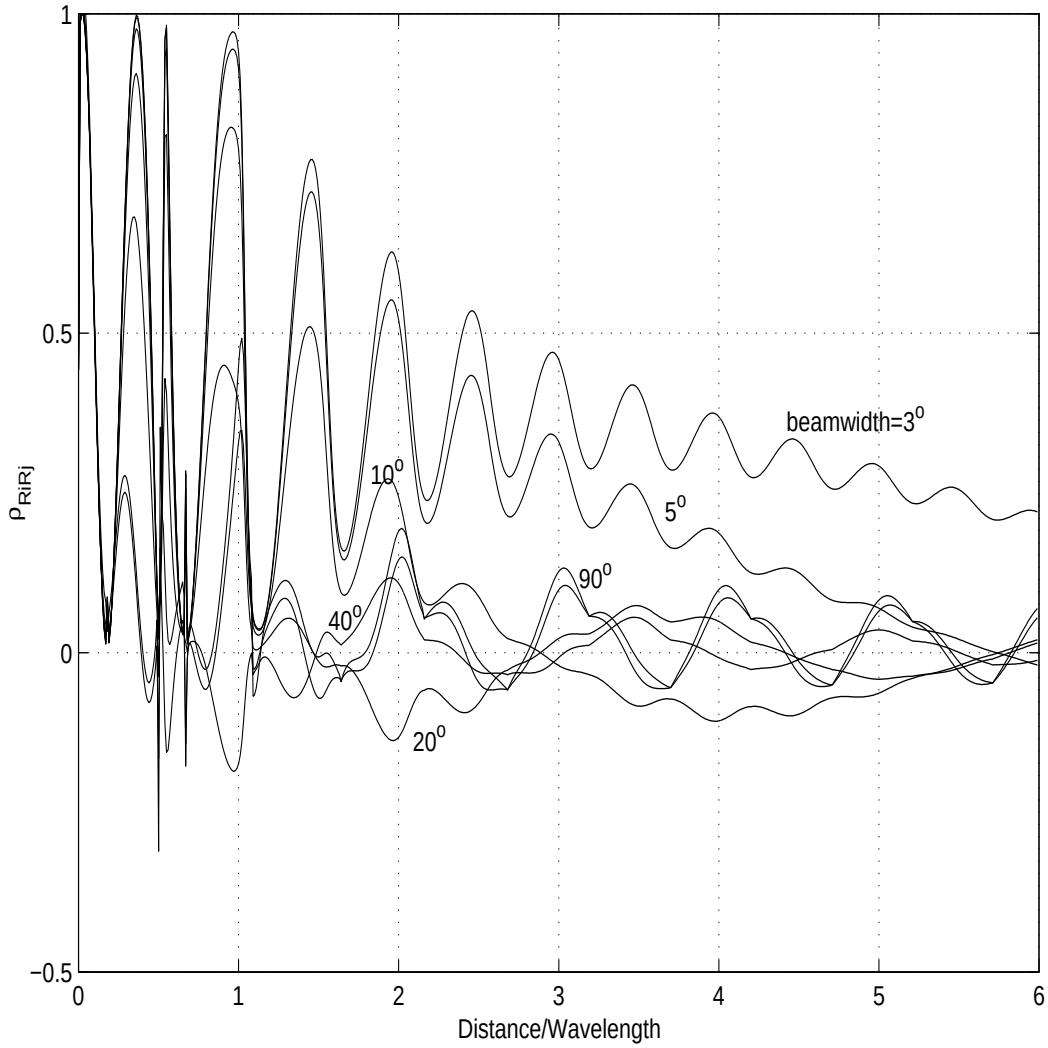


Figure 4.8: Correlation of the real portion of the fading versus antenna spacing for $\theta = 0^o$ and Uniform angle-of-arrival distribution (mutual coupling effects included)

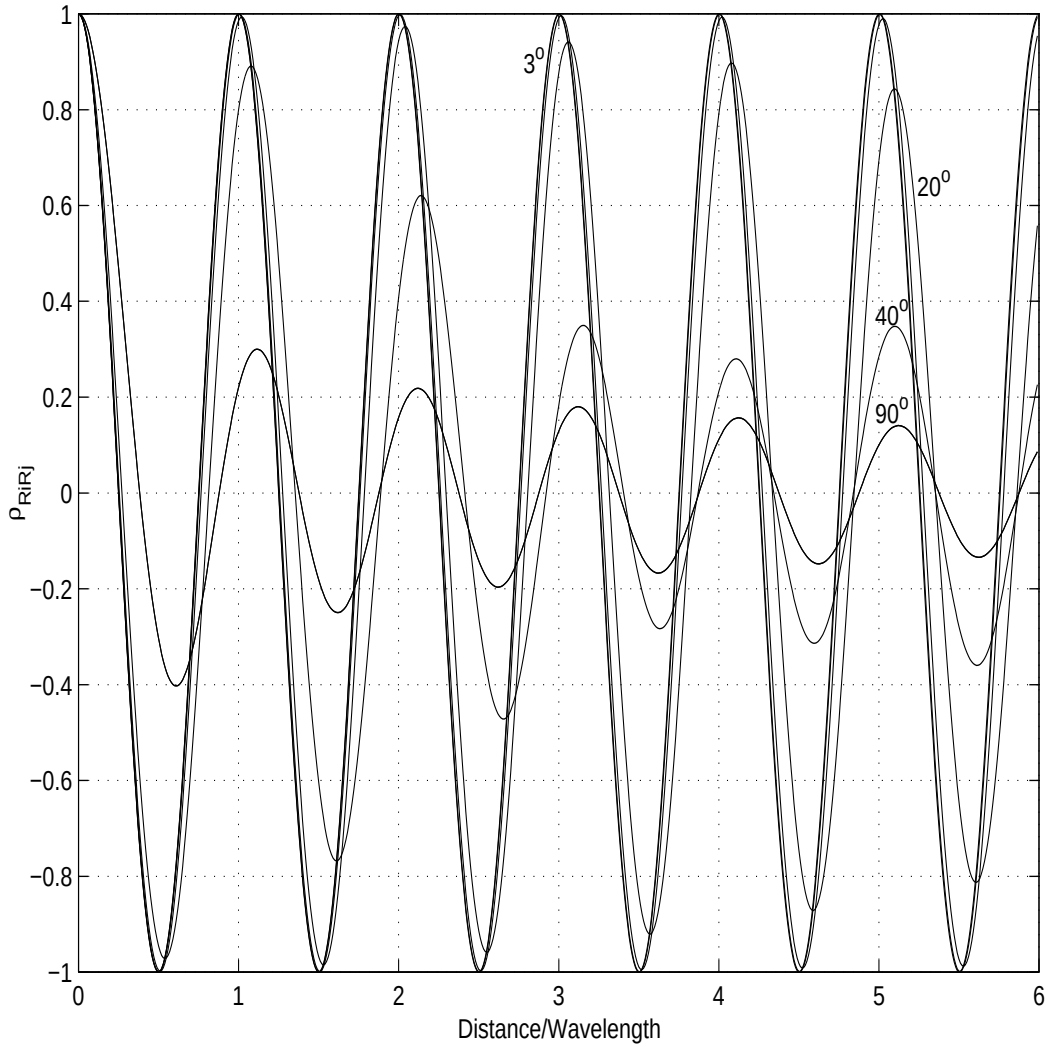


Figure 4.9: Correlation of the real portion of the fading versus antenna spacing for $\theta = 90^o$ and Uniform angle-of-arrival distribution (mutual coupling effects ignored)

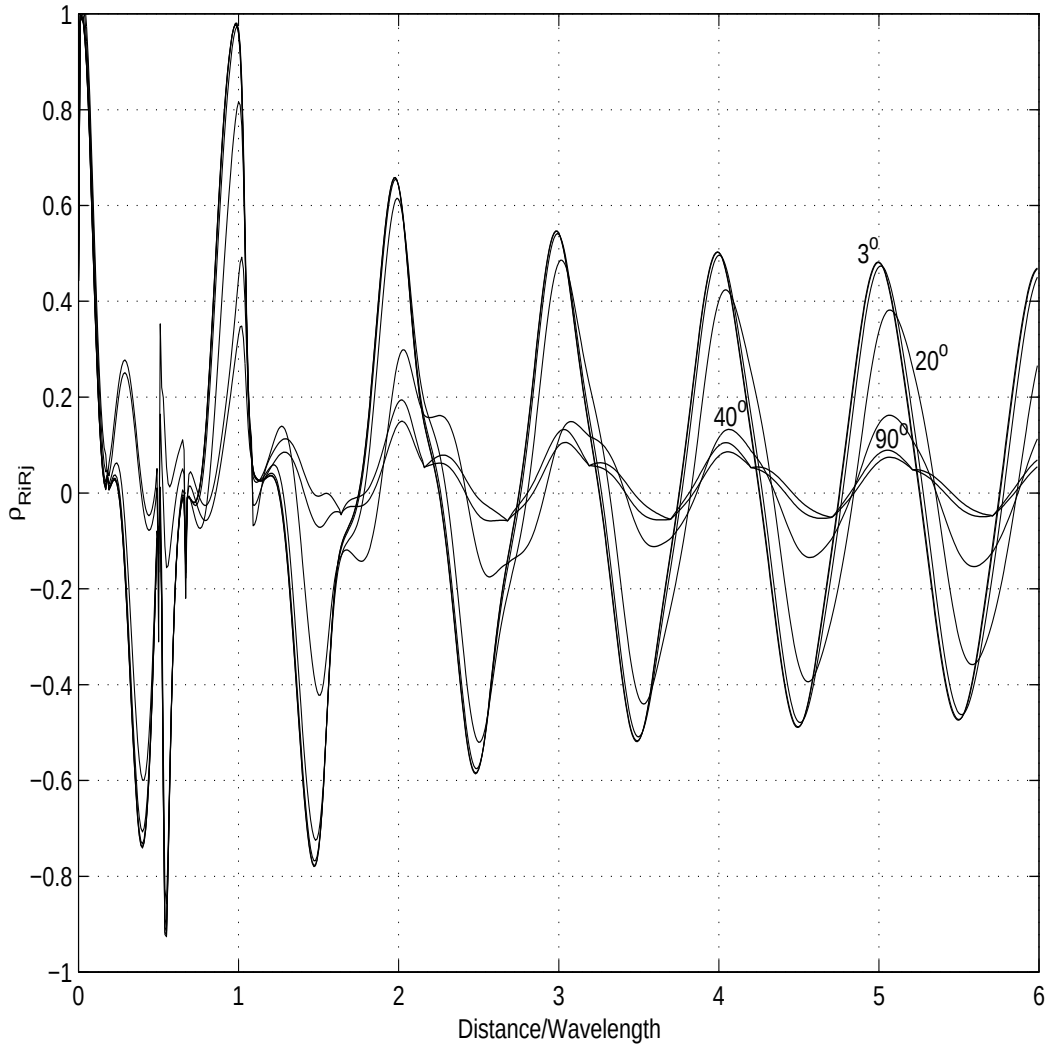


Figure 4.10: Correlation of the real portion of the fading versus antenna spacing for $\theta = 90^o$ and Uniform angle-of-arrival distribution (mutual coupling effects included)

## 4.4 System Capacity Prediction

In this section, we extend the system capacity prediction technique of Section 3.4 to the case of scattering environments.

Although the work Colman presented in [12] provided some insight into this enhancement of system capacity predictions, Colman approached this problem using two different methods: the Beampattern Method in Section 4.4.1 of [12], and the Mobile Power Prediction Using Cross-Correlation Statistics Method in Section 4.4.2 of [12]. Colman claimed that the first method provided an overly pessimistic view on the power levels and capacity of the system, while the second method was considered more in-depth and thus relatively more accurate, exhibiting significant capacity benefits even in high scatter environments. After a closer inspection of the analysis conducted in [12], it appears that Colman's conclusions were inaccurate due to an incomplete setup of the analysis. Ironically, these two methods which Colman derived complemented one another in the sense that the Beampattern Method analyzed the effects of scattering on the received phase information while the Cross-Correlation Statistics Method analyzed the effects of scattering on the received amplitude information.

In the method which we shall present in the following subsection, both the received amplitude and phase information account for the effects of the scattering environment. Furthermore, our method also includes the effects of mutual coupling in the base station antenna array.

### 4.4.1 Determining $E\{\phi_k\}$ and $E\{\phi_d\}$

To assess the capacity of CDMA systems, we first derive the expected interference

and mobile power, $E\{\phi_k\}$ and $E\{\phi_d\}$ respectively, in a scattering environment where the effects of mutual coupling in the array are accounted for. The effects of mutual coupling were analyzed using the induced EMF method, as described in Section 3.3.1.1, and is used throughout this section.

Assuming that maximum SNR beamforming is performed in a circular antenna array, our beamforming weight vector is given as

$$\bar{\omega}\left(\theta_d\right) = \begin{bmatrix} e^{jw_0(\theta_d)} \\ e^{jw_1(\theta_d)} \\ e^{jw_2(\theta_d)} \\ \vdots \\ e^{jw_{(N_A-1)}(\theta_d)} \end{bmatrix} \tag{4.46}$$

where the phase delay for $i$th element of the array, $w_i\left(\theta_d\right)$, is

$$w_i\left(\theta_d\right) = \frac{\pi \cos\left(\theta_d - i\frac{2\pi}{N_A}\right)}{2\sin\left(\frac{\pi}{N_A}\right)} \tag{4.47}$$

It should be noted that these beamforming weights can be changed to correspond to other array geometries without loss of generality.

To account for the effects of mutual coupling, the $N_A \times N_A$ mutual impedance matrix $[Z]$ derived in Section 3.3.1.1 is used in the matrix equation

$$\bar{\omega}_{MC}\left(\theta_d\right) = [Z]^{-1}\bar{\omega}\left(\theta_d\right) = [Y]\bar{\omega}\left(\theta_d\right) \tag{4.48}$$

where the information concerning the effects of mutual coupling is included in the modified beamforming weight vector $\bar{\omega}_{MC}\left(\theta_d\right)$, $[Z]^{-1}$ is the matrix inverse of $[Z]$, $[Y]$ is equal to $[Z]^{-1}$, and both $[Y]$ and $[Z]$ are $N_A \times N_A$ dimensioned matrices where $N_A$ is the number of array elements.

Using Equation (2.2), we need to modified the array response vector in this derivation to account for the received signal power due to mobile $k$ at element $i$, which we

denote as $\beta_{ki}$. We define the $N_A \times N_A$ received signal power matrix $[\beta_k]$ as

$$[\beta_k] = \begin{bmatrix} \beta_{k1} & 0 & \cdots & 0 \\ 0 & \beta_{k2} & & \vdots \\ \vdots & & \ddots & 0 \\ 0 & \cdots & 0 & \beta_{kN_A} \end{bmatrix} \tag{4.49}$$

where the diagonal matrix elements are the corresponding values of $\beta_{ki}$.

Therefore, the modified array response vector $\bar{a}_{\beta_k}$ can be obtained using matrix multiplication, yielding

$$\bar{a}_{\beta_k}(\theta_k) = [\beta_k]\bar{a}(\theta_k) = \begin{bmatrix} \beta_{k1} \\ \beta_{k2} e^{j\alpha_1(\theta_k)} \\ \beta_{k3} e^{j\alpha_2(\theta_k)} \\ \vdots \\ \beta_{kN_A} e^{j\alpha_{(N_A-1)}(\theta_k)} \end{bmatrix} \tag{4.50}$$

where the phase delay for $i$th element of the array, $\alpha_i$, is

$$\alpha_i(\theta_k) = \frac{\pi \cos\left(\theta_k - i\frac{2\pi}{N_A}\right)}{2\sin\left(\frac{\pi}{N_A}\right)} \tag{4.51}$$

and $\bar{a}_\beta$ contains the received signal strength information.

Using Equations (4.48) and (4.50), the normalized amount of interference power seen from an interferer $k$ at an angle-of-arrival $\theta_k$ is

$$\phi_k(\theta_d, \theta_k) = \left| \frac{\bar{\omega}_{MC}^{\mathbf{H}}(\theta_d)}{\|\bar{\omega}_{MC}^{\mathbf{H}}(\theta_d)\|} \frac{\bar{a}_{\beta_k}(\theta_k)}{\|\bar{a}_{\beta_k}(\theta_k)\|} \right|^2 \tag{4.52}$$

where $\bar{\omega}_{MC}^{\mathbf{H}}(\theta_d)$ denotes the complex conjugate transpose of $\bar{\omega}_{MC}(\theta_d)$ and $\|.\|$ is the Euclidean norm.

In its current form, Equation (4.52) is not a convenient representation and requires further manipulation. We proceed by excluding the normalizing factors $\left\|\bar{\omega}_{MC}^{\mathbf{H}}(\theta_d)\right\|$

and $\|\bar{a}_{\beta_k}(\theta_k)\|$ for the time being. Therefore, without normalization, Equation (4.52) becomes

$$\begin{aligned}
\left|\bar{\omega}_{MC}^{\mathbf{H}}(\theta_d)\bar{a}_{\beta_k}(\theta_k)\right|^2 &= \left|\left([Y]\bar{\omega}(\theta_d)\right)^{\mathbf{H}}\left([\beta_k]\bar{a}(\theta_k)\right)\right|^2 \\
&= \left|\bar{\omega}^{\mathbf{H}}(\theta_d)[Y]^{\mathbf{H}}[\beta_k]\bar{a}(\theta_k)\right|^2 \\
&= \left(\bar{\omega}^{\mathbf{H}}(\theta_d)[Y]^{\mathbf{H}}[\beta_k]\bar{a}(\theta_k)\right)\left(\bar{\omega}^{\mathbf{H}}(\theta_d)[Y]^{\mathbf{H}}[\beta_k]\bar{a}(\theta_k)\right)^{\mathbf{H}} \\
&= \left(\bar{\omega}^{\mathbf{H}}(\theta_d)[Y]^{\mathbf{H}}[\beta_k]\bar{a}(\theta_k)\right)\left(\bar{a}^{\mathbf{H}}(\theta_k)[\beta_k]^{\mathbf{H}}[Y]\bar{\omega}(\theta_d)\right) \\
&= \bar{\omega}^{\mathbf{H}}(\theta_d)[Y]^{\mathbf{H}}[\beta_k]\bar{a}(\theta_k)\bar{a}^{\mathbf{H}}(\theta_k)[\beta_k]^{\mathbf{H}}[Y]\bar{\omega}(\theta_d) \qquad (4.53)
\end{aligned}$$

Using the following transformations

$$\begin{aligned}
a_i &= \frac{\pi\cos\left(\theta_k-(i-1)\frac{2\pi}{N_A}\right)}{2\sin(\pi/N_A)} \qquad a_r = \frac{\pi\cos\left(\theta_k-(r-1)\frac{2\pi}{N_A}\right)}{2\sin(\pi/N_A)} \\
w_p &= \frac{\pi\cos\left(\theta_d-(p-1)\frac{2\pi}{N_A}\right)}{2\sin(\pi/N_A)} \qquad w_l = \frac{\pi\cos\left(\theta_d-(l-1)\frac{2\pi}{N_A}\right)}{2\sin(\pi/N_A)} \qquad (4.54)
\end{aligned}$$

and after extensive manipulations, Equation (4.53) can equivalently be written in a component form involving multiple summations as

$$\left|\bar{\omega}_{MC}^{\mathbf{H}}(\theta_d)\bar{a}_{\beta_k}(\theta_k)\right|^2 = \sum_{i=1}^{N_A}\sum_{l=1}^{N_A}\sum_{p=1}^{N_A}\sum_{r=1}^{N_A}\beta_{ki}\beta_{kr}^{*}Y_{li}^{*}Y_{rp}e^{j(a_i+w_p-a_r-w_l)} \qquad (4.55)$$

where $Y_{li}$ and $Y_{rp}$ are the normalized elements of the admittance matrix $[Y]$, the inverse of the mutual impedance matrix $[Z]$.

Returning to Equation (4.52), the normalizing factors, $\left\|\bar{\omega}_{MC}^{\mathbf{H}}(\theta_d)\right\|$ and $\|\bar{a}_{\beta_k}(\theta_k)\|$ can be expressed as

$$\begin{aligned}
\|\bar{a}_{\beta_k}(\theta_k)\| &= \left(\left([\beta_k]\bar{a}(\theta_k)\right)^{\mathbf{H}}\left([\beta_k]\bar{a}(\theta_k)\right)\right)^{\frac{1}{2}} \\
&= \left(\bar{a}^{\mathbf{H}}(\theta_k)[\beta_k]^{\mathbf{H}}[\beta_k]\bar{a}(\theta_k)\right)^{\frac{1}{2}} \\
&= \sum_{i=1}^{N_A}\beta_{ki}^2 \qquad (4.56)
\end{aligned}$$

$$\begin{aligned}\left\|\bar{\omega}_{MC}^{\mathbf{H}}(\theta_d)\right\| &= \left(\left(\bar{\omega}_{MC}^{\mathbf{H}}(\theta_d)\right)^{\mathbf{H}}\left(\bar{\omega}_{MC}^{\mathbf{H}}(\theta_d)\right)\right)^{\frac{1}{2}} \\ &= \left(\bar{\omega}^{\mathbf{H}}(\theta_d)[Y]^{\mathbf{H}}[Y]\bar{\omega}(\theta_d)\right)^{\frac{1}{2}} \\ &= \sum_{h=1}^{N_A}\sum_{s=1}^{N_A}\sum_{m=1}^{N_A} e^{j(w_h-w_s)}Y_{sm}^{*}Y_{mh} \end{aligned} \tag{4.57}$$

using the transformations

$$w_h = \frac{\pi\cos\left(\theta_d-(h-1)\frac{2\pi}{N_A}\right)}{2\sin(\pi/N_A)} \qquad w_s = \frac{\pi\cos\left(\theta_d-(s-1)\frac{2\pi}{N_A}\right)}{2\sin(\pi/N_A)} \tag{4.58}$$

Using Equations (4.55), (4.56), and (4.57) in Equation (4.52), we would obtain a form convenient for numerical computation. Before proceeding, Equations (4.55) and (4.56) require some additional modifications concerning the received signal strength $\beta_{ki}$.

Defining $\beta_{ki} = \eta_k R_{ki}$, Equation (4.55) and Equation (4.56), respectively, can be rewritten as

$$\begin{aligned}&\sum_{i=1}^{N_A}\sum_{l=1}^{N_A}\sum_{p=1}^{N_A}\sum_{r=1}^{N_A}\beta_{ki}\beta_{kr}^{*}Y_{li}^{*}Y_{rp}e^{j(a_i+w_p-a_r-w_l)} \\ &\qquad = \sum_{i=1}^{N_A}\sum_{l=1}^{N_A}\sum_{p=1}^{N_A}\sum_{r=1}^{N_A}\eta_k^2 R_{ki}R_{kr}Y_{li}^{*}Y_{rp}e^{j(a_i+w_p-a_r-w_l)}\end{aligned} \tag{4.59}$$

$$\sum_{i=1}^{N_A}\beta_{ki}^2 = \sum_{i=1}^{N_A}\eta_k^2 R_{ki}^2 \tag{4.60}$$

where $\eta_k$ is the path loss and shadowing effects factor at mobile $k$, and $R_{ki}$ and $R_{kr}$ are Rayleigh fading random variables for mobile $k$ at array elements $i$ and $r$, respectively. Both $\eta_k$ and $R_{ki}$ are functions of two Gaussian-distributed random variables. The factor $\eta_k$ is assumed to be independent of $R_{ki}$ and is identically distributed across the antenna array.

We assume that both $\theta_k$ and $\theta_d$ are random variables uniformly distributed over $[0^o, 360^o)$. The expected values of Equations (4.59) and (4.60) conditioned on $\theta_k$, $\theta_d$,

and $\sigma_\Delta^2$ are, respectively,

$$E\left\{\sum_{i=1}^{N_A}\sum_{l=1}^{N_A}\sum_{p=1}^{N_A}\sum_{r=1}^{N_A}\eta_k^2 R_{ki}R_{kr}Y_{li}^*Y_{rp}e^{j(a_i+w_p-a_r-w_l)}\middle|\,\theta_k,\theta_d,\sigma_\Delta^2\right\}$$
$$= E\left\{\eta_k^2\right\}\sum_{i=1}^{N_A}\sum_{l=1}^{N_A}\sum_{p=1}^{N_A}\sum_{r=1}^{N_A}E\left\{R_{ki}R_{kr}\middle|\,\sigma_\Delta^2\right\}Y_{li}^*Y_{rp}e^{j(a_i+w_p-a_r-w_l)} \quad (4.61)$$

$$E\left\{\sum_{i=1}^{N_A}\eta_k^2 R_{ki}^2\middle|\,\theta_k,\theta_d,\sigma_\Delta^2\right\} = E\left\{\eta_k^2\right\}\sum_{i=1}^{N_A}E\left\{R_{ki}^2\middle|\,\sigma_\Delta^2\right\} \quad (4.62)$$

where $\sigma_\Delta^2$ is the variance of the spatial AOA distribution $P(\theta)$.

Using the second-order statistics of the cross-correlation model derived in Section 4.3, the cross-correlation matrix between antenna elements $i$ and $j$, $\mathcal{R}$, is

$$\mathcal{R} = \begin{bmatrix} \rho_{R_iR_i} & \rho_{R_iI_i} & \rho_{R_iR_j} & \rho_{R_iI_j} \\ \rho_{I_iR_i} & \rho_{I_iI_i} & \rho_{I_iR_j} & \rho_{I_iI_j} \\ \rho_{R_iR_j} & -\rho_{I_iR_j} & \rho_{R_jR_j} & \rho_{R_jI_j} \\ \rho_{R_iI_j} & \rho_{I_iI_j} & \rho_{I_jR_j} & \rho_{I_jI_j} \end{bmatrix} \quad (4.63)$$

which simplifies to

$$\mathcal{R} = \begin{bmatrix} b_o & 0 & \rho_{R_iR_j} & \rho_{R_iI_j} \\ 0 & b_o & \rho_{I_iR_j} & \rho_{I_iI_j} \\ \rho_{R_iR_j} & -\rho_{I_iR_j} & b_o & 0 \\ \rho_{R_iI_j} & \rho_{I_iI_j} & 0 & b_o \end{bmatrix} \quad (4.64)$$

where, referring to Equation (4.38), $\rho_{RiRj}$ is the correlation coefficient between the real component of the Rayleigh fading at antenna $i$ and the real component of the Rayleigh fading at antenna $j$. Furthermore, as shown in Equation (4.39), $\rho_{RiIk}$ is the correlation coefficient between the real component of the Rayleigh fading at antenna $i$ and the imaginary component of the Rayleigh fading at antenna $j$. Finally $b_o$ is the mean-squared value of the real or imaginary component of the Rayleigh fading at antenna $i$ or antenna $j$, as shown in Equation (4.37).

Davenport and Root in [15] have shown that $E\{R_{ki}R_{kj}\}$, the cross-correlation between the Rayleigh distributed random variables at antennas $i$ and $j$ due to mobile $k$, can be given in terms of the confluent hypergeometric function ${}_2F_1\left(-\frac{1}{2},-\frac{1}{2};1;.\right)$ yielding

$$E\{R_{ki}R_{kj}\} = \frac{\pi}{2}b_o\left({}_2F_1\left(-\frac{1}{2},-\frac{1}{2};1;\zeta_{ji}^2\right)\right) \tag{4.65}$$

where

$$\zeta_{ji}^2 = \frac{\rho_{R_iR_j}^2 + \rho_{R_iI_j}^2}{b_o^2} \tag{4.66}$$

such that for the case of maximum correlation between array elements, Equation (4.65) equals 2. Furthermore, as the correlation decreases, Equation (4.65) decreases to a minimum of $\frac{\pi}{2}$. The decrease of correlation will occur when the angle-of-arrival distribution variance increases, affecting the off-main diagonal matrix elements of $\mathcal{R}$.

Using Equations (4.65), (4.61), (4.57), and (4.62), Equation (4.52) can be rewritten as

$$\begin{aligned}\phi_k(\theta_d,\theta_k) &= \frac{\left(E\{\eta_k^2\}\sum_{i=1}^{N_A}\sum_{l=1}^{N_A}\sum_{p=1}^{N_A}\sum_{r=1}^{N_A}E\{R_{ki}R_{kr}|\,\sigma_\Delta^2\}Y_{li}^*Y_{rp}e^{j(a_i+w_p-a_r-w_l)}\right)}{\left(E\{\eta_k^2\}\sum_{i=1}^{N_A}E\{R_{ki}^2|\,\sigma_\Delta^2\}\right)\left(\sum_{h=1}^{N_A}\sum_{s=1}^{N_A}\sum_{m=1}^{N_A}e^{j(w_h-w_s)}Y_{sm}^*Y_{mh}\right)} \\ &= \frac{\sum_{i=1}^{N_A}\sum_{l=1}^{N_A}\sum_{p=1}^{N_A}\sum_{r=1}^{N_A}\frac{\pi}{2}b_o\left({}_2F_1\left(-\frac{1}{2},-\frac{1}{2};1;\zeta_{ji}^2\right)\right)Y_{li}^*Y_{rp}e^{j(a_i+w_p-a_r-w_l)}}{2N_A\sum_{h=1}^{N_A}\sum_{s=1}^{N_A}\sum_{m=1}^{N_A}e^{j(w_h-w_s)}Y_{sm}^*Y_{mh}}\end{aligned} \tag{4.67}$$

where $a_i$, $a_r$, $w_p$, $w_l$, $w_h$, and $w_s$ are defined in Equations (4.54) and (4.58).

Using Equation (4.67), the interference power contribution of interferer $k$

$$P_{I_k} = \phi_k P_R \tag{4.68}$$

can be determined, where $P_{I_k}$ is the received interference power from $k$th mobile and $P_R$ is the received signal power due to the desired user.

Thus, the expected total inference power would be

$$\begin{aligned} E\{P_I\} &= E\left\{\sum_{k=1}^{N_I} P_{I_k}\right\} \\ &= E\left\{\sum_{k=1}^{N_I} \phi_k P_R\right\} \\ &= E\left\{P_R \sum_{k=1}^{N_I} \phi_k\right\} \\ &= P_R \sum_{k=1}^{N_I} E\{\phi_k\} \\ &= P_R N_I E\{\phi_k\} \end{aligned} \tag{4.69}$$

such that the individual paths will be suppressed according to the beamforming pattern and its position relative to the base station antenna array.

In order to compute $E\{\phi_k\}$, Equation (4.67) must be averaged over uniformly-distributed $\theta_k$ and $\theta_d$, yielding

$$E\{\phi_k\} = \frac{1}{N_\theta^2} \sum_{\theta_d \in \Theta_d} \sum_{\theta_k \in \Theta_k} \phi_k(\theta_k, \theta_d) \tag{4.70}$$

where $\Theta_k$ and $\Theta_d$ are sets of $N_\theta$ angles-of-arrival that range uniformly over $[0^o, 360^o)$.

Similarly, due to the fact that some of the desired signal will be suppressed because not all of the signal is located at the maximum of the spatial filter corresponding to the maximum SNR beamformer, the percentage of the desired signal being passed by the beamforming pattern for a mean angle-of-arrival $\theta_d$ must be determined. This may be accomplished by using Equation (4.67), yielding

$$\phi_d = \frac{2\pi}{N_\theta} \sum_{\theta \in \Theta} P(\theta) \phi_k(\theta, \theta_d) \tag{4.71}$$

where $P(\theta)$ is the spatial distribution of the incoming signal, and $\Theta$ is a set of $N_\theta$ angles-of-arrival that range uniformly over $[0^o, 360^o)$.

For the general case where $P(\theta)$ is not specified, the expected percentage of the desired signal being passed by the beamforming pattern, $E\{\phi_d\}$, is determined by

averaging Equation (4.71) uniformly over $\theta_d$, resulting in

$$E\{\phi_d\} = \frac{1}{N_\theta}\frac{2\pi}{N_\theta}\sum_{\theta_d\in\Theta_d}\sum_{\theta\in\Theta} P(\theta)\phi_k(\theta,\theta_d) \tag{4.72}$$

where $\Theta_d$ is a set of $N_\theta$ angles-of-arrival that range uniformly over $[0^o, 360^o)$.

In the following two sub-sections, the expected percentage of the desired signal being passed by the beamforming pattern will be derived for the cases of Gaussian and uniform $P(\theta)$, respectively.

#### 4.4.1.1 Determining $E\{\phi_d\}$ for a Gaussian $P(\theta)$

A Gaussian $P(\theta)$ with mean $\theta_d$ and variance equivalent to that of a uniform distribution over $[\theta_d - \Delta, \theta_d + \Delta]$ is defined as

$$P(\theta) = \sqrt{\frac{3}{2\pi\Delta^2}}e^{-\frac{3(\theta-\theta_d)^2}{2\Delta^2}} \tag{4.73}$$

where $\sigma_\Delta^2 = \frac{\Delta^2}{3}$.

Therefore, the expected percentage of the desired signal being passed by the beamforming pattern, $E\{\phi_d\}$, is determined by averaging Equation (4.71) uniformly over $\theta_d$. Thus, using Equations (4.72) and (4.73) yields

$$E\{\phi_d\} = \frac{\sqrt{6\pi}}{N_\theta^2}\frac{1}{|\Delta|}\sum_{\theta_d\in\Theta_d}\sum_{\theta\in\Theta} e^{-\frac{3(\theta-\theta_d)^2}{2\Delta^2}}\phi_k(\theta,\theta_d) \tag{4.74}$$

where $\Theta$ and $\Theta_d$ are sets of $N_\theta$ angles-of-arrival that range uniformly over $[0^o, 360^o)$.

A set of values of $E\{\phi_d\}$ and $E\{\phi_k\}$ using Gaussian angle-of-arrival distributions with and without mutual coupling are shown in Tables 4.4, 4.5, 4.8, and 4.9.

#### 4.4.1.2 Determining $E\{\phi_d\}$ for a Uniform $P(\theta)$

A Uniform $P(\theta)$ with mean $\theta_d$ distributed over $[\theta_d - \Delta, \theta_d + \Delta]$ is defined as

$$P(\theta) = \frac{1}{2\Delta}\left(U(\theta + (\theta_d - \Delta)) - U(\theta - (\theta_d + \Delta))\right) \tag{4.75}$$

where $U(.)$ is a unit step, defined as

$$U(x) = \begin{cases} 1 & , \quad x \geq 0 \\ 0 & , \quad x < 0 \end{cases} \tag{4.76}$$

Therefore, the expected percentage of the desired signal being passed by the beamforming pattern, $E\{\phi_d\}$, is determined by averaging Equation (4.71) uniformly over $\theta_d$. Thus, using Equations (4.72) and (4.75) yields

$$E\{\phi_d\} = \frac{1}{N_\theta}\frac{2\pi}{N_\theta}\sum_{\theta_d\in\Theta_d}\sum_{\theta\in\Theta}\frac{1}{2\Delta}\left(U\left(\theta+(\theta_d-\Delta)\right)-U\left(\theta-(\theta_d+\Delta)\right)\right)\phi_k(\theta,\theta_d) \tag{4.77}$$

where $\Theta$ and $\Theta_d$ are sets of $N_\theta$ angles-of-arrival that range uniformly over $[0^o, 360^o)$.

The results for $E\{\phi_d\}$ and $E\{\phi_k\}$ using uniform angle-of-arrival distributions with and without mutual coupling are shown in Tables 4.2, 4.3, 4.6, and 4.7.

### 4.4.2 Power and Capacity Prediction

Referring to Section 2.3, the numerical calculations can be performed to yield the expected values for the desired and interfering mobile powers as well as the system capacity predictions.

Using Equation (2.20), namely

$$\frac{E_b}{N_o} = \frac{P_R/R_B}{P_I/B + N_A\sigma_n^2} \tag{4.78}$$

we can replace $P_R$ by $E\{\phi_d\}P_R$ and $P_I$ with $E\{\phi_k\}P_R N_I$, where $N_I$ is the number of interfering mobiles. Equation (4.78) becomes

$$\frac{E_b}{N_o} = \frac{E\{\phi_d\}P_R/R_B}{E\{\phi_k\}P_R N_I/B + N_A\sigma_n^2} \tag{4.79}$$

Solving for $P_R$ yields

$$P_R = N_A\sigma_n^2\left(\frac{E_b}{N_o}\right)\left\{\frac{E\{\phi_d\}}{R_B} - \frac{E\{\phi_k\}N_I}{B}\left(\frac{E_b}{N_o}\right)\right\}^{-1} \tag{4.80}$$

Isolating $N_I$ in Equation (4.80), the number of interfering mobiles within the cell is

$$N_I = \left\lfloor \frac{B}{E\{\phi_k\}} \left( \frac{E\{\phi_d\}}{\left(\frac{E_b}{N_o}\right) R_B} - \frac{N_A \sigma_n^2}{P_R} \right) \right\rfloor \tag{4.81}$$

Therefore, the total number of mobiles within a cell is

$$\begin{aligned} N_M &= N_I + 1 \\ &= \left\lfloor \frac{B}{E\{\phi_k\}} \left( \frac{E\{\phi_d\}}{\left(\frac{E_b}{N_o}\right) R_B} - \frac{N_A \sigma_n^2}{P_R} \right) \right\rfloor + 1 \end{aligned} \tag{4.82}$$

which can then be approximated, as was done with Equation (2.30), to yield

$$N_M \approx \left\lfloor \frac{E\{\phi_d\}}{E\{\phi_k\}} \frac{B}{R_B \left(E_b/N_o\right)} \right\rfloor + 1 \tag{4.83}$$

where $\lfloor . \rfloor$ is the floor function. It should be pointed out that the effects of mutual coupling are included in $E\{\phi_k\}$ and $E\{\phi_d\}$.

Equation (4.83) is applied to the cases with and without mutual coupling effects for uniform and Gaussian angle-of-arrival distributions and the results are shown in Figures 4.11 to 4.14.

### 4.4.3 Results

Observing the results provided in Tables 4.2 through to 4.9 as well as Figures 4.11 to 4.14, we notice several very significant effects occurring.

Unlike the conclusion reached in [12], where it was stated that the effects on power due to scatter, may, in fact be quite small, suggesting that beamforming would still provide significant capacity benefits, even in high angle spread environments. Tables 4.2 to 4.9 as well as Figures 4.11 to 4.14 show the opposite conclusion, namely that the capacity converges to single antenna capacity as the angle spread is increased.

The fact that the capacity for multiple antenna arrays converges to the case of a single antenna makes intuitive sense since, as angle spread increases, spatial discrimination is lost and the beamforming process breaks down.

Comparing the values in Tables 4.2 through 4.9 for the expected fractions of the desired and interfering mobiles' signal power passed by the beamforming weights, $E\{\phi_d\}$ and $E\{\phi_k\}$, respectively, two observations can be made:

1. When comparing the results which do and do not include mutual coupling effects, whether the results are for $E\{\phi_d\}$ or $E\{\phi_k\}$, the results which do include the effects of mutual coupling are, on average, greater than the results which do not contain these effects for all angle spreads.

2. There are only minor differences between the results which use a Gaussian angle-of-arrival distribution and the results which use an uniform angle-of-arrival distribution.

Furthermore, mutual coupling reduces the capacity of the system. When the angle spread is small or zero, the deteriorating effects of mutual coupling are prevalent when compared to models which do not consider mutual coupling effects. Yet, when the angle spread increases, the effects of mutual coupling diminishes as the scattering becomes the dominant deteriorating factor. To demonstrate these differences, refer to Figures 4.13 and 4.14. We notice that for $\Delta = 10^o$, the difference in system capacity between cases which do and do not include mutual coupling, when $N_A = 2$, 3, 4, 5, and 6 antennas, is 13.0, 14.3, 14.5, 14.3, and 10.4 percent, respectively. When the angle spread increases, say $\Delta = 60^o$, the corresponding difference becomes 0.0, 0.0, 2.4, 2.0, and 12.0 percent, respectively. Finally, when $\Delta = 180^o$, the difference is 5.0 percent at most, with all the system capacity predictions close to the case of a single antenna. Moreover, in Figure 4.13, the system capacity decreases by 56.5, 65.1, 71.1,

75.5, and 78.3 percent when the angle spread increases from $\Delta = 10^o$ to $\Delta = 180^o$ for $N_A = 2$, 3, 4, 5, and 6 antennas, respectively.

It should be noted that the models using Gaussian angle-of-arrival distributions are limited to a certain angle spread range. It has been determined that angle spreads between $\Delta = 0^o$ and $\Delta = 8.5^o$, not inclusive, will not provide accurate results when used in the previously derivations. The reason for this is when $\Delta \in [0^o, 8.5^o]$, Equation (4.74) produces values greater than one, which is impossible since the expected fraction of desired mobile $d$'s signal power passed by the beamforming weights can never exceed one. Therefore, a different method must be derived to specifically compute $E\{\phi_d\}$ for Gaussian angle-of-arrival distributions when $\Delta \in [0^o, 8.5^o]$.

Comparing the difference between uniform and Gaussian angle-of-arrival distributions with respect to system capacity predictions, it is observed that as the angle spread increases, all the multiple antenna capacity predictions converge to that of the single antenna capacity for both distributions. Furthermore, the capacity predictions which use a Gaussian angle-of-arrival distribution converges slowly relative to capacity predictions using an uniform angle-of-arrival distribution. Thus, in environments with small to medium angle spreads, models perform relatively better when a Gaussian angle-of-arrival distribution is assumed.

| $\Delta^o$ | $0^o$ | $3^o$ | $5^o$ | $10^o$ | $20^o$ | $40^o$ | $90^o$ | $180^o$ |
|---|---|---|---|---|---|---|---|---|
| $N_A = 1$ | 1.0000 | 1.0000 | 1.0000 | 1.0000 | 1.0000 | 1.0000 | 1.0000 | 1.0000 |
| $N_A = 2$ | 0.5463 | 0.5464 | 0.5468 | 0.5485 | 0.5543 | 0.5691 | 0.5902 | 0.5957 |
| $N_A = 3$ | 0.3950 | 0.3952 | 0.3955 | 0.3969 | 0.4017 | 0.4149 | 0.4354 | 0.4406 |
| $N_A = 4$ | 0.3241 | 0.3243 | 0.3247 | 0.3266 | 0.3328 | 0.3459 | 0.3601 | 0.3627 |
| $N_A = 5$ | 0.2460 | 0.2463 | 0.2469 | 0.2494 | 0.2568 | 0.2697 | 0.2789 | 0.2829 |
| $N_A = 6$ | 0.2058 | 0.2063 | 0.2070 | 0.2102 | 0.2190 | 0.2312 | 0.2366 | 0.2390 |

Table 4.2: Expected fraction of interferer $k$'s signal power passed by the beamforming weights, $E\{\phi_k\}$, for an uniform angle-of-arrival distribution with no mutual coupling

| $\Delta^o$ | $0^o$ | $3^o$ | $5^o$ | $10^o$ | $20^o$ | $40^o$ | $90^o$ | $180^o$ |
|---|---|---|---|---|---|---|---|---|
| $N_A = 1$ | 1.0000 | 1.0000 | 1.0000 | 1.0000 | 1.0000 | 1.0000 | 1.0000 | 1.0000 |
| $N_A = 2$ | 0.5907 | 0.5908 | 0.5908 | 0.5911 | 0.5920 | 0.5941 | 0.5962 | 0.5963 |
| $N_A = 3$ | 0.4608 | 0.4609 | 0.4610 | 0.4614 | 0.4628 | 0.4666 | 0.4719 | 0.4719 |
| $N_A = 4$ | 0.3782 | 0.3782 | 0.3782 | 0.3784 | 0.3788 | 0.3798 | 0.3809 | 0.3811 |
| $N_A = 5$ | 0.2952 | 0.2952 | 0.2952 | 0.2954 | 0.2961 | 0.2972 | 0.2982 | 0.2984 |
| $N_A = 6$ | 0.2362 | 0.2362 | 0.2363 | 0.2365 | 0.2372 | 0.2382 | 0.2387 | 0.2390 |

Table 4.3: Expected fraction of interferer $k$'s signal power passed by the beamforming weights, $E\{\phi_k\}$, for an uniform angle-of-arrival distribution with mutual coupling

| $\Delta^o$ | $0^o$ | $8.5^o$ | $10^o$ | $20^o$ | $40^o$ | $60^o$ | $90^o$ | $180^o$ |
|---|---|---|---|---|---|---|---|---|
| $N_A = 1$ | 1.0000 | 1.0000 | 1.0000 | 1.0000 | 1.0000 | 1.0000 | 1.0000 | 1.0000 |
| $N_A = 2$ | 0.5463 | 0.5480 | 0.5485 | 0.5541 | 0.5682 | 0.5796 | 0.5890 | 0.5953 |
| $N_A = 3$ | 0.3950 | 0.3964 | 0.3968 | 0.4016 | 0.4142 | 0.4248 | 0.4339 | 0.4402 |
| $N_A = 4$ | 0.3241 | 0.3259 | 0.3266 | 0.3325 | 0.3450 | 0.3532 | 0.3589 | 0.3624 |
| $N_A = 5$ | 0.2460 | 0.2484 | 0.2493 | 0.2564 | 0.2686 | 0.2747 | 0.2788 | 0.2825 |
| $N_A = 6$ | 0.2058 | 0.2089 | 0.2101 | 0.2183 | 0.2300 | 0.2345 | 0.2368 | 0.2388 |

Table 4.4: Expected fraction of interferer $k$'s signal power passed by the beamforming weights, $E\{\phi_k\}$, for a Gaussian angle-of-arrival distribution with no mutual coupling

| $\Delta^o$ | $0^o$ | $8.5^o$ | $10^o$ | $20^o$ | $40^o$ | $60^o$ | $90^o$ | $180^o$ |
|---|---|---|---|---|---|---|---|---|
| $N_A = 1$ | 0.9954 | 0.9898 | 0.9891 | 0.9789 | 0.9581 | 0.9373 | 0.9088 | 0.9074 |
| $N_A = 2$ | 0.5886 | 0.5858 | 0.5851 | 0.5800 | 0.5715 | 0.5656 | 0.5620 | 0.5691 |
| $N_A = 3$ | 0.4550 | 0.4542 | 0.4540 | 0.4532 | 0.4528 | 0.4523 | 0.4520 | 0.4584 |
| $N_A = 4$ | 0.3766 | 0.3761 | 0.3760 | 0.3756 | 0.3735 | 0.3683 | 0.3626 | 0.3650 |
| $N_A = 5$ | 0.2946 | 0.2945 | 0.2946 | 0.2956 | 0.2975 | 0.2987 | 0.2997 | 0.2993 |
| $N_A = 6$ | 0.2363 | 0.2362 | 0.2362 | 0.2367 | 0.2380 | 0.2389 | 0.2396 | 0.2396 |

Table 4.5: Expected fraction of interferer $k$'s signal power passed by the beamforming weights, $E\{\phi_k\}$, for a Gaussian angle-of-arrival distribution with mutual coupling

| $\Delta^o$ | $0^o$ | $3^o$ | $5^o$ | $10^o$ | $20^o$ | $40^o$ | $90^o$ | $180^o$ |
|---|---|---|---|---|---|---|---|---|
| $N_A = 1$ | 1.0000 | 1.0000 | 1.0000 | 1.0000 | 1.0000 | 1.0000 | 1.0000 | 1.0000 |
| $N_A = 2$ | 1.0000 | 0.9976 | 0.9937 | 0.9788 | 0.9383 | 0.8478 | 0.6217 | 0.5957 |
| $N_A = 3$ | 1.0000 | 0.9026 | 0.8403 | 0.7276 | 0.6151 | 0.5362 | 0.4778 | 0.4406 |
| $N_A = 4$ | 1.0000 | 0.8045 | 0.7241 | 0.6126 | 0.5248 | 0.4428 | 0.3747 | 0.3627 |
| $N_A = 5$ | 1.0000 | 0.8390 | 0.7692 | 0.6740 | 0.5986 | 0.5328 | 0.4045 | 0.2829 |
| $N_A = 6$ | 1.0000 | 0.7711 | 0.6931 | 0.5999 | 0.5448 | 0.4573 | 0.3185 | 0.2390 |

Table 4.6: Expected fraction of desired mobile $d$'s signal power passed by the beamforming weights, $E\{\phi_d\}$, for an uniform angle-of-arrival distribution with no mutual coupling

| $\Delta^o$ | $0^o$ | $3^o$ | $5^o$ | $10^o$ | $20^o$ | $40^o$ | $90^o$ | $180^o$ |
|---|---|---|---|---|---|---|---|---|
| $N_A = 1$ | 1.0000 | 1.0000 | 1.0000 | 1.0000 | 1.0000 | 1.0000 | 1.0000 | 1.0000 |
| $N_A = 2$ | 1.0000 | 0.9985 | 0.9958 | 0.9845 | 0.9484 | 0.8327 | 0.6167 | 0.5960 |
| $N_A = 3$ | 1.0000 | 0.9663 | 0.9409 | 0.8823 | 0.7776 | 0.6101 | 0.5293 | 0.4716 |
| $N_A = 4$ | 1.0000 | 0.8891 | 0.8156 | 0.6783 | 0.5242 | 0.4350 | 0.3988 | 0.3805 |
| $N_A = 5$ | 1.0000 | 0.9333 | 0.8867 | 0.7945 | 0.6854 | 0.5510 | 0.3968 | 0.2979 |
| $N_A = 6$ | 1.0000 | 0.9006 | 0.8378 | 0.7269 | 0.6109 | 0.5218 | 0.3172 | 0.2386 |

Table 4.7: Expected fraction of desired mobile $d$'s signal power passed by the beamforming weights, $E\{\phi_d\}$, for an uniform angle-of-arrival distribution with mutual coupling

| $\Delta^o$ | $0^o$ | $8.5^o$ | $10^o$ | $20^o$ | $40^o$ | $60^o$ | $90^o$ | $180^o$ |
|---|---|---|---|---|---|---|---|---|
| $N_A = 1$ | 1.0000 | 0.9890 | 0.9880 | 0.9748 | 0.9490 | 0.9234 | 0.8849 | 0.7698 |
| $N_A = 2$ | 1.0000 | 0.9805 | 0.9758 | 0.9293 | 0.8080 | 0.6987 | 0.5931 | 0.4661 |
| $N_A = 3$ | 1.0000 | 0.9781 | 0.9721 | 0.9166 | 0.7734 | 0.6450 | 0.5185 | 0.3729 |
| $N_A = 4$ | 1.0000 | 0.9729 | 0.9645 | 0.8914 | 0.7140 | 0.5708 | 0.4434 | 0.3075 |
| $N_A = 5$ | 1.0000 | 0.9661 | 0.9544 | 0.8600 | 0.6526 | 0.5075 | 0.3904 | 0.2616 |
| $N_A = 6$ | 1.0000 | 0.9582 | 0.9424 | 0.8248 | 0.5950 | 0.4559 | 0.3471 | 0.2251 |

Table 4.8: Expected fraction of desired mobile $d$'s signal power passed by the beamforming weights, $E\{\phi_d\}$, for a Gaussian angle-of-arrival distribution with no mutual coupling

| $\Delta^o$ | $0^o$ | $8.5^o$ | $10^o$ | $20^o$ | $40^o$ | $60^o$ | $90^o$ | $180^o$ |
|---|---|---|---|---|---|---|---|---|
| $N_A = 1$ | 1.0000 | 0.9811 | 0.9797 | 0.9591 | 0.9180 | 0.8770 | 0.8181 | 0.7085 |
| $N_A = 2$ | 1.0000 | 0.9193 | 0.9150 | 0.8757 | 0.7767 | 0.6797 | 0.5762 | 0.4518 |
| $N_A = 3$ | 1.0000 | 0.9487 | 0.9438 | 0.9007 | 0.7903 | 0.6850 | 0.5683 | 0.4075 |
| $N_A = 4$ | 1.0000 | 0.9526 | 0.9451 | 0.8823 | 0.7283 | 0.5903 | 0.4553 | 0.3140 |
| $N_A = 5$ | 1.0000 | 0.9683 | 0.9590 | 0.8843 | 0.7082 | 0.5666 | 0.4342 | 0.2812 |
| $N_A = 6$ | 1.0000 | 0.9641 | 0.9524 | 0.8648 | 0.6723 | 0.5283 | 0.3960 | 0.2412 |

Table 4.9: Expected fraction of desired mobile $d$'s signal power passed by the beamforming weights, $E\{\phi_d\}$, for a Gaussian angle-of-arrival distribution with mutual coupling

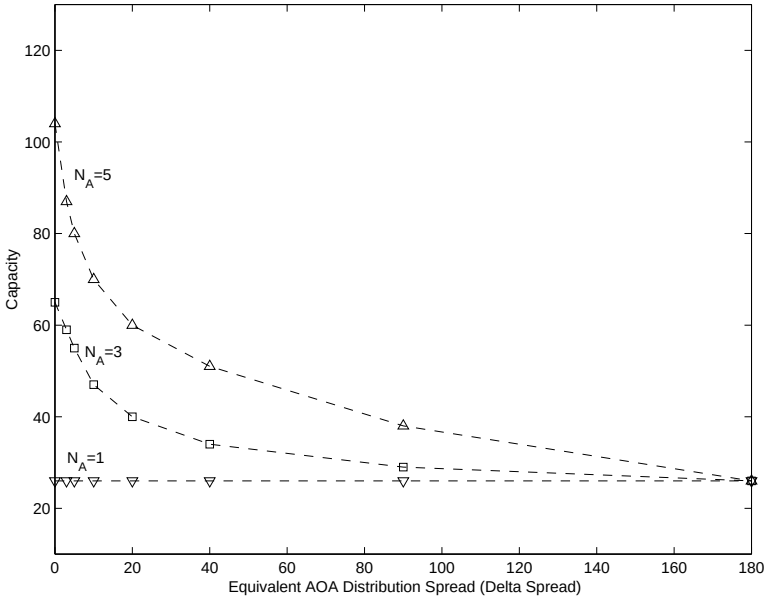


Figure 4.11: System capacity predictions for an uniform angle-of-arrival distribution with no mutual coupling

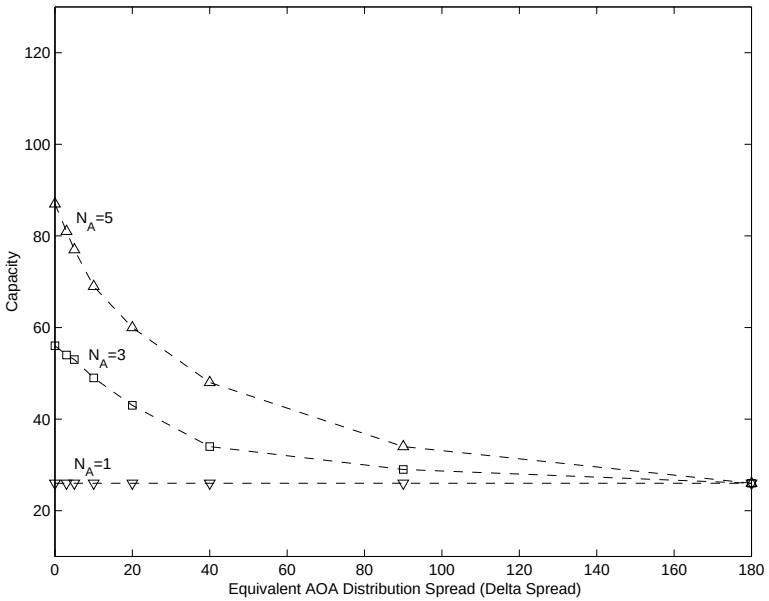


Figure 4.12: System capacity predictions for an uniform angle-of-arrival distribution with mutual coupling

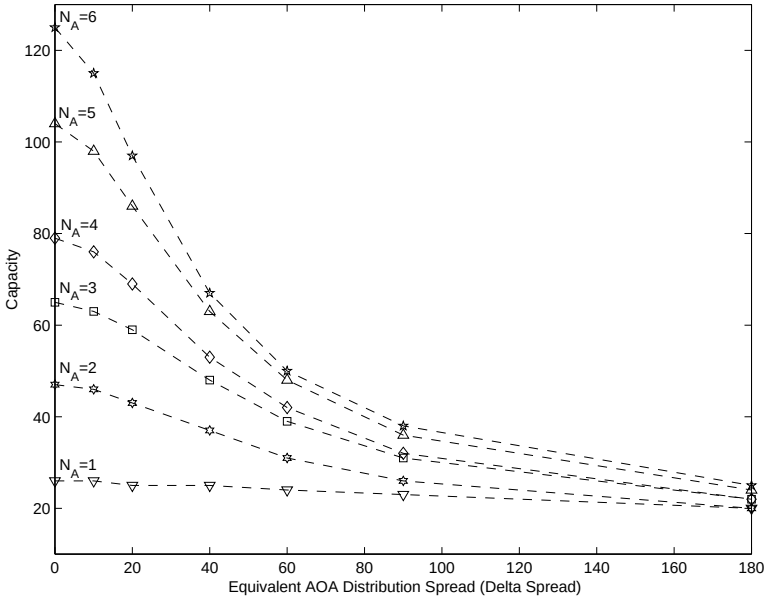


Figure 4.13: System capacity predictions for a Gaussian angle-of-arrival distribution with no mutual coupling

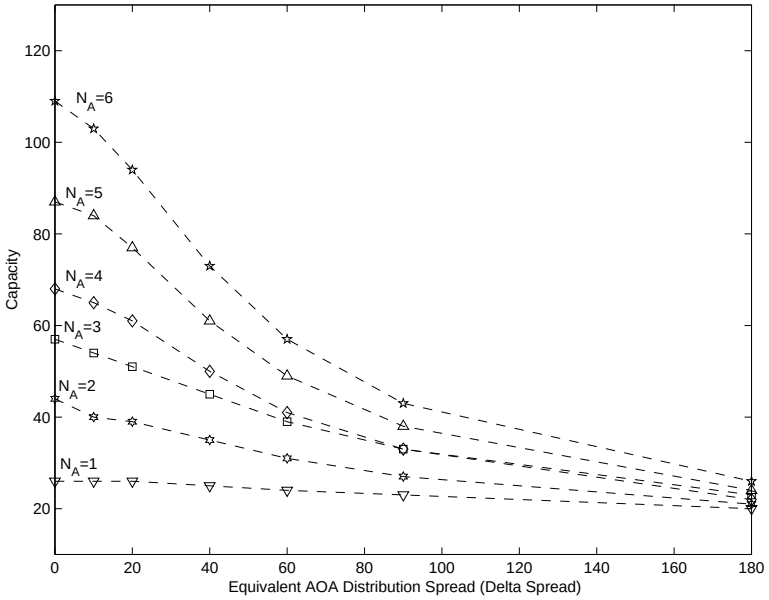


Figure 4.14: System capacity predictions for a Gaussian angle-of-arrival distribution with mutual coupling

## 4.5 Chapter Summary

In this chapter, we have presented a model given in [8], [12], [33], and [74] for the cross-correlation factor for the envelope of a quadrature signal arriving at a pair of antennas. Although the model was generalized to an arbitrary $P(\theta)$, we specifically examined the cases of the Gaussian and uniform angel-of-arrival distributions. We then applied this model to the analysis of system capacity predictions in an environment containing scattering due to multipath. In particular, we formulated a method where both the received amplitude and phase information are accounted for in the analysis by using the cross-correlation statistics and the beampattern of the antenna array, respectively. The results obtained show that mutual coupling effects have a noticeable adverse effect on system capacity predictions when the angle spread is small or non-existent while at high angle spreads, scattering is the dominant factor of degradation. For instance, if we look at $\Delta = 10^o$ in Figures 4.13 and 4.14, the capacity difference between cases which do and do not include mutual coupling effects ranges between 10 and 14.5 percent. Yet, as the angle spread increases and approaches $\Delta = 180^o$ , the system capacity decreases such that the multiple antenna capacity reduces to that of a single antenna.

# Chapter 5

# Imperfect Power Control

## 5.1 Introduction

Power control is a critical component of CDMA systems. If the ratio between the received power from a given mobile and the received interference power is too low, then an intolerably large number of errors in the data flow will occur. Moreover, if this same ratio is too high, the mobile will generate excessive interference for the other users within the cell. Thus, it is necessary to balance the transmission power level for each mobile such that a state of equilibrium within the system is achieved.

For system performance evaluation purposes, we consider two types of power control in CDMA systems: perfect and imperfect. Perfect power control occurs when the system controls the transmission power of each mobile to a desired level instantaneously so that users interfere with each other only to a desired amount. However, it has been shown that using a perfect power control assumption yields overly-optimistic performance predictions. Therefore, many studies employ an imperfect power control assumption to attain more realistic performance analysis. Imperfect power control occurs when the base station is unable to control the transmission power levels of all

mobiles perfectly due to physical factors.

Although much effort has gone into the study of power control, none of these studies have analyzed the effects of power control on the system performance when mutual coupling and scattering effects are included. This is required since these effects change the statistics of the received power levels, such as the mean and variance, which in turn affects the power controllability. Therefore, the performance predictions of these previous studies are potentially less accurate compared to analyses which include these effects.

### 5.1.1 Chapter Outline

In this chapter, we present an approach to the evaluation of the reverse link capacity of a CDMA system using digital beamforming and employing a base station antenna array under imperfect power control. Furthermore the effects of mutual coupling and scatter due to multipath are included.

We first carry out the derivation for the probability of outage for a system with perfect power control using an approach based on [91] and [92]. The end result is two expressions for the outage probability, one is an upper bound and other is a Gaussian approximation.

We then extend our derivation to the case of imperfect power control, also obtaining the upper-bound and Gaussian approximation of the outage probability.

Finally, we present some comparisons which highlight the relative effects of digital beamforming with different numbers of antenna elements, mutual coupling, scatter due to multipath, and power control.

## 5.2 Probability of Outage

### 5.2.1 Erlang Capacity of Reverse Links

Referring to [73], [91], and [92], assuming we have a very large population of users in a cell, the arrivals occur randomly at Poisson-distributed intervals with total average arrival rate $\lambda$ calls per second. Suppose this process is modeled as a sequence of binary random variables, in successive infinitesimal time intervals $\Delta t$. Then the probability of a single arrival per interval occurring is $\lambda(\Delta t)$. Assuming the call service time per user is assumed to exponentially distributed, the probability that the service time $\gamma$ exceeds $T$ is

$$Pr(\gamma > T) = e^{-\mu T} \quad , \quad T > 0 \tag{5.1}$$

where the average call duration is $1/\mu$ seconds.

Therefore, the probability that the call terminates during an interval $\Delta t$ seconds long is

$$\begin{aligned} Pr(T < \gamma < T + \Delta t | \gamma < T) &= \frac{\left[e^{-\mu T} - e^{-\mu(T+\Delta t)}\right]}{e^{-\mu T}} \\ &= 1 - e^{-\mu \Delta t} \\ &\sim \mu(\Delta t) + o(\Delta t) \end{aligned} \tag{5.2}$$

where $o(\Delta t) \to 0$ as $\Delta t \to 0$. Suppose the maximum number of users that can be served simultaneously is equal to $K_o$, then as the number of active calls $k$ is less than or equal to $K_o$, all $k$ calls will be serviced. Therefore, the probability that one of the calls will end in $\Delta t$ is on the order of $k\mu(\Delta t)$. In the case that more than one call terminates within $\Delta t$, the probability is $o(\Delta t)$, which becomes negligible as $\Delta t \to 0$.

In this chapter, the model used for determining the occupancy distribution and the probability of lost calls is the "lost call held" (LCH) model. In this model, it is

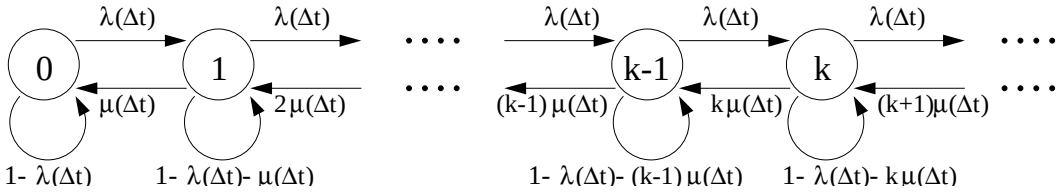


Figure 5.1: Transition probabilities represented as a Markov chain state diagram for the Erlang C model

assumed that the unserved users repeat their attempts to place a call immediately and thus remain in the system, though unserved. This model is illustrated as a Markov process in Figure 5.1. In this case, the number of states is infinite, where each state represents the number of users in the system.

Therefore, the Markov state equations for the LCH model can be written in terms of the steady-state occupancy probability, namely

$$P_k = \begin{cases} [1-\lambda(\Delta t)]\,P_k + \mu(\Delta t)\,P_{k+1} & , \quad k=0 \\ \lambda(\Delta t)\,P_{k-1} + [1-(\lambda+k\mu)\,\Delta t]\,P_k + (k+1)\,\mu(\Delta t)\,P_{k+1} & , \quad k=1,2,3,... \end{cases} \tag{5.3}$$

Thus, by induction and using Equation (5.3), the steady-state occupancy probability for the $k$th state is

$$P_k = \frac{(\lambda/\mu)}{k} P_{k-1} \quad , \quad k=1,2,3,... \tag{5.4}$$

which can be rewritten as

$$P_k = \frac{(\lambda/\mu)^k}{k!} P_0 \quad , \quad k=1,2,3,... \tag{5.5}$$

and

$$1 = \sum_{k=0}^{\infty} P_k = P_0 \sum_{k=0}^{\infty} \frac{(\lambda/\mu)^k}{k!} = P_0 e^{\lambda/\mu} \tag{5.6}$$

Therefore, the LCH model can be presented as a Poisson formula, namely

$$P_k = \frac{(\lambda/\mu)^k}{k!} e^{-\lambda/\mu} \quad , \quad k = 0, 1, 2, 3, ... \tag{5.7}$$

The blocking probability is the probability that when a new user arrives these are $K_o$ or more users in the system, either being served or seeking service. Thus, the *blocking probability* for LCH model is

$$P_B = \sum_{k=K_o}^{\infty} P_k = e^{-\lambda/\mu} \sum_{k=K_o}^{\infty} \frac{(\lambda/\mu)}{k!} \tag{5.8}$$

which is just the sum of the tail of a Poisson distribution.

In the following, Equation (5.7) will be used often to determine a closed-form for the outage probability of the system.

### 5.2.2 Derivation of $P_{out}$

The derivation for the probability of outage found in the next two subsections is based upon the approach developed in [91] and [92]. Although the general approach is similar, there are several significant differences. The first difference is that the derivations found in [91] and [92] are meant for a single antenna base station while our derivation extends [91] and [92] to base stations employing multiple antennas. A second difference is that our derivations include the effects of mutual coupling. Third, unlike [91] and [92], we account for the effects of scatter due to multipath propagation. As a result, the expressions that we obtain are more realistic in terms encompassing more complex propagation conditions, relative to that found in [91] and [92].

#### 5.2.2.1 Perfect Power Control

Assuming that we have a single cell occupied by $k_u$ perfectly power-controlled users, such that each user is received by the base station at the same power level,

the total average power received by the cell, assuming stationary arrivals and user activity, is

$$Total \quad Power \quad = \sum_{i=1}^{k_u} \psi_i v_i E_b R_B + E\{\phi_k\} N_A N_o B \tag{5.9}$$

where $B$ is the total bandwidth occupancy, $R_B$ is the user data rate, $N_o$ is the background noise, $E_b$ is the perfectly controlled bit energy, $k_u$ is the number of users within a single cell, $v_i$ is a binary random variable indicating whether or not the $i$th user is active at any instant, $\alpha$ is the activity factor, defined as $\alpha = Pr\{v_i = 1\} = 1 - Pr\{v_i = 1\}$, $N_A$ is the number of array elements, and $\psi_i$ is defined as

$$\psi_i = \begin{cases} E\{\phi_d\} & , \quad i = 1 \\ E\{\phi_k\} & , \quad i \neq 1 \end{cases} \tag{5.10}$$

where, as defined in Chapter 4, $E\{\phi_k\}$ is the expected fraction of interferer $k$'s signal power passed by the beamforming weights of the array, $E\{\phi_d\}$ is the expected fraction of desired mobile $d$'s signal power passed by the beamforming weights of the array, and $i = 1$ refers to desired mobile number one without loss of generality.

Since the total received power is the sum of noise, interference power, and desired user power, we can express the average noise-plus-interference power, $I_o B$, as

$$I_o B = \sum_{i=2}^{k_u} v_i \psi_i E_b R_B + E\{\phi_k\} N_A N_o B \tag{5.11}$$

where $I_o$ is the noise-plus-interference power, and $B$ is the bandwidth.

For dynamic range limitations on the multiple access receiver of bandwidth $B$, we should limit the total received noise-plus-interference power-to-background noise, or equivalently $I_o B / N_o B$, such that

$$\frac{I_o}{N_o} = \frac{1}{\tau} \tag{5.12}$$

where $\tau$ typically ranges between 0.25 and 0.1.

Therefore, we can determine the probability of outage, $P_{out}$, by determining the condition by which the system is deemed to be in outage. To obtain the condition for non-outage, we can rewrite Equation (5.11) as

$$\begin{aligned} I_o B - E\{\phi_k\} N_A N_o B &= \sum_{i=2}^{k_u} v_i \psi_i E_b R_B \\ B\left(I_o - N_o N_A E\{\phi_k\}\right) &= \sum_{i=2}^{k_u} v_i \psi_i E_b R_B \end{aligned}$$

and then apply Equation (5.12) to get the inequality

$$\begin{aligned} B\left(I_o - I_o \tau N_A E\{\phi_k\}\right) &> \sum_{i=2}^{k_u} v_i \psi_i E_b R_B \\ I_o B\left(1 - \tau N_A E\{\phi_k\}\right) &> \sum_{i=2}^{k_u} v_i \psi_i E_b R_B \\ \sum_{i=2}^{k_u} v_i \psi_i &< \frac{I_o B\left(1 - \tau N_A E\{\phi_k\}\right)}{E_b R_B} \end{aligned} \tag{5.13}$$

In order to reflect the fact that the bit energy-to-noise ratio is affected by the beamforming applied to the desired user, we divide the bit energy-to-noise ratio by $E\{\phi_d\}$. Thus, Equation (5.13) becomes

$$\begin{aligned} \sum_{i=2}^{k_u} v_i \psi_i &< \frac{(B/R_B)\left(1 - \tau N_A E\{\phi_k\}\right)}{\frac{1}{E\{\phi_d\}} \frac{E_b}{I_o}} \\ &= K_o \end{aligned} \tag{5.14}$$

where both the $v_i$ and $k_u$ are independent random variables. Note that when the condition of Equation (5.14) is not met, the system is said to be in an *outage condition*.

Thus, the probability of outage, $P_{out}$, is

$$\begin{aligned} P_{out} &= Pr\left\{\sum_{i=2}^{k_u} v_i \psi_i > K_o\right\} \\ &< Pr\left\{\sum_{i=1}^{k_u} v_i \psi_i > K_o\right\} \end{aligned} \tag{5.15}$$

where we have upper-bounded $P_{out}$ by including in the summation the desired signal variable, $v_1$, as done in [91] [92]. Unfortunately, including $v_1$ in the outage probability

expression will loosen it since the $v_1$ term in the outage probability summation contains $\psi_i = E\{\phi_d\}$, referring to Equation (5.10), and thus this term will dominate over the other terms since they have $\psi_i = E\{\phi_k\}$. As was shown in previous chapters, the value of $E\{\phi_d\}$ is larger than $E\{\phi_k\}$ on average.

We employ a stricter outage condition, namely

$$\begin{aligned} P_{out} &= Pr\left\{\sum_{i=2}^{k_u} v_i\psi_i > K_o\right\} \\ &= Pr\left\{\sum_{i=2}^{k_u} v_i E\{\phi_k\} > \frac{(B/R_B)(1-\tau N_A E\{\phi_k\})}{\frac{1}{E\{\phi_d\}}\frac{E_b}{I_o}}\right\} \\ &= Pr\left\{\sum_{i=2}^{k_u} v_i > \frac{(B/R_B)(1-\tau N_A E\{\phi_k\})}{\frac{E\{\phi_k\}}{E\{\phi_d\}}\frac{E_b}{I_o}}\right\} \\ &= Pr\left\{\sum_{i=2}^{k_u} v_i > K_o'\right\} \end{aligned} \tag{5.16}$$

To simplify the derivation, suppose we let $k_u' = k_u - 1$, where $k_u'$ is the number of interfering mobiles within the cell. Therefore, we can rewrite Equation (5.16) as

$$P_{out} = Pr\left\{\sum_{l=1}^{k_u'} v_i > K_o'\right\} \tag{5.17}$$

Thus, the outage probability can be determined by the distribution of the sum of $k_u'$ independent random variables, each with probability $\alpha$. According to Subsection 5.2.1, since we are assuming that the users remain in the system through outage, then $k_u'$ has a Poisson distribution given by Equation (5.7), namely

$$p_{k_u'} = Pr\{\ k_u' \quad active \quad users/sector\ \} = \frac{(\lambda/\mu)^{k_u'}}{k_u'!}e^{-\lambda/\mu} \tag{5.18}$$

where $\lambda$ is the total average call arrival rate, $\mu$ is the average call duration, and $\lambda/\mu$ is the average number of calls which is the mean as well as the variance of $p_{k_u'}$.

Therefore, we define the random variable

$$Z = \sum_{l=1}^{k_u'} v_l \tag{5.19}$$

in order to facilitate the derivation of $P_{out}$. One method of computing the distribution of $Z$ is to derive its moment-generating function, thus obtaining

$$\begin{aligned} E\left\{e^{sZ}\right\} &= E_{k'_u}\prod_{l=1}^{k'_u} E_{v_l}\left(e^{sv_l}\right) \\ &= E_{k'_u}\prod_{l=1}^{k'_u}\left[Pr\left\{v_l=1\right\}e^{s\{v_l=1\}}+Pr\left\{v_l=0\right\}e^{s\{v_l=0\}}\right] \\ &= E_{k'_u}\prod_{l=1}^{k'_u}\left[\alpha e^s+(1-\alpha)\right] \\ &= E_{k'_u}\left[\alpha e^s+(1-\alpha)\right]^{k'_u} \\ &= E_{k'_u}\left[\alpha\left(e^s-1\right)+1\right]^{k'_u} \end{aligned}$$

and then applying Equation (5.18) yields

$$\begin{aligned} E\left\{e^{sZ}\right\} &= \sum_{k'_u=0}^{\infty}\frac{\left(\lambda/\mu\right)^{k'_u}}{k_u!}e^{-\lambda/\mu}\left[\alpha\left(e^s-1\right)+1\right]^{k'_u} \\ &= \sum_{k'_u=0}^{\infty}\frac{\left(\left(\lambda/\mu\right)\left[\alpha\left(e^s-1\right)+1\right]\right)^{k'_u}}{k_u!}e^{-\lambda/\mu} \\ &= e^{((\lambda/\mu)[\alpha(e^s-1)+1])}e^{-\lambda/\mu} \\ &= e^{((\alpha\lambda/\mu)(e^s-1))} \end{aligned} \tag{5.20}$$

Since Equation (5.20) is, in fact, the moment generating function of a Poisson Distribution (refer to Example 5-30 in [61]), the outage probability is just the sum of Poisson tails, namely

$$P_{out} = e^{-\alpha\lambda/\mu}\sum_{k=\lfloor K'_o\rfloor}^{\infty}\frac{\left(\alpha\lambda/\mu\right)^k}{k!} \tag{5.21}$$

where $P_{out}$ can be solved numerically.

Alternatively, $P_{out}$ may also be evaluated using the moment generating function in obtaining its Chernoff bound, yielding

$$\begin{aligned} P_{out} &< \min_{s>0}\left\{E\left\{e^{s(Z-K'_o)}\right\}\right\} \\ &= \min_{s>0}\left\{e^{\frac{\alpha\lambda}{\mu}(e^s-1)}e^{-sK'_o}\right\} \end{aligned}$$

where the minimum value of $s$ is

$$\begin{aligned} \frac{\partial}{\partial s}\left\{e^{\frac{\alpha\lambda}{\mu}(e^s-1)}e^{-sK'_o}\right\} &= 0 \\ e^{\frac{\alpha\lambda}{\mu}(e^s-1)}e^{-sK'_o}\left(\frac{\alpha\lambda}{\mu}e^s - K'_o\right) &= 0 \\ s &= \ln\left(\frac{K'_o\mu}{\alpha\lambda}\right) \end{aligned}$$

Therefore, $P_{out}$ becomes

$$\begin{aligned} P_{out} &< e^{\frac{\alpha\lambda}{\mu}e^{\ln(K'_o\mu/\alpha\lambda)}-\frac{\alpha\lambda}{\mu}-\ln\left(\frac{K'_o\mu}{\alpha\lambda}\right)K'_o} \\ &= e^{K'_o-\frac{\lambda\alpha}{\mu}-K'_o-K'_o\ln\left(\frac{K'_o\mu}{\alpha\lambda}\right)} \\ &= e^{-K'_o\left(\ln\left(\frac{K'_o}{\alpha\lambda/\mu}\right)-1+\frac{\alpha\lambda/\mu}{K'_o}\right)} \end{aligned} \tag{5.22}$$

We can further approximate Equation (5.22), for large $K'_o$, by a Gaussian variable with a mean and variance of $\alpha\lambda/\mu$, yielding

$$P_{out} \approx Q\left(\frac{K'_o - \alpha\lambda/\mu}{\sqrt{\alpha\lambda/\mu}}\right) \tag{5.23}$$

#### 5.2.2.2 Imperfect Power Control

Suppose now we loosen our restriction on power control and assume imperfect power control. Therefore, a user that is controlled to a desired $E_b/I_o$ level, which may vary due to multipath propagation conditions, will exhibit a received $E_b/I_o$ level at a desired cell base station which varies according to a log-normal distribution with a standard deviation of about 1.5 to 2.5dB [91] [92].

To model the effects of imperfect power control, we must modify the derivation in Section 5.2.2.1 to account for the variable bit energy of each user within the cell. Thus, instead of a constant $E_b$, let us define the bit energy to be $E_{b_l} = \epsilon_l E_{b_o}$, which

is log-normally distributed. Thus, using this modification, Equation (5.17) becomes

$$P_{out} = Pr\left\{Z' = \sum_{l=1}^{k'_u} \epsilon_l v_l > K'_o\right\} \tag{5.24}$$

where

$$K'_o = \frac{\frac{B}{R_B}(1-\tau(N_A E\{\phi_k\}))}{\frac{E\{\phi_k\}}{E\{\phi_d\}}\frac{E_b}{I_o}} \tag{5.25}$$

and $k'_u$ is a Poisson variable with parameter $\alpha(\lambda/\mu)$. Therefore, since $E_{b_l} = \epsilon_l E_{b_o}$ is log-normally distributed, we can define the following transformed random variables

$$x_l = 10\log_{10}(E\{\phi_k\}\epsilon_l E_{b_o}/I_o) \tag{5.26}$$

to be normally distributed random variable with mean $m_c$ and standard deviation $\sigma_c$. Thus, inverting Equation (5.26) yields

$$\frac{E_{b_o}}{I_o}\epsilon_l E\{\phi_k\} = 10^{\frac{x_l}{10}} = e^{\beta x_l} \tag{5.27}$$

where $\beta = \ln(10)/10$.

To solve for the moment-generating function of the random variable $Z'$, we evaluate the $n$th moment of $\epsilon_l$ using $x_l$. Thus, since $x_l$ is Gaussian with mean $m_c$ and standard deviation $\sigma_c$, we get

$$\begin{aligned} E\{\epsilon_l^n\} &= \left(\frac{E_{b_o}}{I_o}E\{\phi_k\}\right)^{-n}\int_{-\infty}^{\infty} e^{n\beta x_l}\frac{e^{-(x_l-m_c)^2/\left(2\sigma_c^2\right)}}{\sqrt{2\pi\sigma_c^2}}dx_l \\ &= \frac{\left(e^{\beta m_c}\right)^n}{\left(\frac{E_{b_o}}{I_o}\right)^n(E\{\phi_k\})^n}e^{n^2(\beta\sigma_c)^2/2} \end{aligned} \tag{5.28}$$

Since $E_{b_o}$ was defined as an arbitrary constant, let us assign it a convenient value such that

$$E\{\phi_k\}\frac{E_{b_o}}{I_o} = e^{\beta m_c} = 10^{\frac{m_c}{10}} \tag{5.29}$$

Therefore, using Equation (5.29), Equation (5.28) becomes

$$E\left\{\epsilon_l^n\right\} = e^{n^2(\beta\sigma_c)^2/2} \tag{5.30}$$

Since the moment-generating function of $\epsilon$ does not exist, we resort to a modified Chernoff Bound for obtaining the outage probability. This is accomplished by using a truncated moment-generating function approach, where the outage probability expression is broken up into two components. The first part is conditioned on $v_l\epsilon_l < T$ for all $i$, for some sufficiently large $T$, while the second part is conditioned on the complementary event. Therefore the probability of outage, upper-bounding the second part of the expression by unity, becomes

$$\begin{aligned}
P_{out} &= Pr\left\{\sum_{l=1}^{k'_u} v_l\epsilon_l > K'_o; v_l\epsilon_l < T\right\} + Pr\left\{\sum_{l=1}^{k'_u} v_l\epsilon_l > K'_o; v_l\epsilon_l \geq T\right\} \\
&< Pr\left\{\sum_{l=1}^{k'_u} v_l\epsilon_l > K'_o; v_l\epsilon_l < T\right\} + Pr\left\{v_l\epsilon_l \geq T\right\} \\
&< E_{k'_u}\prod_{l=1}^{k'_u} E_{v_l}\left(e^{sv_l\epsilon_l}; \epsilon_l < T\right)e^{-sK'_o} + E_{k'_u}\sum_{l=1}^{k'_u} Pr\left\{\epsilon_l \geq T\right\} Pr\left\{v_l = 1\right\} \\
&< \min_{s>0,T>0}\left\{E_{k'_u}\left\{\left[\alpha E_\epsilon e^{s\epsilon} + (1-\alpha)\right]^{k'_u}; \epsilon < T\right\}e^{-sK'_o} + E_{k'_u}\left\{k'_u Pr\left\{\epsilon \geq T\right\}\alpha\right\}\right\} \\
&< \min_{s>0,T>0}\left\{e^{\alpha\left(\frac{\lambda}{\mu}\right)E\{e^{s\epsilon_T}-1\}-sK'_o} + \alpha\left(\frac{\lambda}{\mu}\right)Pr\left\{\epsilon \geq T\right\}\right\}
\end{aligned} \tag{5.31}$$

Furthermore,

$$E\left\{e^{s\epsilon_T}\right\} = E\left\{e^{se^{\beta\xi}}; \xi \leq \frac{\ln(T)}{\beta}\right\} \tag{5.32}$$

and

$$Pr\left\{\epsilon \geq T\right\} = Pr\left\{\xi \geq \frac{\ln(T)}{\beta}\right\} \tag{5.33}$$

where $\xi = \ln(\epsilon)/\beta = x - m_c$, referring to Equations (5.27) through (5.29). Therefore, $\xi$ is Gaussian with zero mean and standard deviation $\sigma_c$. Thus, defining $\theta = \ln(T)/\beta$,

Equations (5.33) and (5.32) become, respectively,

$$\begin{aligned} Pr\left\{\epsilon \geq T\right\} &= \frac{1}{\sqrt{2\pi\sigma_c}} \int_{\frac{\ln(T)}{\beta}}^{\infty} e^{-\xi^2/2\sigma_c^2} d\xi \\ &= Q\left(\frac{\ln(T)}{\beta\sigma_c}\right) \\ &= Q\left(\frac{\theta}{\sigma_c}\right) \end{aligned} \tag{5.34}$$

and

$$\begin{aligned} E\left\{e^{s\epsilon_T}\right\} &= \frac{1}{\sqrt{2\pi\sigma_c^2}} \int_{-\infty}^{\theta} e^{se^{\beta\xi}} e^{-\xi^2/2\sigma_c^2} d\xi \\ &= \sum_{n=0}^{\infty} \frac{s^n}{n!\sqrt{2\pi}\sigma_c} \int_{-\infty}^{\theta} e^{n\beta\xi} e^{-\xi^2/2\sigma_c^2} d\xi \\ &= \sum_{n=0}^{\infty} \frac{s^n}{n!} e^{n^2(\beta\sigma_c)^2/2} Q\left(n\beta\sigma_c - \frac{\theta}{\sigma_c}\right) \end{aligned} \tag{5.35}$$

As was described previously in Section 5.2.2.1 for the case of perfect power control, we can rewrite Equation (5.24) in the form of a Gaussian approximation. Furthermore, it is no longer necessary to truncate the moments, since the untruncated first and second moments exist. Therefore, approximating the distribution of $Z'$ in Equation (5.24) yields

$$P_{out} \approx Q\left(\frac{K_o' - E\left\{Z'\right\}}{\sqrt{var\left(Z'\right)}}\right) \tag{5.36}$$

where

$$\begin{aligned} E\left\{Z'\right\} &= E\left\{\sum_{l=1}^{k_u'} v_l \epsilon_l\right\} \\ &= E\left\{k_u'\right\} E\left\{v\right\} E\left\{\epsilon\right\} \\ &= \left(\frac{\lambda}{\mu}\right) \alpha e^{(\beta\sigma_c)^2/2} \end{aligned} \tag{5.37}$$

and since $k_u'$ is a Poisson variable, then $E\left\{k_u'\right\} = var\left(k_u'\right) = \frac{\lambda}{\mu}$, therefore

$$var\left(Z'\right) = var\left(\sum_{l=1}^{k_u'} v_l \epsilon_l\right)$$

$$
\begin{aligned}
&= E\left\{k'_u\right\} var\left(v\epsilon\right) + var\left(k'_u\right) E^2\left\{v\epsilon\right\} \\
&= \left(\frac{\lambda}{\mu}\right) var\left(v\epsilon\right) + \left(\frac{\lambda}{\mu}\right) E^2\left\{v\epsilon\right\} \\
&= \left(\frac{\lambda}{\mu}\right)\left(var\left(v\epsilon\right) + E^2\left\{v\epsilon\right\}\right) \\
&= \left(\frac{\lambda}{\mu}\right)\left(\left(E\left\{v^2\epsilon^2\right\} - E^2\left\{v\epsilon\right\}\right) + E^2\left\{v\epsilon\right\}\right) \\
&= \left(\frac{\lambda}{\mu}\right)\left(\left(E\left\{v^2\right\} E\left\{\epsilon^2\right\} - E\left\{v^2\right\} E\left\{\epsilon^2\right\}\right) + E^2\left\{v\epsilon\right\}\right) \\
&= \left(\frac{\lambda}{\mu}\right)\left(E^2\left\{v\epsilon\right\}\right) \\
&= \left(\frac{\lambda}{\mu}\right)\left(E\left\{v^2\right\} E\left\{\epsilon^2\right\}\right) \\
&= \left(\frac{\lambda}{\mu}\right)\alpha e^{2(\beta\sigma_c)^2} \qquad (5.38)
\end{aligned}
$$

Therefore, the Gaussian approximation of the outage probability can be expressed, using Equations (5.37) and (5.38), as

$$
P_{out} \approx Q\left(\frac{K'_o - \alpha\left(\frac{\lambda}{\mu}\right) e^{(\beta\sigma_c)^2/2}}{\sqrt{\alpha\left(\frac{\lambda}{\mu}\right) e^{2(\beta\sigma_c)^2}}}\right) \qquad (5.39)
$$

## 5.3 Results

Using Equations (5.21), (5.23), (5.31), and (5.39) from Sections 5.2.2.1 and 5.2.2.2, we have plotted Figures 5.2 through 5.8 in order to examine the impact of several different factors, including mutual coupling effects, scattering effects, as well as power control, on the performance of CDMA systems employing smart antennas.

In all the figures, we have plotted the logarithm of the probability of outage, $P_{out}$, versus the normalized average user occupancy, $(\lambda/\mu)\,\alpha\,(1+f)$, in terms of Erlangs. The term $(\lambda/\mu)$ represents the occupancy rate of the system, in Erlangs, where $\lambda$ is the total mean call arrival rate per unit time and $\mu$ is the mean service rate (average

number of calls per unit time). Multiplying $(\lambda/\mu)$ by the activity factor $\alpha$, which is defined as the fraction of the time during which the user's signal is present, reduces the occupancy rate by $\alpha < 1$. As for $f$, it is defined as the percentage of users controlled by other cell base stations which introduce interference power into a given base station. Thus, since our derivations are only based on a single cell model, we let $f = 0$. Furthermore, we assume a data transmission activity factor of $\alpha = 1$, a spread bandwidth of $B = 1228800$Hz, a data rate of $R_B = 9600$bits/second, $\tau = 0.1$, and $\sigma_c = 2.5$dB. To be consistent with the rest of this thesis, the array has a circular geometry with half-wavelength distances between adjacent array elements. Of course, the derivations of Sections 5.2.2.1 and 5.2.2.2 are equally applicable to other geometries. Finally, we use the Gaussian angle-of-arrival spatial distribution for the scatter, although other distributions can be used as well.

Figure 5.2 exhibits the effects on performance as a function of the number of array elements. In this case, we have assumed perfect power control, no mutual coupling effects, and no scatter. Using Equations (5.21) and (5.23) for a base station antenna array consisting of $N_A = 1$,3, and 5 antennas, as the number of antennas increases, the outage probability decreases. The approximate linear improvement with the number of antennas, observation agrees with the other results in this thesis as well as with other references. Furthermore, the curves generated using Equation (5.21) give the upper-bound performance of each case, as predicted. For example, suppose we compare the upper-bound curves, corresponding to Equation (5.21), for $N_A = 1$ and 5 antennas. Fixing $\log(P_{out})$ to $-3.0$, we observe the normalized average user occupancy to be 10 Erlangs for $N_A = 1$ antenna while 64 Erlangs for $N_A = 5$ antennas. Therefore, for a fixed outage probability, a system with $N_A = 5$ antennas is capable of achieving a greater capacity relative to a system with only $N_A = 1$ antenna. Interpreting this example another way, if we fix the normalized average

user occupancy, the probability of outage would be greater for a system with $N_A = 1$ antenna relative to system with $N_A = 5$ antennas.

In Figure 5.3, we further examine the impact of the number of array elements on the performance of our system, where imperfect power control is assumed and neither the effects of mutual coupling nor scatter are included. Using Equations (5.31) and (5.39), we have determined the outage probability for base station antenna arrays consisting of $N_A$ = 1,3, and 5 antennas. We observe that the probability of outage decreases as the number of array elements increases, therefore the capacity of the system increases. Furthermore, the curves generated using Equation (5.31) give the upper-bound performance of each case, as predicted. For instance, suppose we compare the $N_A = 1$ and 5 antennas cases by fixing $\log(P_{out})$ to $-3.0$. The normalized average user occupancy of a system with only $N_A = 1$ array element is 5 Erlangs, when the upper bound expression of Equation (5.31) is used, or 10 Erlangs, when the Gaussian approximation of Equation (5.39) is employed. Moreover, the normalized average user occupancy of a system with $N_A = 5$ array elements is 52 Erlangs, when the upper bound expression of Equation (5.31) is used, or 61 Erlangs, when the Gaussian approximation of Equation (5.39) is used. Therefore, for a fixed outage probability, a system with $N_A = 5$ antennas is capable of achieving a greater capacity relative to a system with only $N_A = 1$ antenna. Thus, for a fixed normalized average user occupancy the probability of outage would be greater for a system with $N_A = 1$ antenna relative to system with $N_A = 5$ antennas. Comparing Figures 5.3 and 5.2, we observe that the normalized average user occupancy in Figure 5.3 is lower relative to Figure 5.2. For example, the normalized average user occupancy for the $N_A = 1$ array element case at $\log(P_{out}) = -3.0$ on the upper bound curve of Figure 5.3 is 50 percent lower relative to the corresponding point in Figure 5.2. This observation agrees with open literature, especially [91], since systems with perfect power control,

on average, provide overly-optimistic results with respect to Erlang capacity.

Referring to Figure 5.4, we examine the effects of mutual coupling and scatter on the system performance. Assuming perfect power control (both upper bound and Gaussian approximation) and an $N_A = 5$ element antenna array, we have plotted curves where both mutual coupling and scattering effects are included, only mutual coupling effects are included, and the ideal case where neither mutual coupling nor scattering effects are included in our system model. When scattering is included, angle spreads of $\Delta = 15^o$ and $\Delta = 60^o$, corresponding to hilly (macro) and microcell (mall) environments [56], respectively, are used. Referring to Figure 5.4, the following observations are made:

1. As expected, when mutual coupling is included and scatter is $\Delta = 60^o$, the performance of the system is the worst of the four cases. For instance, fixing $\log(P_{out})$ to $-3.0$ and referring to the upper-bound curve where mutual coupling and scatter ($\Delta = 60^o$) are both included, we observe that the normalized average user occupancy is 24 Erlangs, as opposed to 64 Erlangs when both mutual coupling and scatter are not included.

2. When the scatter is decreased to $\Delta = 15^o$, the performance is somewhat better although still not as good as the case where only mutual coupling effects are included. For example, the normalized average user occupancy, when both mutual coupling and scatter ($\Delta = 15^o$) are included and the upper bound curve is used, is 46 Erlangs, when $\log(P_{out})$ is fixed to $-3.0$. This is higher than 24 Erlangs when $\Delta = 60^o$, yet lower compared to 49 Erlangs when only mutual coupling is included.

3. Finally, when none of these effects are included, the system performs at its best. Comparing the above values for the normalized average user occupancy when

$\log(P_{out})$ is fixed to $-3.0$, we get 64 Erlangs when none of these effects are included.

These results agree strongly with the results from the rest of this thesis and serve as a baseline for the following power control studies.

Figures 5.5 to 5.8 demonstrate the effects of power control on system performance. Assuming that all figures include the effects of mutual coupling and both imperfect and perfect power control, Figure 5.5 corresponds to an $N_A = 3$ antenna array system where the angle spread is $\Delta = 15^o$, Figure 5.6 corresponds to a $N_A = 3$ antenna array system where the angle spread is $\Delta = 60^o$, Figure 5.7 corresponds to a $N_A = 5$ antenna array system where the angle spread is $\Delta = 15^o$, and Figure 5.8 corresponds to a $N_A = 5$ antenna array system where the angle spread is $\Delta = 60^o$. From these figures, three major observations can be made:

1. Imperfect power control using Equation (5.31) gave the lowest capacity values, followed by imperfect power control using Equation (5.39), then perfect power control using Equation (5.21), and finally perfect power control using Equation (5.23) yielded the highest capacity values. For example, fixing $\log(P_{out})$ is fixed to $-3.0$ in Figure 5.5, we notice that the normalized average user occupancy for the curves generated using Equations (5.31), (5.39), (5.21), and (5.23) are 20, 24, 27, and 28 Erlangs, respectively. This agrees with the literature, especially [91], since systems with imperfect power control, on average, do not perform as well as systems with perfect power control. Moreover, the upper bound equations establish the worst case scenario that a system could obtain. Therefore, it makes sense that the upper bound always performs worse relative to the Gaussian approximation.

2. The curves of Figures 5.5 and 5.7 indicate better performance relative to the

curves of Figures 5.6 and 5.8, respectively. This is due to the fact that the scatter in Figures 5.5 and 5.7 has an angle spread of $\Delta = 15^o$ while the scatter in Figures 5.6 and 5.8 has an angle spread of $\Delta = 60^o$. Therefore, since the scatter is larger in Figures 5.6 and 5.8, the curves in those figures indicate the increased degrading due to scattering effects. For example, comparing the curves generated using Equations (5.31), (5.39), (5.21), and (5.23) in Figure 5.5 to the corresponding curves in Figure 5.6, we notice a difference in normalized average user occupancy of 35.0, 29.1, 33.3, and 28.6 percent, when $\log(P_{out})$ is fixed to $-3.0$, where all the curves in Figure 5.5 have relatively higher normalized average user occupancy.

3. System performance is improved when the array consists of $N_A = 5$ antennas relative to the $N_A = 3$ antennas case. This is obvious when comparing Figures 5.5 and 5.7 as well as Figures 5.6 and 5.8. This agrees with the general consensus that as the number of array elements increases, the performance improves. For instance, the difference in normalized average user occupancy, with respect to the curves generated using Equations (5.31), (5.39), (5.21), and (5.23), between Figures 5.5 and 5.7 is 44.4, 42.9, 40.0, and 40.4 percent, respectively, when $\log(P_{out})$ is fixed to $-3.0$. Note that Figure 5.7 possess the higher values for the normalized average user occupancy.

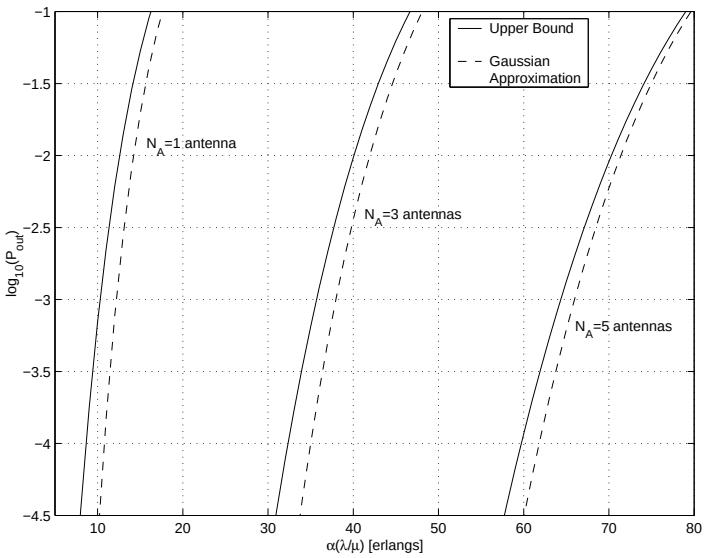


Figure 5.2: Effect of the number of array elements on the outage probability [no mutual coupling, no scatter, perfect power control]

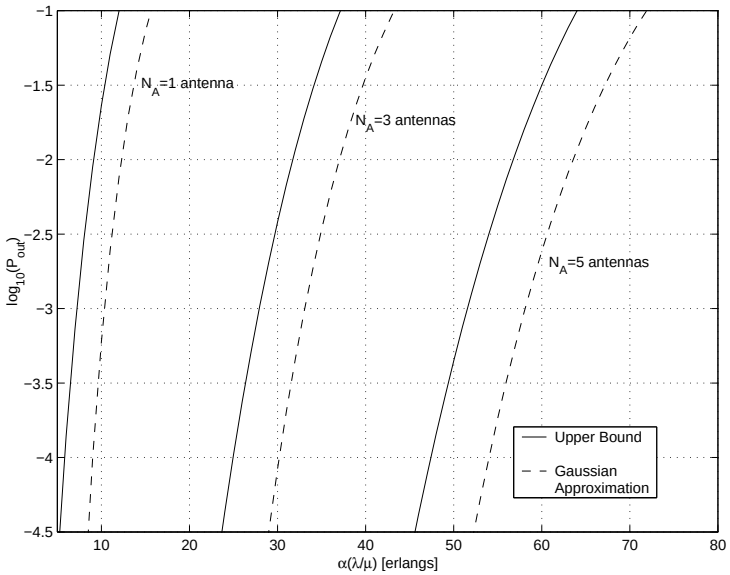


Figure 5.3: Effect of the number of array elements on the outage probability [no mutual coupling, no scatter, imperfect power control]

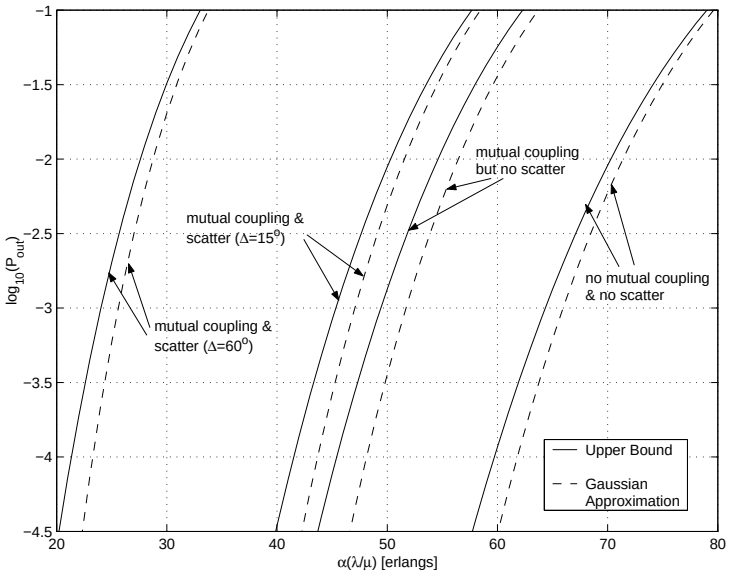


Figure 5.4: Effect of mutual coupling and scatter on the outage probability [$N_A = 5$ antennas, perfect power control]

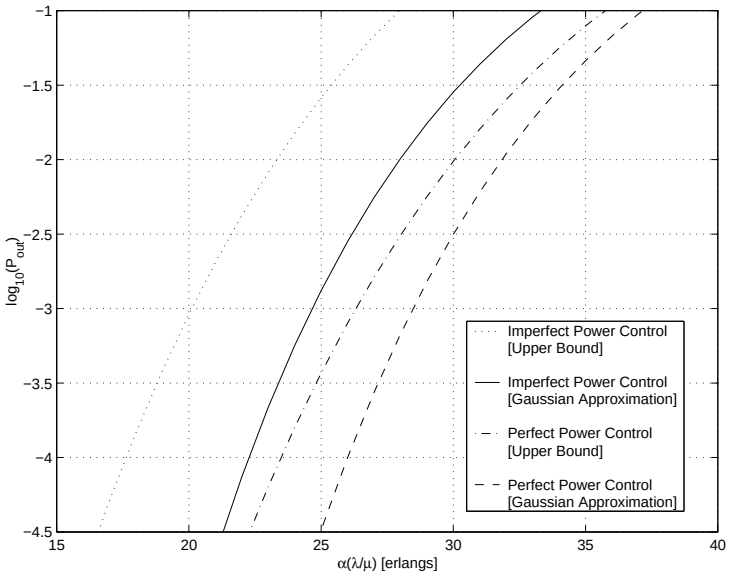


Figure 5.5: Effect of imperfect power control on the outage probability [$N_A = 3$ antennas, mutual coupling included, scatter included ($\Delta = 15^o$)]

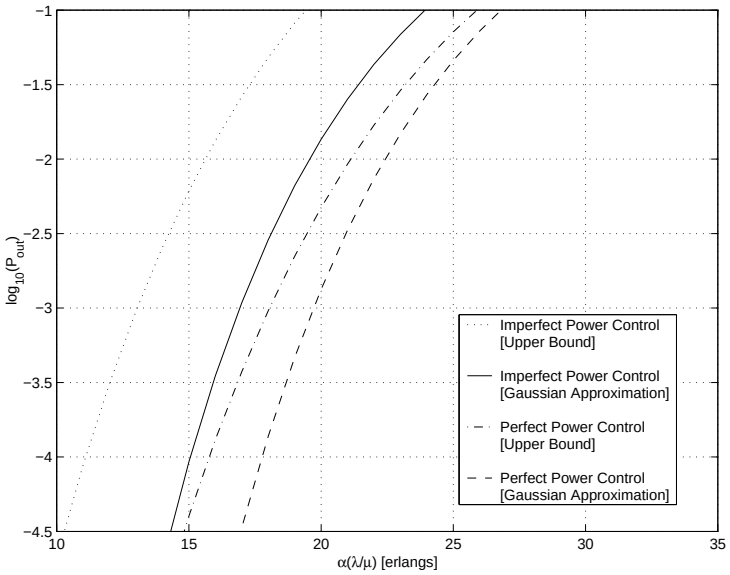


Figure 5.6: Effect of imperfect power control on the outage probability [$N_A = 3$ antennas, mutual coupling included, scatter included ($\Delta = 60^o$)]

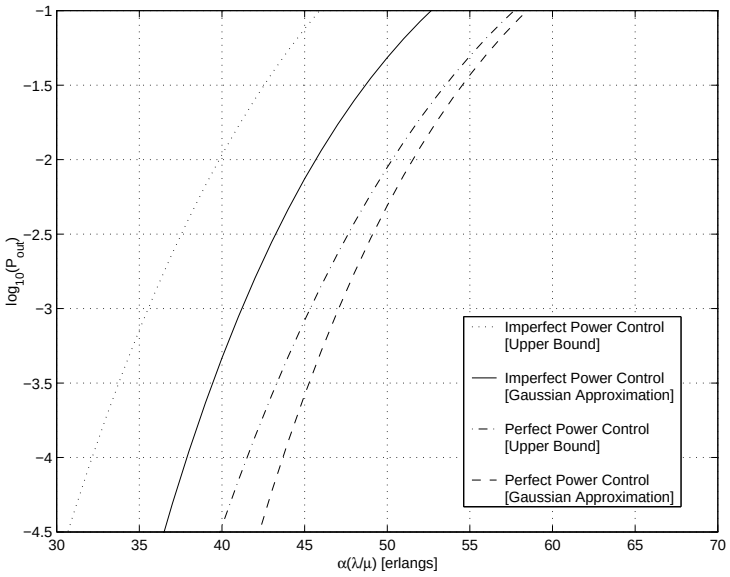


Figure 5.7: Effect of imperfect power control on the outage probability [$N_A = 5$ antennas, mutual coupling included, scatter included ($\Delta = 15^o$)]

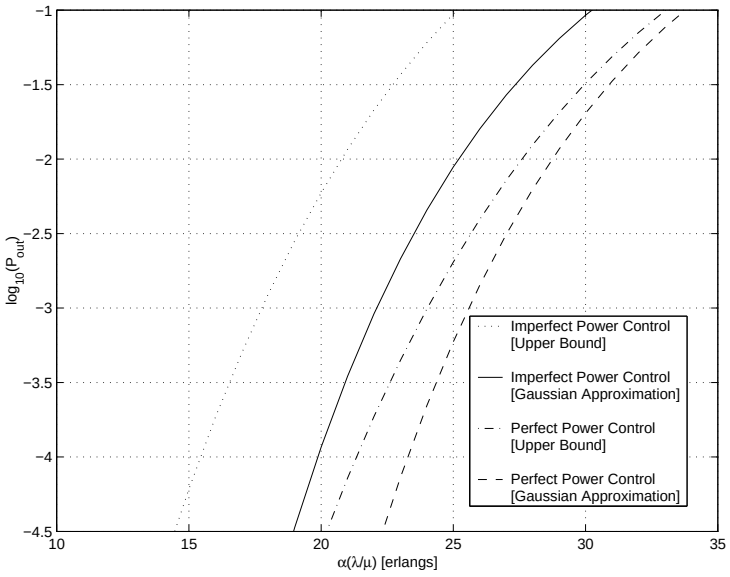


Figure 5.8: Effect of imperfect power control on the outage probability [$N_A = 5$ antennas, mutual coupling included, scatter included ($\Delta = 60^o$)]

## 5.4 Chapter Summary

We have presented a detailed analysis of the effects of power control on system performance where multi-antenna arrays are used and mutual coupling as well as scattering effects are included.

From this analysis, the results indicate that the performance of systems which use imperfect power control is lower relative to systems using perfect power control. This agrees with the open literature on this subject and provides us with a sanity check.

Moreover, the effects of mutual coupling and scatter further degrades performance of these systems. Although this part of the analysis has never been done before, the results make intuitive sense and agrees with the results found in the rest of this thesis.

Finally, as the number of antennas within the array increases, system performance also improves. Thus, the use of base station antenna arrays in increase system capacity is justified.

# Chapter 6

# Summary and Future Work

## 6.1 Introduction

This chapter provides some perspective for the major contributions of this thesis, and outlines several possible extensions and enhancements which could be performed.

## 6.2 Summary of Contributions

The major contributions of this thesis are:

- Two analytical methods, the Induced EMF Method, from [37], and the Method of Moments, from [30], as well as a full-wave electromagnetic numerical computation, from [98], were used to include the effects of mutual coupling in our beampattern synthesis models and system capacity predictions. Our beampatterns which include the effects of mutual coupling exhibit higher sidelobe levels, shallower nulls, and wider beamwidths relative to beampatterns which do not include mutual coupling. Moreover, the beampatterns which do account for mutual coupling effects, which were generated using the three methods, all compare

very closely with one another. Furthermore, the predicted capacity results for the cases where mutual coupling effects are included show a noticeable decrease relative to the case where the mutual coupling is unaccounted for. For example, we observe a difference in system capacity of six to eleven percent when the effects of mutual coupling are and are not considered in the $N_A = 5$ antennas case.

- The improved system model we developed, where the effects of mutual coupling are included, is taken one step further by assuming the environment also includes the effects of scatter due to multipath. This is achieved by determining the cross-correlation statistics between antennas of the array, as was performed by Salz and Winters [75], and improving it by including the effects of mutual coupling as well as using an unspecified angle-of-arrival spatial distribution. Hence, we can further increase the accuracy of our system model by including both the effects of mutual coupling and scatter. The results obtained show that mutual coupling effects have a noticeable adverse effect on system capacity predictions when the angle spread is small or non-existent while at high angle spreads, scattering is the dominant factor of degradation. For instance, if we look at $\Delta = 10^o$ in Figures 4.13 and 4.14, the capacity difference between cases which do and do not include mutual coupling effects ranges between 10 and 14.5 percent. Yet, as the angle spread increases and approaches $\Delta = 180^o$, the system capacity decreases such that the multiple antenna capacity reduces to that of a single antenna.

- An approach for evaluating the reverse link capacity of a CDMA system using digital beamforming and employing a base station antenna array under imperfect power control where the effects of mutual coupling and scatter due to

multipath are included. The derivation for the probability of outage for a system with perfect power control uses an approach based on [91] and [92]. The end result is two expressions for the outage probability, one is an upper bound and other is a Gaussian approximation. This derivation is then extended to the case of imperfect power control, where the upper-bound and Gaussian approximation of the outage probability are obtained. From this analysis, the results indicate that the performance of systems which use imperfect power control is lower relative to systems using perfect power control, which is in agreement with the open literature on this subject. Moreover, the effects of mutual coupling and scatter further degrades performance of these systems. Although this part of the analysis is novel, the results are intuitive by reasonable sense and agree with the results found in the rest of this thesis. Finally, as the number of antennas within the array increases, system performance also improves. Thus, the use of base station antenna arrays in increase system capacity is justified.

## 6.3 Future Work

Suggested areas of researcher which would compliment this thesis are:

- Throughout this thesis we have adopted the same base station antenna array setup used by Colman [12] and Earnshaw [19] for the sake of comparison, namely, a circular array consisting of one to six dipole antenna elements with half wavelength adjacent spacing. Unfortunately, it has been shown that CDMA systems using adaptive arrays with circular geometries do not perform as well as other geometries, such as linear, triangular, and golomb. Therefore, to study the system performance where other array geometries are used, the analysis

in this thesis must be modified to account for the new relative positions and distances of the array elements.

- Several researchers have suggested that there exist several values for the adjacent separation between dipole antennas in the array that the effects of mutual coupling may be potentially beneficial to the system performance, such as Diouris, McLaughlin, and Zeidler in [16]. The adjacent separation of dipole antennas in this thesis has been fixed to one half wavelength, keep with the spirit of research conducted by Colman [12] and Earnshaw [19]. Unfortunately, in many of the derived expressions have the adjacent separation of one half wavelength "hard-coded" into them. Thus, to study the impact on performance by array element adjacent separation, one must modify the expressions by allowing for an adjacent distance variable.

- Throughout this thesis, we have assumed that capacity prediction being derived is for a single cell system. Although extending the derivation of the system capacity to a multi-cell environment is simple in some cases, such as the derivation for the Erlang capacity in Chapter 5, the modifications of the system capacity derivations in the majority of this thesis will be extensive.

- This thesis focused primarily on the performance issues of CDMA systems using digital beamforming and employing base station antenna arrays. We have chosen, as performance measures, the system capacity and the beampatterns of the base station antenna array to indicate how well or how poorly our system is performing when the effects of mutual coupling, scatter, and/or power control are included. Another performance measure which could be use is the receiver bit-error-rate (BER), as in [56]-[59]. Using the probability of bit error, the performance of the CDMA system as a function of the number of users within the

cell could be calculated.

- In Chapter 3, the full-wave electromagnetic numerical software, IE3D, by Zeland Software is capable of producing beampatterns in our analysis of CDMA systems employing smart antennas. Furthermore, the beampatterns produced with the full-wave electromagnetic numerical computation are in agreement with the beampatterns produced with analytical methods. Thus, the rationale for the full-wave electromagnetic numerical computation is that it is capable of predicting beampatterns for a larger class of antenna arrays and antenna types which cannot be analytically studied, such as those which have directional radiation that could be used in fixed wireless applications. Therefore, the full-wave electromagnetic numerical computation could be used in an investigation of the performance of CDMA systems employing base station antenna arrays where the array geometry and/or antenna type cannot be analytically studied.

- Throughout this thesis, we have only investigated the uplink system performance, where the effects of mutual coupling, scatter due to multipath, and power control have all been accounted-for. In the future, this work can be extend to the case of the downlink system performance, such that these effects are also included. It should be noted that according to the Reciprocity Theorem, the mutual coupling information is identical in both the uplink and downlink cases.

## 6.4 Conclusion

In this thesis, we have significantly improved the accuarcy of the work carried out in [12] and [19] by including in the system performance analysis the effects of mutual

coupling, scatter due to multipath, and power control. We observe that by including these effects, the performance of a CDMA communication system employing digital beamforming and a base station antenna array degrades significantly relative to the case when one of more of these effects are not present. Furthermore, the limitations of smart antennas are exhibited when these effects are significant, as in the case of beamforming in high-scatter environments, for example.

# Appendix A

# Derivation of Complex Second Moments

In this appendix, we derive the complex second moments of the total received voltage amplitudes at antennas $i$ and $k$ in Section 4.3 such that its joint probability distribution is determined. These complex second moments are $\overline{B_{1c}B_{1c}^*}$, $\overline{B_{1s}B_{1s}^*}$, $\overline{B_{2c}B_{2c}^*}$, $\overline{B_{2s}B_{2s}^*}$, $\overline{B_{1c}B_{2c}^*}$, $\overline{B_{1s}B_{2s}^*}$, $\overline{B_{1c}B_{1s}^*}$, $\overline{B_{2c}B_{2s}^*}$, $\overline{B_{1c}B_{2s}^*}$, and $\overline{B_{2c}B_{1s}^*}$, where $\overline{(\cdot)}$ is the expectation of $(\cdot)$, and $B_{1c}$, $B_{1s}$, $B_{2c}$, and $B_{2s}$ are defined by Equations (4.24) through (4.27), respectively.

Before we begin with the derivations, we must recall several equations from Section 4.3 which are used extensively throughout this appendix.

From Equation (4.9), the mean-squared signal amplitude at antennas $i$ and $k$ is

$$\overline{A_1^2} = \overline{A_2^2} = \sum_{r=1}^{n} a_r^2$$

which is required in every derivation to transform the resulting expression into a usable form.

Furthermore, since our derivations are based on the basic definition of the mean, we require the use of Equations (4.24) through (4.27), namely

$$B_{1c} \;=\; |Y_{ii}|A_1\cos(\Psi_1)e^{j\angle Y_{ii}} + |Y_{ik}|A_2\cos(\Psi_2)e^{j\angle Y_{ik}}$$

$$= |Y_{ii}|\sum_{r=1}^{m} a_r \cos(\psi_r + \chi_r) e^{j\angle Y_{ii}} + |Y_{ik}|\sum_{r=1}^{m} a_r \cos(\psi_r - \chi_r) e^{j\angle Y_{ik}}$$

$$\begin{aligned} B_{1s} &= |Y_{ii}| A_1 \sin(\Psi_1) e^{j\angle Y_{ii}} + |Y_{ik}| A_2 \sin(\Psi_2) e^{j\angle Y_{ik}} \\ &= |Y_{ii}|\sum_{r=1}^{m} a_r \sin(\psi_r + \chi_r) e^{j\angle Y_{ii}} + |Y_{ik}|\sum_{r=1}^{m} a_r \sin(\psi_r - \chi_r) e^{j\angle Y_{ik}} \end{aligned}$$

$$\begin{aligned} B_{2c} &= |Y_{ki}| A_1 \cos(\Psi_1) e^{j\angle Y_{ki}} + |Y_{kk}| A_2 \cos(\Psi_2) e^{j\angle Y_{kk}} \\ &= |Y_{ki}|\sum_{r=1}^{m} a_r \cos(\psi_r + \chi_r) e^{j\angle Y_{ki}} + |Y_{kk}|\sum_{r=1}^{m} a_r \cos(\psi_r - \chi_r) e^{j\angle Y_{kk}} \end{aligned}$$

$$\begin{aligned} B_{2s} &= |Y_{ki}| A_1 \sin(\Psi_1) e^{j\angle Y_{ki}} + |Y_{kk}| A_2 \sin(\Psi_2) e^{j\angle Y_{kk}} \\ &= |Y_{ki}|\sum_{r=1}^{m} a_r \sin(\psi_r + \chi_r) e^{j\angle Y_{ki}} + |Y_{kk}|\sum_{r=1}^{m} a_r \sin(\psi_r - \chi_r) e^{j\angle Y_{kk}} \end{aligned}$$

respectively, where

$$\chi_r = \frac{\pi d}{\lambda}\cos(\theta_{k_r})$$

Finally, since the phase angles $\psi_r$ are assumed to be random and $m$ is assumed to be large, we can then say that $B_{1c}$, $B_{1s}$, $B_{2c}$, and $B_{2s}$ are each distributed normally with zero mean.

Therefore, we commence with the expression for $\overline{B_{1c}B_{1c}^*}$ by using Equation (4.24), and applying the definition of the mean squared value, thus yielding

$$\begin{aligned} \overline{B_{1c}B_{1c}^*} &= E\left\{\left(|Y_{ii}| A_1 \cos(\Psi_1) e^{j\angle Y_{ii}} + |Y_{ik}| A_2 \cos(\Psi_2) e^{j\angle Y_{ik}}\right)\right. \\ &\quad \left.\cdot \left(|Y_{ii}| A_1 \cos(\Psi_1) e^{j\angle Y_{ii}} + |Y_{ik}| A_2 \cos(\Psi_2) e^{j\angle Y_{ik}}\right)^*\right\} \\ &= E\left\{\left(|Y_{ii}| A_1 \cos(\Psi_1) e^{j\angle Y_{ii}} + |Y_{ik}| A_2 \cos(\Psi_2) e^{j\angle Y_{ik}}\right)\right. \\ &\quad \left.\cdot \left(|Y_{ii}| A_1 \cos(\Psi_1) e^{-j\angle Y_{ii}} + |Y_{ik}| A_2 \cos(\Psi_2) e^{-j\angle Y_{ik}}\right)\right\} \\ &= E\left\{|Y_{ii}|^2 A_1^2 \cos^2(\Psi_1) + |Y_{ik}|^2 A_2^2 \cos^2(\Psi_2)\right. \\ &\quad \left.+|Y_{ii}|\,|Y_{ik}|\, A_1 A_2 \cos(\Psi_1)\cos(\Psi_2)\, e^{j\left(\angle Y_{ii} - \angle Y_{ik}\right)}\right. \end{aligned}$$

$$
\begin{aligned}
&+ |Y_{ii}|\,|Y_{ik}|\,A_1A_2\cos(\Psi_1)\cos(\Psi_2)\,e^{j\left(\angle Y_{ik}-\angle Y_{ii}\right)}\Big\} \\
= \;& E\Big\{|Y_{ii}|^2\,A_1^2\left(\frac{1}{2}+\frac{1}{2}\cos(2\Psi_1)\right)+|Y_{ik}|^2\,A_2^2\left(\frac{1}{2}+\frac{1}{2}\cos(2\Psi_2)\right) \\
&+2\,|Y_{ii}|\,|Y_{ik}|\,A_1A_2\cos(\Psi_1)\cos(\Psi_2)\cos(\angle Y_{ii}-\angle Y_{ik})\} \\
= \;& E\Big\{|Y_{ii}|^2\,A_1^2\left(\frac{1}{2}+\frac{1}{2}\cos(2\Psi_1)\right)+|Y_{ik}|^2\,A_2^2\left(\frac{1}{2}+\frac{1}{2}\cos(2\Psi_2)\right) \\
&+|Y_{ii}|\,|Y_{ik}|\,A_1A_2\left(\cos(\Psi_1+\Psi_2)+\cos(\Psi_1-\Psi_2)\right)\cos(\angle Y_{ii}-\angle Y_{ik})\} \\
= \;& \frac{1}{2}\,|Y_{ii}|^2\,\overline{A_1^2}+\frac{1}{2}\,|Y_{ik}|^2\,\overline{A_2^2} \\
&+|Y_{ii}|\,|Y_{ik}|\,\overline{A_1A_2}\cos(\Psi_1-\Psi_2)\cos(\angle Y_{ii}-\angle Y_{ik}) \\
= \;& \left(|Y_{ii}|^2+|Y_{ik}|^2\right)\frac{1}{2}\sum_{r=1}^{m}{a_r}^2 \\
&+|Y_{ii}||Y_{ik}|\sum_{r=1}^{m}{a_r}^2\cos\left(\frac{2\pi d}{\lambda}\cos(\theta_{k_r})\right)\cos(\angle Y_{ii}-\angle Y_{ik}) \qquad \text{(A.1)}
\end{aligned}
$$

which agrees with Equation (4.29). Furthermore, using the same approach for determining $\overline{B_{1c}B_{1c}^*}$, we are able to derive the expressions for $\overline{B_{1s}B_{1s}^*}$, as well as $\overline{B_{2c}B_{2c}^*}$ and $\overline{B_{2s}B_{2s}^*}$, yielding Equations (4.29) and (4.30), respectively.

We next deal with the expression for $\overline{B_{1c}B_{2c}^*}$, which we use Equations (4.24) and (4.26), and applying the definition of the mean, thus yielding

$$
\begin{aligned}
\overline{B_{1c}B_{2c}^*} \;=\;& E\Big\{\left(|Y_{ii}|A_1\cos(\Psi_1)e^{j\angle Y_{ii}}+|Y_{ik}|A_2\cos(\Psi_2)e^{j\angle Y_{ik}}\right) \\
&\cdot\left(|Y_{ki}|A_1\cos(\Psi_1)e^{j\angle Y_{ki}}+|Y_{kk}|A_2\cos(\Psi_2)e^{j\angle Y_{kk}}\right)^*\Big\} \\
=\;& E\Big\{\left(|Y_{ii}|A_1\cos(\Psi_1)e^{j\angle Y_{ii}}+|Y_{ik}|A_2\cos(\Psi_2)e^{j\angle Y_{ik}}\right) \\
&\cdot\left(|Y_{ki}|A_1\cos(\Psi_1)e^{-j\angle Y_{ki}}+|Y_{kk}|A_2\cos(\Psi_2)e^{-j\angle Y_{kk}}\right)\Big\} \\
=\;& E\Big\{|Y_{ii}|\,|Y_{ki}|\,A_1A_1\cos^2(\Psi_1)\,e^{j\left(\angle Y_{ii}-\angle Y_{ki}\right)} \\
&+|Y_{ik}|\,|Y_{kk}|\,A_2A_2\cos^2(\Psi_2)\,e^{j\left(\angle Y_{ik}-\angle Y_{kk}\right)} \\
&+|Y_{ii}|\,|Y_{kk}|\,A_1A_2\cos(\Psi_1)\cos(\Psi_2)\,e^{j\left(\angle Y_{ii}-\angle Y_{kk}\right)} \\
&+|Y_{ik}|\,|Y_{ki}|\,A_1A_2\cos(\Psi_1)\cos(\Psi_2)\,e^{j\left(\angle Y_{ik}-\angle Y_{ki}\right)}\Big\} \\
=\;& E\Big\{|Y_{ii}|\,|Y_{ki}|\,A_1^2\left(\frac{1}{2}+\frac{1}{2}\cos(2\Psi_1)\right)e^{j\left(\angle Y_{ii}-\angle Y_{ki}\right)}
\end{aligned}
$$

$$
\begin{aligned}
&+|Y_{ik}|\,|Y_{kk}|\,A_2^2\left(\frac{1}{2}+\frac{1}{2}\cos\left(2\Psi_2\right)\right)e^{j\left(\angle Y_{ik}-\angle Y_{kk}\right)}\\
&+\frac{1}{2}|Y_{ii}|\,|Y_{kk}|\,A_1A_2(\cos\left(\Psi_1+\Psi_2\right)+\cos\left(\Psi_1-\Psi_2\right))e^{j\left(\angle Y_{ii}-\angle Y_{kk}\right)}\\
&+\frac{1}{2}|Y_{ik}|\,|Y_{ki}|\,A_1A_2(\cos\left(\Psi_1+\Psi_2\right)+\cos\left(\Psi_1-\Psi_2\right))e^{j\left(\angle Y_{ik}-\angle Y_{ki}\right)}\Big\}\\
=\;&\frac{1}{2}|Y_{ii}|\,|Y_{ki}|\,\overline{A_1^2}e^{j\left(\angle Y_{ii}-\angle Y_{ki}\right)}\\
&+\frac{1}{2}|Y_{ik}|\,|Y_{kk}|\,\overline{A_2^2}e^{j\left(\angle Y_{ik}-\angle Y_{kk}\right)}\\
&+\frac{1}{2}|Y_{ii}|\,|Y_{kk}|\,\overline{A_1A_2\cos\left(\Psi_1-\Psi_2\right)}e^{j\left(\angle Y_{ii}-\angle Y_{kk}\right)}\\
&+\frac{1}{2}|Y_{ik}|\,|Y_{ki}|\,\overline{A_1A_2\cos\left(\Psi_1-\Psi_2\right)}e^{j\left(\angle Y_{ik}-\angle Y_{ki}\right)}\\
=\;&|Y_{ii}||Y_{ki}|\frac{1}{2}\sum_{r=1}^{m}a_r^2e^{j\left(\angle Y_{ii}-\angle Y_{ki}\right)}\\
&+|Y_{ik}||Y_{kk}|\frac{1}{2}\sum_{r=1}^{m}a_r^2e^{j\left(\angle Y_{ik}-\angle Y_{kk}\right)}\\
&+|Y_{ii}||Y_{kk}|\frac{1}{2}\sum_{r=1}^{m}a_r^2\cos\left(\frac{2\pi d}{\lambda}\cos\left(\theta_{k_r}\right)\right)e^{j\left(\angle Y_{ii}-\angle Y_{kk}\right)}\\
&+|Y_{ik}||Y_{ki}|\frac{1}{2}\sum_{r=1}^{m}a_r^2\cos\left(\frac{2\pi d}{\lambda}\cos\left(\theta_{k_r}\right)\right)e^{j\left(\angle Y_{ik}-\angle Y_{ki}\right)}
\end{aligned}
\tag{A.2}
$$

which agrees with Equation (4.33). Similarly, using the approach to determine $\overline{B_{1c}B_{2c}^*}$, we are able to derive the expression for $\overline{B_{1s}B_{2s}^*}$ yielding Equation (4.33).

We next deal with the expression for $\overline{B_{1c}B_{1s}^*}$, which we use Equations (4.24) and (4.25), and applying the definition of the mean, thus yielding

$$
\begin{aligned}
\overline{B_{1c}B_{1s}^*} \;=\;& E\Big\{\Big(|Y_{ii}|A_1\cos(\Psi_1)e^{j\angle Y_{ii}}+|Y_{ik}|A_2\cos(\Psi_2)e^{j\angle Y_{ik}}\Big)\\
&\cdot\Big(|Y_{ii}|A_1\sin(\Psi_1)e^{j\angle Y_{ii}}+|Y_{ik}|A_2\sin(\Psi_2)e^{j\angle Y_{ik}}\Big)^*\Big\}\\
=\;& E\Big\{\Big(|Y_{ii}|A_1\cos(\Psi_1)e^{j\angle Y_{ii}}+|Y_{ik}|A_2\cos(\Psi_2)e^{j\angle Y_{ik}}\Big)\\
&\cdot\Big(|Y_{ii}|A_1\sin(\Psi_1)e^{-j\angle Y_{ii}}+|Y_{ik}|A_2\sin(\Psi_2)e^{-j\angle Y_{ik}}\Big)\Big\}\\
=\;& E\Big\{|Y_{ik}|\,|Y_{ii}|\,A_2A_1\cos\left(\Psi_2\right)\sin\left(\Psi_1\right)e^{j\left(\angle Y_{ik}-\angle Y_{ii}\right)}\\
&+|Y_{ik}|\,|Y_{ik}|\,A_2A_2\cos\left(\Psi_2\right)\sin\left(\Psi_2\right)\\
&+|Y_{ii}|\,|Y_{ii}|\,A_1A_1\cos\left(\Psi_1\right)\sin\left(\Psi_1\right)
\end{aligned}
$$

$$
\begin{aligned}
&+ |Y_{ii}|\,|Y_{ik}|\,A_1A_2\cos(\Psi_1)\sin(\Psi_2)\,e^{j\left(\angle Y_{ii}-\angle Y_{ik}\right)}\Big\} \\
= \;& E\Big\{\frac{1}{2}\,|Y_{ik}|\,|Y_{ii}|\,A_2A_1\left(\sin(\Psi_1+\Psi_2)+\sin(\Psi_1-\Psi_2)\right)e^{j\left(\angle Y_{ik}-\angle Y_{ii}\right)} \\
&+\frac{1}{2}\,|Y_{ik}|\,|Y_{ik}|\,A_2A_2\left(\sin(\Psi_2+\Psi_2)+\sin(\Psi_2-\Psi_2)\right) \\
&+\frac{1}{2}\,|Y_{ii}|\,|Y_{ii}|\,A_1A_1\left(\sin(\Psi_1+\Psi_1)+\sin(\Psi_1-\Psi_1)\right) \\
&+\frac{1}{2}\,|Y_{ii}|\,|Y_{ik}|\,A_1A_2\left(\sin(\Psi_2+\Psi_1)+\sin(\Psi_2-\Psi_1)\right)e^{j\left(\angle Y_{ii}-\angle Y_{ik}\right)}\Big\} \\
= \;& E\Big\{\frac{1}{2}\,|Y_{ik}|\,|Y_{ii}|\,A_2A_1\left(\sin(\Psi_1+\Psi_2)+\sin(\Psi_1-\Psi_2)\right)e^{j\left(\angle Y_{ik}-\angle Y_{ii}\right)} \\
&+\frac{1}{2}\,|Y_{ik}|\,|Y_{ik}|\,A_2A_2\sin(2\Psi_2)+\frac{1}{2}\,|Y_{ii}|\,|Y_{ii}|\,A_1A_1\sin(2\Psi_1) \\
&+\frac{1}{2}\,|Y_{ii}|\,|Y_{ik}|\,A_1A_2\left(\sin(\Psi_2+\Psi_1)+\sin(\Psi_2-\Psi_1)\right)e^{j\left(\angle Y_{ii}-\angle Y_{ik}\right)}\Big\} \\
= \;& \frac{1}{2}\,|Y_{ik}|\,|Y_{ii}|\,\overline{A_2A_1\sin(\Psi_1-\Psi_2)}e^{j\left(\angle Y_{ik}-\angle Y_{ii}\right)} \\
&+\frac{1}{2}\,|Y_{ii}|\,|Y_{ik}|\,\overline{A_1A_2\sin(\Psi_2-\Psi_1)}e^{-j\left(\angle Y_{ik}-\angle Y_{ii}\right)} \\
= \;& |Y_{ik}|\,|Y_{ii}|\,\overline{A_2A_1\sin(\Psi_1-\Psi_2)}j\sin\left(j\left(\angle Y_{ik}-\angle Y_{ii}\right)\right) \\
= \;& j\,|Y_{ii}|\,|Y_{ik}|\sin\left(\angle Y_{ik}-\angle Y_{ii}\right)\sum_{r=1}^{m}a_r^2\sin\left(\frac{2\pi d}{\lambda}\cos\left(\theta_{k_r}\right)\right) \qquad \text{(A.3)}
\end{aligned}
$$

which agrees with Equation (4.31). Similarly, using the approach to determine $\overline{B_{1c}B_{1s}^*}$, we are able to derive the expression for $\overline{B_{2c}B_{2s}^*}$ yielding Equation (4.32).

Finally, we deal with the expression for $\overline{B_{1c}B_{2s}^*}$, which we use Equations (4.24) and (4.27), and applying the definition of the mean, thus yielding

$$
\begin{aligned}
\overline{B_{1c}B_{2s}^*} \;=\; & E\Big\{\Big(|Y_{ii}|A_1\cos(\Psi_1)e^{j\angle Y_{ii}}+|Y_{ik}|A_2\cos(\Psi_2)e^{j\angle Y_{ik}}\Big) \\
&\cdot\Big(|Y_{ki}|A_1\sin(\Psi_1)e^{j\angle Y_{ki}}+|Y_{kk}|A_2\sin(\Psi_2)e^{j\angle Y_{kk}}\Big)^*\Big\} \\
= \;& E\Big\{\Big(|Y_{ii}|A_1\cos(\Psi_1)e^{j\angle Y_{ii}}+|Y_{ik}|A_2\cos(\Psi_2)e^{j\angle Y_{ik}}\Big) \\
&\cdot\Big(|Y_{ki}|A_1\sin(\Psi_1)e^{-j\angle Y_{ki}}+|Y_{kk}|A_2\sin(\Psi_2)e^{-j\angle Y_{kk}}\Big)\Big\} \\
= \;& E\Big\{|Y_{ii}|\,|Y_{ki}|\,A_1A_1\cos(\Psi_1)\sin(\Psi_1)\,e^{j\left(\angle Y_{ii}-\angle Y_{ki}\right)} \\
&+|Y_{ik}|\,|Y_{kk}|\,A_2A_2\cos(\Psi_2)\sin(\Psi_2)\,e^{j\left(\angle Y_{ik}-\angle Y_{kk}\right)} \\
&+|Y_{ik}|\,|Y_{ki}|\,A_1A_2\cos(\Psi_1)\sin(\Psi_2)\,e^{j\left(\angle Y_{ik}-\angle Y_{ki}\right)}
\end{aligned}
$$

$$
\begin{aligned}
&+ |Y_{ii}|\,|Y_{kk}|\,A_1A_2\cos(\Psi_2)\sin(\Psi_1)\,e^{j\left(\angle Y_{ii}-\angle Y_{kk}\right)}\Big\} \\
= \;& E\Big\{\frac{1}{2}\,|Y_{ii}|\,|Y_{ki}|\,A_1A_1\left(\sin(\Psi_1+\Psi_1)+\sin(\Psi_1-\Psi_1)\right)e^{j\left(\angle Y_{ii}-\angle Y_{ki}\right)} \\
&+\frac{1}{2}\,|Y_{ik}|\,|Y_{kk}|\,A_2A_2\left(\sin(\Psi_2+\Psi_2)+\sin(\Psi_2-\Psi_2)\right)e^{j\left(\angle Y_{ik}-\angle Y_{kk}\right)} \\
&+\frac{1}{2}\,|Y_{ik}|\,|Y_{ki}|\,A_1A_2\left(\sin(\Psi_2+\Psi_1)+\sin(\Psi_2-\Psi_1)\right)e^{j\left(\angle Y_{ik}-\angle Y_{ki}\right)} \\
&+\frac{1}{2}\,|Y_{ii}|\,|Y_{kk}|\,A_1A_2\left(\sin(\Psi_1+\Psi_2)+\sin(\Psi_1-\Psi_2)\right)e^{j\left(\angle Y_{ii}-\angle Y_{kk}\right)}\Big\} \\
= \;& \frac{1}{2}\,|Y_{ik}|\,|Y_{ki}|\,\overline{A_1A_2\sin(\Psi_2-\Psi_1)}e^{j\left(\angle Y_{ik}-\angle Y_{ki}\right)} \\
&+\frac{1}{2}\,|Y_{ii}|\,|Y_{kk}|\,\overline{A_1A_2\sin(\Psi_1-\Psi_2)}e^{j\left(\angle Y_{ii}-\angle Y_{kk}\right)} \\
= \;& -|Y_{ii}||Y_{kk}|\frac{1}{2}\sum_{r=1}^{m}a_r^2\sin\left(\frac{2\pi d}{\lambda}\cos(\theta_{k_r})\right)e^{j\left(\angle Y_{ii}-\angle Y_{kk}\right)} \\
&+|Y_{ik}||Y_{ki}|\frac{1}{2}\sum_{r=1}^{m}a_r^2\sin\left(\frac{2\pi d}{\lambda}\cos(\theta_{k_r})\right)e^{j\left(\angle Y_{ki}-\angle Y_{ik}\right)} \qquad \text{(A.4)}
\end{aligned}
$$

which agrees with Equation (4.34). Similarly, using the approach to determine $\overline{B_{1c}B_{2s}^*}$, we are able to derive the expression for $\overline{B_{2c}B_{1s}^*}$ yielding Equation (4.34).

# Appendix B

# Dipole Antenna Array Model in IE3D

## B.1 Introduction

IE3D is a full-wave electromagnetic numerical computation and optimization software package for the analysis and design of 3-dimensional structures, such as antennas, printed circuit and digital boards, etc [98].

As was mentioned in Section 6.3, IE3D is capable of predicting beampatterns for a larger class of antenna arrays and antenna types which cannot be analytically studied. Furthermore, it comes with several useful software tools to assist the user in the design and analysis process: the layout editor MGRID, the schematic editor MODUA, the current display post processor CURVIEW, and the radiation pattern post processor PATTERNVIEW [98].

Unfortunately, like other proprietary software packages, the specific way in which IE3D operates is unknown to the end-user and is essentially a "black box". Thus, the accuracy of the design and analysis is dependent on the user's input to the software. For example, the beampatterns of Figures 3.9, 3.13, 3.17, 3.21, and 3.25 were generated using IE3D. Upon comparison with the Method of Moments-generated

beampatterns of Figures 3.8, 3.12, 3.16, 3.20, and 3.24, respectively, we notice that the sidelobe levels are relatively smaller in the latter. As was explained in Subsection 3.3.2, it turns out that the way the dipole antennas were implemented in IE3D led to the difference in the beampatterns.

In this appendix, we will briefly cover the modeling of wire structures in IE3D, followed by an example of implementing a dipole antenna in IE3D.

## B.2 Modeling Wires in IE3D

Usually, a wire is modeled with separated field and observation points. To avoid the possibility of the occurrence of a singularity in the numerical computation, it is assumed that the electric current is at the center of the wire and the observation point is on the surface of the wire. Such a model will inherently introduce some error since it is known that the current also flows on the surface of the wire.

In IE3D, the software models the surface currents of metallic structures and tests the field on them. Thus, a thin wire can be modeled as a metallic strip or a polygonal tube, depending on the accuracy requirements.

Since both the metallic strip or tube model assumes both the current source and observation point to be on the surface, this tends to increase the accuracy of the design and analysis.

## B.3 Example: Dipole Antenna

We will now go through a quick design example for a simple dipole antenna.

In this example, we fix the length of the dipole to 15 mm, the dipole radius to 0.075 mm, and a resonant frequency of about 10 GHz. It should be pointed out that this design process is applicable to other dipole lengths, radii, and frequencies.

1. Using MGRID, select **New** in **File** menu. When the window pops up, select **mm** as the **Length Unit**. When prompted for the **Layout and Grid**, add a new grid and enter the **Grid Size** of 0.15 mm. Click **OK**.

2. Define the following **Dielectric Parameters**:

   (a) $Ztop = 0mm, \epsilon_r = (1, 0), \mu_r = (1, 0), \sigma = (0, 0)$

   (b) $Ztop = 1.0 \times 10^{15}mm, \epsilon_r = (1, 0), \mu_r = (1, 0), \sigma = (0, 0)$

3. Define the following **Metallic Strip Parameters**:

   (a) $Thickness = 0.075mm, \epsilon_r = (1, 0), \mu_r = (1, 0), \sigma = (4.9 \times 10^7, 0)$

4. Define the **Discretization Parameters**:

   (a) $Fmax = 15GHz$

   (b) $Ncell = 15$

5. Choose **Create and Edit Vertices** in the **Input** menu and click the **Import** button. Then click **OK** when prompted.

6. Since the IE3D software package comes with some ready made examples and designs, let us choose the dipole design found in

   `C:\ie3d\samples\dipole.txt`

   and then click **OK** until the MGRID is back in 2D mode.

7. Choose **Build Wire Path** in **Adv Edit** menu. Input 6 for the **Number of Segments for Circle** and 0.075 mm for the **Radius**. Click **OK** to create the dipole. To view the whole circuit, choose **Whole Circuit** in the **View** menu.

8. Remove the small bend in the dipole by choosing **Select Polygon Group** in the **Edit** menu. Form a window over the bend area and select **Delete Objects** in the **Edit** menu.

9. To attach the ports to this dipole antenna, choose **Port for Edge group** in the **Port** Menu, followed by **Extension for MMIC** scheme. Using the left mouse button, define one of the terminals (created via the deletion of the bend in the previous step) as "+1" and use the right mouse button to define the remaining terminal as "−1". Then choose **Exit Port** in the **Port** menu to return to 2D mode.

10. Save the structure as

    `C:\my documents\dipole.geo`

    which can then be used by the other software programs found in IE3D. In particular, CURVIEW can be used to generated the beampattern for this antenna, or an array of antennas. Please refer to the IE3D User Manual for information on how to use these packages [98].

It should be noted that the dipole antenna arrays designed in IE3D for this thesis were created in the same fashion described in this section.

# Bibliography


[1] M. Abramowitz and I. A. Stegun. *Handbook of Mathematical Functions with Formulas, Graphs, and Mathematical Tables*. 55. National Bureau of Standards, June 1964.

[2] A. T. Adams and B. J. Strait. Modern analysis methods for emc. *IEEE/EMC Symposium*, pages 383–393, July 1970.

[3] R. S. Adve and T. K. Sarkar. Compensation for the effects of mutual coupling on direct data domain adaptive algorithms. *IEEE Transactions on Antennas and Propagation*, 48(1):86–94, January 2000.

[4] J. B. Andersen. Antenna arrays in mobile communications: Gain, diversity, and channel capacity. *IEEE Antennas and Propagation Magazine*, 42(2):12–16, April 2000.

[5] S. P. Applebaum. Adaptive arrays. *IEEE Transactions on Antennas and Propagation*, 24(5):585–598, September 1976.

[6] A. Baiocchi, F. Delli Priscoli, and F. Sestini. Improving the erlang capacity of a cdma cellular network under bursty user mobility. *The Fifth IEEE International Conference on Universal Personal Communications*, 1:194–199, 1996.

[7] C. A. Balanis. *Antenna Theory: Analysis and Design*. John Wiley and Sons, 2nd edition, 1997.

[8] E. N. Bramley. Diversity effects in spaced-aerial reception of ionospheric waves. *IEE Proceedings*, 98(3):19–25, 1951.

[9] R. Cameron and B. Woerner. Performance analysis of cdma with imperfect power control. *IEEE Transactions on Communications*, 44(7):777–781, July 1996.

[10] P. S. Carter. Circuit relations in radiating systems and applications to antenna problems. *Proceedings of the IEEE*, 20(6):1004–1041, June 1932.

[11] D. K. Cheng. Optimization techniques for antenna arrays. *Proceedings of the IEEE*, 59(12):1664–1674, December 1971.

[12] G. W. K. Colman. An investigation into the capacity of cellular cdma commnications systems with beamforming in environments with scatter. Master's thesis, Queen's University at Kingston, 1998.

[13] R. T. Compton. *Adaptive Antennas: Concept and Performance*. Prentice-Hall, Inc., 1988.

[14] G. E. Corazza, G. De Maio, and F. Vatalaro. Cdma cellular system performance with fading, shadowing, and imperfect power control. *IEEE Transactions on Vehicular Technology*, 47(2):450–459, May 1998.

[15] W. B. Davenport, Jr. and W. L. Root. *An Introduction to the Theory of Random Signals and Noise*. McGraw-Hill, Inc., 1994.

[16] J. F. Diouris, S. McLaughlin, and J. Zeidler. Sensitivity analysis of the performance of a diversity receiver. *1999 IEEE International Conference on Communications*, CD-ROM(S40A-4):1–5, 1999.

[17] R. C. Dixon. *Spread Spectrum Systems*. John Wiley and Sons, Inc., 1976.

[18] J. Duggan. Adaptive beamforming with a focal-fed offset parabolic reflector antenna. Master's thesis, Queen's University at Kingston, 1997.

[19] A. M. Earnshaw. *An Investigation into Improving Performance of Cellular CDMA Communication Systems with Digital Beamforming*. PhD thesis, Queen's University at Kingston, 1997.

[20] A. M. Earnshaw and S. D. Blostein. Efficient evaluation of adaptive digital beamforming for multi-service provision in a cellular cdma system. *48th IEEE Vehicular Technology Conference*, 3:1665–1669, 1998.

[21] R. S. Elliott. *Antenna Theory and Design*. Prentice-Hall, Inc., 1981.

[22] R. B. Ertel, P. Cardieri, K. W. Sowerby, T. S. Rappaport, and J. H. Reed. Overview of spatial channel models for antenna array communication systems. *IEEE Personal Communications*, 5(1):10–22, 1998.

[23] R. B. Ertel and J. H. Reed. Angle and time of arrival statistics for circular and elliptical scattering models. *IEEE Journal on Selected Areas in Communications*, 17(11):1829–1840, November 1999.

[24] G. Femenias, F. J. Perez-Briceno, A. Gelonch, and I. Furio. Transmitter power control for ds/cdma cellular mobile radio networks. *The Sixth IEEE International Symposium on Personal, Indoor and Mobile Radio Communications*, 1:46–50, 1995.

[25] B. Friedlander and A. J. Weiss. Direction finding in the presence of mutual coupling. *IEEE Transactions on Antennas and Propagation*, 39(3):273–284, March 1991.

[26] H. Gao and P. J. Smith. Exact sinr calculations for optimum linear combining in wireless systems. *Probability in the Engineering and Informational Sciences*, 12:261–281, 1998.

[27] K. S. Gilhousen, I. M. Jacobs, R. Padovani, A. J. Viterbi, L. A. Weaver, and C. E. Wheatley III. On the capacity of a cellular cdma system. *IEEE Transactions on Vehicular Technology*, 40(2):303–312, May 1991.

[28] P. M. Grant, J. S. Thompson, and B. Mulgrew. Adaptive arrays for narrow-band cdma base stations. *Electronics and Communications Engineering Journal*, 10(4):156–166, August 1998.

[29] I. J. Gupta and A. A. Ksienski. Effect of mutual coupling on the performance of adaptive arrays. *IEEE Transactions on Antennas and Propagation*, 31(5):785–791, Septemeber 1983.

[30] R. F. Harrington. *Field Computation by Moment Method*. MacMillan Co., 1968.

[31] T. Y. Hsu and C. Y. Lee. The outage probability in ds/cdma for cellular mobile radio with imperfect power control. *The Seventh IEEE International Symposium on Personal, Indoor and Mobile Radio Communications*, 1:183–187, 1996.

[32] J. E. Hudson. *Adaptive Array Principles*. Peter Peregrinus Ltd., 1981.

[33] W. C. Jakes. *Mobile Microwave Communications*. John Wiley and Sons, 1974.

[34] C. T. A. Johnk. *Engineering Electromagnetic Fields and Waves*. John Wiley and Sons, 2nd edition, 1988.

[35] D. H. Johnson and D. E. Dudgeon. *Array Signal Processing: Concepts and Techniques*. Prentice Hall, Inc., 1993.

[36] E. C. Jordan. *Electromagnetic Waves and Radiating Systems*. Prentice-Hall, Inc., 1950.

[37] H. E. King. Mutual impedance of unequal length antennas in echelon. *IRE Transactions on Antennas and Propagation*, 5:306–313, July 1957.

[38] J. D. Krauss. *Antennas*. McGraw-Hill, Inc., 2nd edition, 1988.

[39] D. Lee and C. Xu. The effect of narrowbeam antenna and multiple tiers on system capacity in cdma wireless local loop. *IEEE Communications Magazine*, 35(9):110–114, September 1997.

[40] J. S. Lee and L. E. Miller. On the erlang capacity of cdma cellular systems. *IEEE Global Telecommunications Conference*, 3:1877–1883, 1995.

[41] W. C. Y. Lee. Overview of cellular cdma. *IEEE Transactions on Vehicular Technology*, 40(2):291–302, May 1991.

[42] M. L. Leou, C. C. Yeh, and D. R. Ucci. Bearing estimations with mutual coupling present. *IEEE Transactions on Antennas and Propagation*, 37(10):1332–1335, October 1989.

[43] J. C. Liberti and T. S. Rappaport. Analytical results for capacity improvements in cdma. *IEEE Transactions on Vehicular Technology*, 43(3):680–690, August 1994.

[44] F. Lin, X. Huang, and Y. Wu. An uplink power control scheme in cdma mobile communication system. *48th IEEE Vehicular Technology Conference*, 3:2479–2482, 1998.

[45] J. P. M. G. Linnartz. Exact analysis of the outage probability in multiple-user mobile radio. *IEEE Transactions on Communications*, 40(1):20–23, January 1992.

[46] M. P. Lotter and P. van Rooyen. Cellular channel modeling and the performance of ds/cdma systems with antenna arrays. *IEEE Journal on Selected Areas in Communications*, 17(12):2181–2196, December 1999.

[47] M. Lu, T. Lo, and J. Litva. A smart antenna array for cdma systems with noncoherent m-ary orthogonal modulation. *IEEE Global Telecommunications Conference*, 2:589–593, 1997.

[48] T. Luo. Beamforming in the uplink and downlink channels of a cellular cdma communication system. Master's thesis, Queen's University at Kingston, 1998.

[49] R. J. Mailloux. *Phased Array Antenna Handbook*. Artech House, 1994.

[50] J. A. G. Malherbe. Analysis of a linear antenna array including the effects of mutual coupling. *IEEE Transactions on Education*, 32(1):29–34, February 1989.

[51] S. Manji and W. Zhuang. Reverse link power control for packetized ds/cdma in a slowly rayleigh fading environment. *1997 IEEE International Conference on Communications*, 1:101–105, 1997.

[52] S. L. Marple. *Digital Spectral Analysis with Applications*. Prentice-Hall, Inc., 1987.

[53] L. B. Milstein, T. S. Rappaport, and R. Bargouti. Performance evaluation for cellular cdma. *IEEE Journal on Selected Areas in Communications*, 10(4):680–689, May 1992.

[54] R. A. Monzingo and T. W. Miller. *Introduction to Adaptive Arrays*. John Wiley and Sons, 1980.

[55] Motorola, Nokia, LSI Logic, Texas Instruments, Dot Wireless, and Broadcom. Proposed 1xtreme physical layer delta specification. 2000.

[56] A. F. Naguib. *Adaptive Antennas for CDMA Wireless Networks*. PhD thesis, Stanford University, 1995.

[57] A. F. Naguib and A. Paulraj. Performance of wireless cdma with m-ary orthogonal modulation and cell site antenna arrays. *IEEE Journal on Selected Areas in Communications*, 14(9):1770–1783, 1996.

[58] A. F. Naguib, A. Paulraj, and T. Kailath. Capacity improvement with base-station antenna arrays in cellular cdma. *IEEE Transactions on Vehicular Technology*, 43(3):691–698, 1994.

[59] A. F. Naguib, A. Paulraj, and T. Kailath. Performance of cdma cellular networks with base-station antenna arrays: The downlink. *1994 IEEE International Conference on Communications*, pages 795–799, 1994.

[60] R. Padovani. Reverse link performance of is-95 based cellular systems. *IEEE Personal Communications*, 1(3):28–34, 3rd Quarter 1994.

[61] A. Papoulis. *Probability, Random Variables, and Stochastic Processes*. McGraw-Hill, Inc., 3rd edition, 1991.

[62] K. M. Pasala and E. M. Friel. Mutual coupling effects and their reduction in wideband direction of arrival estimation. *IEEE Transactions on Aerospace and Electronic Systems*, 30(4):1116–1122, October 1994.

[63] A. J. Paulraj and C. B. Papadias. Space-time processing for wireless communication. *IEEE Signal Processing Magazine*, pages 49–83, November 1997.

[64] S. U. Pillai. *Array Signal Processing*. Springer-Verlag, 1989.

[65] D. M. Pozar. *Microwave engineering*. John Wiley and Sons, 2nd edition, 1998.

[66] W. H. Press, S. A. Teukolsky, W. T. Vetterling, and B. P. Flannery. *Numerical Recipes in C: The Art of Scientific Computing*. Cambridge University Press, 2nd edition, 1992.

[67] S. L. Preston, D. V. Thiel, T. A. Smith, S. G. O'Keefe, and J. W. Lu. Base-station tracking in mobile communications using a switched parasitic antenna array. *IEEE Transactions on Antennas and Propagation*, 46(6):841–844, June 1998.

[68] J. G. Proakis. *Digital Communications*. McGraw-Hill, Inc., 3rd edition, 1995.

[69] J. G. Proakis and M. Salehi. *Communication Systems Engineering*. Prentice-Hall, Inc., 1994.

[70] Qualcomm Inc. Mobile station-base compatibility standard for dual-mode wide-band spread system. 1993.

[71] S. Ramo, J. R. Whinnery, and T. Van Duzer. *Fields and Waves in Communications Electronics*. John Wiley and Sons, 3rd edition, 1994.

[72] N. N. Rao. *Elements of Engineering Electromagnetics*. Prentice-Hall, Inc., 4th edition, 1994.

[73] T. S. Rappaport. *Wireless Communications: Principles and Practice*. Prentice Hall, Inc., 1996.

[74] J. Salz and J. H. Winters. Effect of fading correlation on adaptive arrays in digital wireless communications. *1993 IEEE International Conference on Communications*, 3:1768–1774, 1993.

[75] J. Salz and J. H. Winters. Effect of fading correlation on adaptive arrays in digital mobile radio. *IEEE Transactions on Vehicular Technology*, 43(4):1049–1057, 1994.

[76] S. A. Schelkunoff and H. T. Friis. *Antennas: Theory and Practice*. John Wiley and Sons, 1952.

[77] Q. Shen and W. Krzymien. The effect of fading on the erlang capacity of the is-95 cdma celluar system. *1996 IEEE International Conference on Communications*, 3:1829–1833, 1996.

[78] W. Y. Shiu. Non-iterative digital beamforming in cdma cellular communications systems. Master's thesis, Queen's University at Kingston, 1998.

[79] H. Stellakis, A. Giordano, A. Aksu, and W. Biagini. Reverse link performance of wireless local loop cdma networks. *IEEE Communications Letters*, 4(2):49–51, February 2000.

[80] B. J. Strait and K. Hirasawa. Array design for a specified pattern by matrix methods. *IEEE Transactions on Antennas and Propagation*, 17(2):237–239, March 1969.

[81] B. T. Strait and A. T. Adams. Analysis and design of wire antennas with applications to emc. *IEEE Transactions on Electromagnetic Compatibility*, 12(2):45–54, May 1970.

[82] G. L. Stuber and C. Kchao. Analysis of a multiple-cell direct-sequence cdma cellular mobile radio system. *IEEE Journal on Selected Areas in Communications*, 10(4):669–679, May 1992.

[83] S. C. Swales, M. A. Beach, D. J. Edwards, and J. P. McGeehan. The performance enhancement of multibeam adaptive base-station antennas for cellular land mobile radio systems. *IEEE Transactions on Vehicular Technology*, 39(1):56–67, 1990.

[84] W. M. Tam and F. C. M. Lau. Analysis of power control and its imperfections in cellular cdma systems. *IEEE Transactions on Vehicular Technology*, 48(5):1706–1717, September 1999.

[85] G. B. Thomas. *Calculus and Analytic Geometry.* Addison-Wesley, 4th edition, 1968.

[86] J. S. Thompson, P. M. Grant, and B. Mulgrew. Smart antenna arrays for cdma systems. *IEEE Personal Communications*, 3(5):16–25, October 1996.

[87] TIA. The cdma2000 itu-r rtt candidate submission. TR45.5, 1998.

[88] N. T. Tin and S. D. Blostein. Wideband cdma smart antenna measurement system. *Proceedings of the Queen's 20th Biennial Symposium on Communications*, pages 186–190, 2000.

[89] G. V. Tsoulos, G. E. Athanasiadou, M. A. Beach, and S. C. Swales. Adaptive antennas for microcellular and mixed cell environments with ds-cdma. *Wireless Personal Communications*, 7(2):147–169, August 1998.

[90] B. D. Van Veen and K. M. Buckley. Beamforming: A versatile approach to spatial filtering. *IEEE Acoustics, Speech, and Signal Processing Magazine*, pages 4–24, April 1988.

[91] A. J. Viterbi. *CDMA: Principles of Spread Spectrum Communication*. Addison-Wesley, 1995.

[92] A. M. Viterbi and A. J. Viterbi. Erlang capacity of a power controlled cdma system. *IEEE Journal on Selected Areas in Communications*, 11(6):892–900, 1993.

[93] Q. Wu, W. L. Wu, and J. P. Zhou. Centralised power control in cdma cellular mobile systems. *Electronics Letters*, 33(2):115–116, January 16th 1997.

[94] A. D. Wunsch. *Complex Variables with Applications*. Addison-Wesley, 2nd edition, 1994.

[95] A. M. Wyglinski and S. D. Blostein. Mutual coupling effects on cellular cdma communication systems using smart antennas. *CITR Technical Report*, 1999.

[96] A. M. Wyglinski and S. D. Blostein. Antenna array mutual coupling effects on cellular cdma communication systems. *Proceedings of the Queen's 20th Biennial Symposium on Communications*, pages 181–185, 2000.

[97] A. M. Wyglinski and S. D. Blostein. Mutual coupling and scattering effects on cellular cdma systems using smart antennas. *IEEE Semiannual Vehicular Technology Conference Fall 2000 (in press)*, 2000.

[98] Zeland Software Inc. *IE3D Electromagnetic Simulator: User Manual*. 5rd edition, 1999.

[99] J. Zhou, Y. Onozato, and U. Yamamoto. On the capacity and outage probability of a cdma hierarchical mobile system with perfect/imperfect power control and sectorization. *IEICE Transactions on Fundamentals*, E82-A(7):1161–1171, July 1999.

# Vita

## Alexander Mieczysl̃aw Wyglinski

### EDUCATION

| | | | |
|---|---|---|---|
| McGill University | Ph.D. | Electrical and Computer Engineering | 2000– |
| Queen's University | M.Sc.(Eng.) | Electrical and Computer Engineering | 1999–2000 |
| McGill University | B.Eng. | Electrical and Computer Engineering | 1995–1999 |

### EXPERIENCE

Research Assistant (2000–),
Electrical and Computer Engineering, McGill University

Research Assistant (1999–2000),
Electrical and Computer Engineering, Queen's University

System Administrator (1999–2000),
Electrical and Computer Engineering, Queen's University

Teaching Assistant (2000),
Electrical and Computer Engineering, Queen's University

Defence Research Assistant (summer 1997 & 1998),
Department of National Defence,
Ottawa, Ontario, Canada

Teaching Assistant (1998),
Civil Engineering and Applied Science, McGill University

## AWARDS

| | |
|---|---|
| NSERC Postgraduate Scholarship (PGS A) | 2000–2002 |
| Ontario Graduate Scholarship | *(declined)* |
| Le Fonds FCAR Bourse de Matrîse en Recherche | 1999–2000 |
| Queen's Graduate Award | 1999–2000 |

## PUBLICATIONS

Alexander M. Wyglinski and Steven D. Blostein (2000). Mutual Coupling and Scattering Effects on Cellular CDMA Systems using Smart Antennas. *Proceedings IEEE Semiannual Vehicular Technology Conference 2000 (Fall).*

Alexander M. Wyglinski and Steven D. Blostein (2000). Effects of Mutual Coupling, Scatter, and Power Control on the Performance of CDMA Systems using Smart Antennas. *2000 Canadian Institute for Telecommunications Research Annual Research Conference.*

Alexander M. Wyglinski and Steven D. Blostein (2000). Antenna Array Mutual Coupling Effects on Cellular CDMA Communication Systems. *Proceedings 20th Queen's Biennial Symposium on Communications.*

Alexander M. Wyglinski and Steven D. Blostein (1999). Mutual Coupling Effects on CDMA Communication Systems with Smart Antennas. *1999 Canadian Institute for Telecommunications Research Annual Research Conference.*

Capt. B. A. Lepine, B. P. Wallace, D. S. Forsyth, A. Wyglinski. (1998) Pulsed Eddy Current Method Developments for Hidden Corrosion Detection in Aircraft Structures. *Canadian Society for Non-Destructive Testing Journal.*